Institut für Nutzpflanzenwissenschaften und Ressourcenschutz

Sorption, Transformation and Transport of Sulfadiazine in a loess and a sandy Soil

Genehmigte Inaugural-Dissertation
zur
Erlangung des Grades

Doktor der Agrarwissenschaften
(Dr. agr.)
der
Landwirtschaftlichen Fakultät
der
Rheinischen Friedrich-Wilhelms-Universität Bonn

von
Dipl. Geoökol. Stephan Sittig
aus
Liebenburg

Meinem Vater

Danksagungen

Abstract

Veterinary antibiotics are unintentionally introduced into the environment and therefore found in ground and surface water, soil and sediments, air, plants etc. They enter these compartments mainly via application of manure or sewage sludge to soils for fertilizing purposes or after application in aquaculture, in form of the parent compound or a transformation product. Generally, sorption, transformation and transport determines the fate of these organic contaminants in soil. Their wide-spread distribution bears several risks, i. e. spreading of resistance genes or occurrence in the food chain.

Long-term (60 days) batch studies were conducted applying radio-labelled sulfadiazine to samples from two agricultural soils to investigate the sorption and sequestration behavior in the plow layers. Sequential extractions at several time-steps served to analyze the dynamics of both processes. A numerical evaluation served to describe instantaneous sorption, the dynamics of sorption and sequestration, and the formation of non-extractable residues. Multiple extractions with the harsh method questioned the concept of non-extractable residues, since with each consecutive extraction step, further sulfadiazine could be extracted.

Analyzing the liquid phase and the extracts from these batch experiments with Radio-HPLC served to improve the understanding of the transformation behavior in soils in different degrees of (bio-)availability. Apart from the deduction of rate-parameters for a compartment model, the resemblance of the compositions in the liquid phases and the harsh extracts was demonstrated. The formation of the up to six transformation products showed distinct dynamics, either spontaneous or with a time-lag.

Laboratory column experiments with multiple applications of sulfadiazine either together with manure from pig-feeding experiments or in liquid solution served to the improved understanding of the transport processes and the transformation during trans-

port. A numerical description of the breakthrough curves elucidated the processes during movement through undisturbed soil. The composition in the outflow was considerably different in terms of transformation products, as a factor of application mode and soil.

This thesis updated the knowledge of the environmental behavior of sulfadiazine, since we investigated the fate in its most important aspects of sorption, transformation and transport.

Zusammenfassung

Veterinärpharmaka werden unbeabsichtigt in die Umwelt eingeführt und sind demzufolge vorhanden in Grund- und Oberflächenwasser, Boden und Sedimenten, Luft, Pflanzen usw. Sie gelangen in diese verschiedenen Kompartimente durch das Ausbringen von Gülle und Klärschlamm auf landwirtschaftliche Felder zum Zwecke der Düngung oder durch den Einsatz in Aquakulturen, entweder unverändert oder in Form von Transformationsprodukten. Das Schicksal von organischen Kontaminanten wird generell bestimmt von Sorption, Transformation und dem Transportverhalten. Die weitreichende Verteilung von Antibiotika aus der Tierhaltung birgt verschiedene Risiken, wie z. B. die Ausbreitung von Resistenzgenen oder den ¨bergang in die menschliche Nahrungskette.

Langzeit-Schüttelversuche (60 Tage) mit radioaktiv markiertem Sulfadiazin und Proben von zwei landwirtschaftlichen Böden wurden durchgeführt mit dem Ziel das Sorptions- und Sequestrierungsverhalten in den beiden Pflughorizonten zu untersuchen. Sequenzielle Extraktion an den verschiedenen Zeitpunkten erlaubte die Analyse der Dynamiken beider Prozesse. Eine numerische Auswertung diente der Beschreibung der instantanen Sequestrierung, dem Verlauf der Sorption und der Bildung nicht-extrahierbarer Rückstände. Mehrfache harsche Extraktionen stellte das Konzept der nicht-extrahierbaren Rück-stände grundsätzlich in Frage, da mit jeder weiteren Extraktion immer mehr Substanz extrahiert werden konnte.

Die Analyse der Flüssigphase und der Extrakte aus diesen Versuchen mit Radio-HPLC zeigte das Transformationsverhalten in verschiedenen Graden der (Bio-)verfügbarkeit. Neben der Ermittlung von Raten-parameter für ein Kompartimentmodell wurde die ähnlichkeit von Flüssigphase und sorbierter Phase demonstriert. Die Formation der bis zu sechs Transformationsprodukte zeigt deutlich unterschiedliche Dynamiken, sowohl spontan als auch mit einer Zeitverzögerung.

Labor-Säulenversuche mit Mehrfachapplikation von Sulfadiazin, entweder in Form von Gülle aus Futterexperimenten oder in wässriger Lösung diente dem besseren Verständnis der Transportprozesse und der Transformation während der Transports. Eine numerische Modellbeschreibung der Durchbruchskurven beleuchtete die Transportprozesse während des Durchbruchs durch ungestörte Bodensäulen. Die Zusammensetzung des Ausflusses war deutlich unterschiedlich in Hinsicht auf die Transformationsprodukte.

Insgesamt tragen die Ergebnisse der verschiedenen Studien in dieser Dissertation zu einem besseren Verständnis des Umweltverhaltens von Sulfadiazin bei, da dessen Verhalten während der Prozesse der Sorption, Transformation und dem Transport untersucht wurde.

Contents

List of Tables

Chapter 1

Introduction

1.1 Rationale

Veterinary antibiotics are used all over the world for preventive and therapeutic treatment and growth promotion in industrial livestock farming as well as in aquaculture [Du and Liu, 2011, Chee-Sanford et al., 2009, Sarmah et al., 2006, Boxall et al., 2003, Halling-Sørensen et al., 1998]. The German Pharmaceutical Law (AMG) restricts the usage of pharmaceuticals on therapeutic use, following the EU legislation, which initially pointed out the environmental risk assessment in 1997 [EAEM, 1997]. Application as growth promoter is prohibited in the EU since 2006 [Council of the European Union., 2001].
While the usage in aquaculture leads to a direct contamination of sediments and aquatic systems, residues from the application in livestock reach the environment via fertilization practices with manure or directly via grazing animals [Sukul and Spiteller, 2006]. A large fraction (approximately 75%) of the applied antibiotics is not absorbed by animals and is subsequently excreted Chee-Sanford et al. [2009]. During passage through a metabolism the parent compounds are partly transformed, leading to more water

soluble metabolites [Halling-Sørensen et al., 1998]. A reduction of the antimicrobial properties occurrs during manure storage due to degradation processes [Mohring et al., 2009, Boxall, 2008].

Hence, these organic xenobiotics reach the distinct environmental compartments, i. e. surface and ground water, soil, and air [Halling-Sørensen et al., 1998]. Their effects range from acute toxicity [Halling-Sørensen, 2000], development of resistance genes [Gullberg et al., 2011, Chee-Sanford et al., 2009] to inhibition of soil bacteria growth and functionality [Thiele-Bruhn, 2003].

Gullberg et al. [2011] showed the development of resistant bacteria even below the minimum inhibitory concentration for tetracyclines and other antibiotics. For effective risk assessment, Ding and He [2010] pointed out the need for further investigations on the effects on microbial communities. Kopmann et al. [2013] showed the influence of manure based application of sulfadiazine on the development of resistance genes and bioavailability on field trials cropped with maize. The abundance of resistance genes was increased in these soils, with less effect on the rhizosphere soil. The structural diversity of microorganisms was reported to be influenced by slurry from medicated pigs in un-rooted bulk soil as well as in the rhizosphere of maize plants. In soil mesocosm experiments for the duration of 63 days, Reichel et al. [2013] found shifts in the genetic patterns.

A comprehensive approach on estimating the vulnerability of soils in the European Union to contamination with veterinary antibiotics based e. g. on land use and sorption and degradation properties is presented by de la Torre et al. [2012]. Nevertheless, there is limited knowledge on fate and consequences of the usage of these emerging contaminants [Boxall, 2012, Pan et al., 2009]. Consequently, further studies are required.

One important group of veterinary antibiotics is that of the sulfonamides, comprising of not less than 5000 different, structural related compounds [Sukul and Spiteller, 2006]. Hruska and Franek [2012] showed in a comprehensive review the emerging relevance of

sulfonamides in scientific literature: between 1991 and 2011, they found 1255 papers in their search in a scientific database (Thomson Reuters, New York, USA).

The antibiotic in the focus of this dissertation is sulfadiazine (IUPAC: 4-amino-N-(2-pyrimidinyl)benzene sulfonamide; SDZ). As it holds true for other organic contaminants as well, the fate of SDZ in soils depends on sorption, degradation, and transport behavior. When applied to pigs, a mixture of the parent compound and two main metabolites is excreted [Lamshöft et al., 2007]. SDZ applied together with manure is proven to affect the microbial biomass and structural composition, and, to a lesser extent the functional processes [Hammesfahr et al., 2011]. Remediation by oxidation can be conducted e. g. by ferrate(VI) which was shown for sulfamethoxazole, the products are less toxic than the parent compounds [Sharma, 2010].

Tappe et al. [2013] isolated *Microbacterium lacus* as SDZ degrading bacterium in soil samples from the toplayer of lysimeter studies. Incubation experiments using this bacterium demonstrated a complete degradation to 2-aminopyrimidine after 10 days, hinting towards a potential mineralization. Jechalke et al. [2013] found a considerably increase of the abundance of resistance genes in soil samples from a field experiment with slurry from SDZ treated pigs. Besides that, a higher transferability in bulk soil and rhizosphere of these genes *sul1* and *sul2* was detected. In samples from the same experiment, Ollivier et al. [2013] found a drastic change in the ratio of ammonia oxidizing bacteria to nitrite oxidizers, resulting to an 15-fold increase toward the ammonia oxidizers. Additionally, the diversity *Nitrobacter*- and *Nitrospira*-like bacteria was significantly incresed. There are strong indications of an acceleration of biodegradation of sulfonamides following long-term exposure. Topp et al. [2013] isolated a microbacterium degrading sulfamethazine and tylosin, but not chlortetracycline.

SDZ is a slightly hydrophilic compound, having a K_{OW} value of -0.09. Consequently, sorption to soil matrix is not mainly due to

hydrophobic partitioning [Tolls, 2001] as it holds true for several other organic xenobiotics such as pesticides, but to other processes such as ion exchange, cation binding at clay surfaces, surface complexation, and hydrogen bonding Sukul and Spiteller [2006]. Thus, other factors than soil organic carbon content and hydrophobicity, such as surrounding pH and clay content are important [Boxall, 2008]. SDZ forms non-extractable residues in soils [Rosendahl et al., 2011, Kreuzig et al., 2003], which were proven to be prone to be subsequently released with harsh extraction methods [Förster et al., 2008].

SDZ undergoes several transformation processes, in which the parent compound can be inactivated (acetylation), transformed into a less toxic state (hydroxylation), or, via SO_2-extrusion transformed to a more polar metabolite with a lower molecular mass. Sukul and Spiteller [2006] pointed out the need for further investigation in transformation pathways in native soils, with or without manure or sludge.

Transport (of organic contaminants) to the ground water occurs via matrix or macropore flow. Land application of animal waste for a sustainable nutrient cycle with or without precedent waste storage leads to the entry of various veterinary antibiotics. To this purpose, the sludge or manure is often incorporated in the soil to avoid a loss of nitrogen [Chee-Sanford et al., 2009], a practice in accordance to German Federal law Düngeverordnung [1996].

Numerical studies on the fate of SDZ on the basis of batch [Kasteel et al., 2010, Wehrhan et al., 2010, Zarfl et al., 2009] and column experiments [Unold et al., 2009a, Wehrhan et al., 2010] are reported. Model descriptions regarding several distinct types of sorption domains including reversible and irreversible sorption process as well as non-linearity and kinetics.

1.2   General objectives and outline of the thesis

The overall objective of this thesis was to improve the understanding of sorption, transformation and transport of the veterinary antibiotic sulfadiazine. To this aim, laboratory experiments with the radio-labeled compound were conducted, achieving mass balance closure in these batch sorption and column transport studies. The results were evaluated applying inverse modeling techniques by means of Monte Carlo Markov Chain (MCMC) simulations. Specific aims were:

- Investigating sorption and sequestration in batch experiments

- Developing enhancements to existing modeling strategies to describe sorption and sequestration, including instantaneous sorption to reversible and irreversible kinetic sorption sites

- Improving the understanding of the course of transformation processes in soils by means of batch and soil column experiments

- Studying the effect of repeated application of pig slurry containing SDZ to soil columns

- Comparing different strategies of MCMC simulation of these results

- Applying the results of the laboratory transport experiments to a real-world scenario of migration of incorporated substance in soil profile to the groundwater

- Comparing the results with the threefold applications from two different soils and numerically describe the breakthroughs with the HYDRUS-1D model [Simunek et al., 2008, Version 4.14].

This thesis was part of the second phase of the research unit: Veterinary Medicines in Soils - Basic Research for Risk Analysis (FOR

566), founded by the Deutsche Forschungsgemeinschaft (DFG). Sorption and sequestration in long-term batch experiments are discussed in Chapter 2. There, an enhanced model description is developed for the sequestration phenomena and investigated the amount of operational defined non-extractable residues. The transformation in the batch experiments is analyzed in Chapter 3, by presenting new transformation processes in soils and evaluating with a compartment model description for the dissipation and transformation of the parent compound and the metabolites in the liquid phase. In Chapter 4 the model description of the results from the column experiments is shown, applying an MCMC simulator. The parameter optimization procedure is conducted with two different formulations of the likelihood function: a standard least squares approach as the common procedure in hydrology with assuming normal distributed errors with a constant variance and secondly, a generalized likelihood approach enabling the description of the errors to be heteroscedastic and non-normal distributed. In Chapter 5 the results of the column experiments with multiple applications are depicted in terms of the breakthrough curves of the SDZ equivalent concentration, the transformation products, and the concentration profiles in the soil columns as well as a numerical description of the breakthrough curves, estimating one set of parameters for all three breakthrough curves simultaneously.

Chapter 2

Long-term sorption and sequestration dynamics of the antibiotic sulfadiazine - a batch study [1]

2.1 Introduction

The spreading of veterinary pharmaceuticals in the environment is of growing concern. The environmental risk was not emphasized until a decade ago [Pan et al., 2009]. The application of contaminated manure leads to pollution of soils [e. g., Sarmah et al., 2006, Christian et al., 2003, Tolls, 2001, Halling-Sørensen et al., 1998], as well as to pollution of surface and ground waters, which are potential resources for drinking water. Furthermore, persisting antibiotics can cause the development of resistant pathogens, as well as the spreading of resistance via gene transfer

---

[1]Adapted from: S. Sittig, R. Kasteel, J. Groeneweg and H. Vereecken. Long-term sorption and sequestration dynamics of the antibiotic sulfadiazine: a batch study. *J. Environ. Qual.*, 41 (2012): 5: 1497–1506, doi: 10.2134/jeq2011.0467

[Thiele-Bruhn, 2003].
The substance studied here is sulfadiazine (SDZ), an antibiotic from the sulfonamide group. Sulfonamides are widely used in animal husbandry as well as in human medicine [Sarmah et al., 2006] and are known to be persistent in soils [e. g., Sukul and Spiteller, 2006, Stoob et al., 2007]. SDZ undergoes transformation to several metabolites, caused by photolysis [Sukul et al., 2008a] or occurring in soils [e. g., Rosendahl et al., 2011, Kasteel et al., 2010, Unold et al., 2009b]. Transformation in soils is assumed to be primarily of biological origin [Kasteel et al., 2010, Sarmah et al., 2006, Yang et al., 2009], although abiotic transformation on specific mineral surfaces has also been reported [Meng, 2011]. The fate and transport of xenobiotics depend among other factors on sorption to the soil matrix. In the context of this study, sorption is defined as the distribution of a substance between the liquid and the solid phase. For SDZ, this process is non-linear and time-dependent, as shown in batch systems [Kasteel et al., 2010, Wehrhan et al., 2010] and column transport studies [Unold et al., 2009b]. In several studies, sorption kinetics was described by various mathematical models consisting of compartments with different mass exchange rates (reversible and irreversible) [Kasteel et al., 2010, Wehrhan et al., 2010, Zarfl et al., 2009, Unold et al., 2009b].
SDZ forms residues relatively quickly, which are neither extractable with mild methods [e. g., Kreuzig et al., 2003, Kreuzig and Höltge, 2005, Hamscher et al., 2005] nor with harsh extractions processes [Stoob et al., 2007, Förster et al., 2008]. The transfer of a contaminant to a state of reduced accessibility that is not readily reversible is defined as sequestration [Lueking et al., 2000]. It is still unknown, whether this strong binding to the soil matrix and a partial, slow subsequent release [Luthy et al., 1997] is due to diffusion processes into soil particles [Schmidt et al., 2008] or to the formation of covalent bonds [Bialk et al., 2005].
Schauss et al. [2009] pointed out the rapid sequestration of SDZ in soils and showed how soil fractions with different sorption strengths

can be distinguished from each other using sequential extraction methods. Sequential extractions provide an answer to the question of the amount of solute that can be potentially released from the sorbed phase. For example, Kreuzig and Höltge [2005] found fast initial sorption of SDZ into less accessible sorption sites. This was confirmed by Rosendahl et al. [2011] and Förster et al. [2009]. Förster et al. [2008] presented a method with the best extraction efficiency for SDZ from soils.

Sequestered compounds which are not accessible by an extraction method without altering the matrix or changing the compound itself are called bound residues [Burauel and Führ, 2007]. Bound residues are therefore always determined by the experimental extraction procedure used. Förster et al. [2009] extracted radiolabeled sulfadiazine from a manure-amended soil in a 218-day experiment. Their extraction design had foreseen distinguishing between four fractions of different availability: the plant-available nutrients (extractable with $0.01\,\mathrm{M}\,CaCl_2$), the aged but still available fraction (methanol-extractable), a residual fraction (extractable with a harsh microwave extraction), and the bound residues (non-extractable residues). Zarfl et al. [2009] described these extraction data with a conceptual kinetic sorption model and defined the following three sorption compartments with different binding strengths: easily accessible fraction (EAS; extracted with $CaCl_2$ and methanol), residual fraction (RES; microwave extraction), and the fraction of non-extractable residues (NER). However, there is still a need for controlled long-term SDZ adsorption experiments combined with sequestration into different soil compartments, taking into account the temporal dynamics of bioavailability and the formation of bound residues. Furthermore, measuring the sorbed phase concentrations is useful for model discrimination, and it can reduce the uncertainty of the estimated parameters compared to analyzing the liquid phases only [Kasteel et al., 2010].

We performed 60-day batch adsorption experiments using soil from the plow layers of a silty loam and a loamy sand, accompanied by a

sequential extraction of the solid phase according to Förster et al. [2009]. The soil was spiked with radiolabeled sulfadiazine. The objectives were (I) to verify the absence of (biologically driven) transformation of SDZ in a sterilized silty loam, (II) to study the sequestration dynamics of SDZ in solid-phase fractions obtained by a sequential extraction using a modified novel model concept, (III) to apply this model concept to ^{14}C SDZ-equivalent concentrations in non-sterile silty loam and loamy sand, and (IV) to assess the amount of NER (bound residues) in the soils by multiple harsh extractions. We used a modified version of the mathematical compartment model 2SIS proposed by Wehrhan et al. [2010] to describe the long-term sorption and sequestration experiments with the sterilized samples from the Merzenhausen plow layer. We hypothesized that the four model compartments can be used to represent the operationally defined fractions obtained by sequential extraction from this soil-like substrate: liquid phase, EAS, RES, and NER. Our model description represented the sorption and sequestration processes of ^{14}C-derived SDZ-equivalent concentrations in the untreated samples from the two plow layers, irrespective of transformation products in these samples.

2.2 Materials and methods

2.2.1 Laboratory experiments

Sulfadiazine (IUPAC: 4-amino-N-(2-pyrimidinyl)benzene sulfonamide; SDZ) was used as a model compound. It was radiolabeled at the C-2-atom of the pyrimidine ring (purity: 99%, specific radioactivity: 8.88 MBq mg^{-1}; BayerHealthCare, Wuppertal, Germany). Kinetic adsorption experiments combined with a sequential extraction of the solid phase were conducted using soil from the

plow layers (Ap horizons) of a silty loam in Merzenhausen (MER; typic Hapludalf) and a loamy sand in Kaldenkirchen (KAL; typic Dystrudept). Both sites are situated in North Rhine-Westphalia (Germany). They are used for agriculture and differ mainly in clay content and pH. Selected soil properties are listed in Table 2.1.

Long-term batch experiments: sterilized soil. Field-moist soil was sieved (2 mm) and stored in the dark at 4°C before usage. The MER soil was autoclaved three times at 120°C for 20 min (2050 ELV, Tuttnauer, Wesel, Germany). A 0.01 M CaCl$_2$ (Merck, Darmstadt, Germany) solution was also autoclaved. The solutions were treated with a sterile filtration in a 0.1 μm filtration device (Stericup-VP 250 ml Millipore, Molsheim, France). The experiments were run in a clean bench (HERAsafe KS 12, Kendro, Hanau, Germany). The sterility of the 60-day sample was tested by streaking the slurry on an agar plate doped with standard nutrient agar I (Carl Roth, Karlsruhe, Germany).

After determining the initial gravimetric water content, 10 g of field-moist soil was weighed into Teflon-lined centrifuge tubes (performed in duplicate). For preconditioning, 10 ml of the 0.01 M CaCl$_2$ solution was added to the tubes, which were then shaken for one week. After preconditioning, the input concentrations of SDZ were achieved by adding 5 ml of an appropriate stock solution. The ki-

Table 2.1: Selected properties of the plow layer (Ap) from the sites in Merzenhausen (MER) and Kaldenkirchen (KAL).

	Soil texture * [mass-%]			pH †	C_{OC} ‡ [mass-%]	CEC § [cmol$_c$kg^{-1}]	θ_i ¶ [mass-%]
	Sand	Silt	Clay				
MER	4.3	82.9	12.8	7.0	0.97	11.4	7.84
KAL	69.7	26.3	4.0	5.7	0.88	7.8	6.47

* Pipette method (diameters: sand 2 mm–64 μm, silt 2–64 μm, clay < 2 μm). Analysis with oven-dried and sieved (2 mm) soil. † pH measured in 0.01 M CaCl$_2$. ‡ Total organic carbon content determined via combustion. § Cation exchange capacity determined from the exchange with a NH$_4$Cl solution. ¶ Initial field-moist water content.

netic sorption experiments were performed at three input concentrations: a low ($1.5\,\mu mol\,l^{-1}$), a medium ($3\,\mu mol\,l^{-1}$), and a high ($14\,\mu mol\,l^{-1}$) concentration. In addition, batch containers with four input concentrations (0.2, 0.3, 0.4, and $0.6\,\mu mol\,l^{-1}$) were run for seven days to cover a larger concentration range for the determination of the shape of the sorption isotherm. Pure ^{14}C SDZ was used for all input concentrations, except for the highest concentration of $14\,\mu mol\,l^{-1}$, where a mixture of ^{12}C/^{14}C SDZ with a ratio of 4:1 was applied (^{12}C-SDZ: purity 99%; Sigma-Aldrich, Steinheim, Germany). All experiments were performed at room temperature in the dark in a head-over-head shaker (Rotoshake RS 12; Gerhardt, Knigswinter, Germany) at 7 rotations min^{-1} under aerobic conditions.

After 0.5, 1, 4, 7, 14, 29, 44 and 60 days, respectively, the liquid and the solid phases were separated by vacuum filtration (Leybold S4B, Oerlikon Leybold Vacuum, Cologne, Germany) using cellulose acetate filters (pore size $0.45\,\mu m$, Sartorius, Gttingen, Germany) with a final vacuum of less than 1 mbar for about 20 min. The liquid phase concentration was measured by means of liquid scintillation counting (LSC; 2500 TR, Packard Bioscience, Dreieich, Germany) and the remaining wet soil in the batch container was further processed using the sequential extraction procedure. Measurements of the total radioactivity with LSC were conducted in two replicates with a counting time of 15 min. To this end, an aliquot of the sample was mixed with an appropriate scintillation cocktail (Instant Scint Gel Plus; Canberra Packard, Dreieich, Germany). The detection limit was 0.4 Bq, the limit of quantification was set to 1.2 Bq ($5.46\cdot10^{-4}\,\mu mol\,l^{-1}$ ^{14}C SDZ).

The sequential extraction was conducted according to Förster et al. [2009]. There, the wet soil was extracted with 25 ml of a $0.01\,M\,CaCl_2$ solution over 24 hours (this constituted the EAS phase), followed by 25 ml methanol over 4 hours (also EAS). Finally, 50 ml of a mixture of acetonitrile and water (1:4, v:v) was placed with the soil in a microwave (MLS-Ethos 1600; MLS, Leutkirch, Germany) at

150°C for 15 min (RES phase). For the MER sterile treatments, we replaced the 0.01 M CaCl$_2$ and methanol extraction steps (both of which attributed to the easily accessible fraction) with one extraction step by shaking the batch containers with 25 ml of a mixture of 0.01 M CaCl$_2$ and methanol (1:1; v:v) for 24 hours. Both EAS extraction methods were tested and shown to provide similar results (data not shown).

The total radioactivity of the remaining soil, constituting the fraction of non-extractable residues (NER), was measured via combustion. Three samples weighing 0.5 g each were analyzed via combustion at 900°C with an oxidizer (Robox 192; Zinsser Analytik, Frankfurt, Germany). The evolving gas was trapped in a scintillation cocktail (Oxysolve C-400; Zinsser Analytik, Frankfurt, Germany) in which the ^{14}C activity was measured with LSC.

The compositions of the solutions were measured by Radio-HPLC (LB 509 detector, Berthold Technologies, Bad Wildbad, Germany), using a reversed phase column (Phenomenex Synergi Fusion RP 80, 250 mm·4.6 mm; Phenomenex, Aschaffenburg, Germany). Elution was conducted with a mixture of water (490 ml) and methanol (10 ml), buffered with 0.5 ml of a 25% phosphoric acid solution. A 0.25 ml aliquot of each sample was injected into the Radio-HPLC. The peak separation was conducted with a gradient with an increasing amount of methanol, initially with 100% water for 6 min. The methanol fraction was increased linearly to 27% after 23 min, followed by an increase to 37% in the next 3 min and to 47% in the following 2 min. After a total of 30 min, the maximum methanol concentration of 57% was reached.

Using this experimental setup for samples of untreated soils, peaks in the chromatograms were detected at approximately the following retention times (the assigned metabolites in parentheses): 3.8 min (2-aminopyrimidine), 5.3 min (M1), 8.2 min (M2), 12.0 min (p-(pyrimidine-2-yl)amino-aniline), 16.6 min (4-OH-SDZ), 17.8 min (SDZ), and 21.2 min (N-acetyl-SDZ). The metabolites M1 and M2 are assumed to be isomeric compounds of 4-(2-iminopyrimidine-

1(2H)-yl)aniline. The latter as well as 2-aminopyrimidine were described in Sukul et al. [2008a] and referred to as "Photoproduct-A" and "Photoproduct-B", respectively. The metabolite p-(pyrimidine-2-yl)amino-aniline is depicted in Meng [2011] and was used as a standard for our study.

Long-term batch experiments: untreated soils. An identical set of experiments was conducted using soils from MER and KAL in order to test the applicability of our model concept for non-sterilized soil. For the MER soil, the sequential extraction procedure was conducted according to Förster et al. [2009]; the KAL experiment was conducted using the protocol applied to the sterilized samples. For preconditioning, we used $10\,ml$ (MER) or $15\,ml$ (KAL) of a $0.01\,M$ $CaCl_2$ solution. During the experiments, both soils were sampled at 1, 4, 7, 14, 29, 44, and 60 days, by means of vacuum filtration for a duration of about $20\,min$ (MER) or about $15\,min$ (KAL).

Multiple extractions. To assess the extraction efficiency of the microwave method, and thus evaluate the bound residue concept, soil was extracted four times with the harsh method in a separate experiment. For the sterilized MER soil, batch containers with SDZ input concentrations of $3.0\,\mu mol\,l^{-1}$ were run for 0.5, 29, 44, and 60 days. For the untreated MER and KAL soils, batch containers with input concentrations of 1.2 and $17\,\mu mol\,l^{-1}$ were shaken for both 7 and 28 days. With the exception of the multiple microwave extractions, the experimental protocol was identical to the modified extraction protocol as described above.

2.2.2 Modeling

Sorption and sequestration model. We used a modified version of the two-stage irreversible sorption (2SIS) model pro-

posed by Wehrhan et al. [2010] to describe the sorption and sequestration behavior of SDZ. This model comprises a physically realistic implementation of NER in the form of irreversible sorption. The solid phase in the model comprises three domains: an equilibrium sorption site, and a kinetic sorption site, which is subdivided into two fractions, exhibiting reversible and irreversible sorption. We aimed to show that these domains represent the experimental fractions of our sequential extraction protocol: EAS (equilibrium sorption), RES (reversible kinetic), and NER (irreversible kinetic).

The change of the liquid phase concentration C_w [M L^{-3}] over time t [T] is expressed by:

$$(V + M f k_f n C_w^{n-1})\frac{dC_w}{dt} = -M\alpha H(S_1 - S_2) \qquad (2.1)$$

where V [L^3] is the volume of water, M [M] is the mass of soil, f [-] is the fraction of equilibrium sorption sites, k_f [M$_{solution}^{1-n}$ L^{3n} M$_{soil}^{-1}$] is the Freundlich coefficient, n [-] is the Freundlich exponent, α [T^{-1}] is a rate coefficient for reversible sorption, γ [-] ($0 \leq \gamma \leq \gamma_{max}$) is the fraction of the kinetic sorption domain that is occupied by irreversible sorption, γ_{max} [-] ($0 \leq \gamma_{max} \leq 1$) is the dimensionless maximal fraction of the kinetic sorption domain that can be occupied by irreversible sorption, S_1 [M M^{-1}] and S_2 [M M^{-1}] are the concentrations on the equilibrium and kinetic sorption sites, respectively, and H is a modified Heavyside step function defined as:

$$H(1 - \frac{\gamma}{\gamma_{max}}, S_1 - S_2) = \begin{cases} 1 & \text{if } 1 - \frac{\gamma}{\gamma_{max}} > 0 \text{ or } 1 - \frac{\gamma}{\gamma_{max}} = 0 \text{ and} \\ & S_1 - S_2 > 0 \\ 0 & \text{if } 1 - \frac{\gamma}{\gamma_{max}} = 0 \text{ and } S_1 - S_2 < 0 \end{cases}$$

$$(2.2)$$

The distribution between the equilibrium sorption site and the liquid phase is described by the Freundlich isotherm:

$$S_1 = k_f C_w^n \qquad (2.3)$$

The change of concentration in the kinetic site S_2 over time is given by:

$$(1 - f)\frac{dS_2}{dt} = \alpha H(S_1 - S_2) \tag{2.4}$$

The course of the fraction of irreversible sorption in the kinetic site is expressed by:

$$\frac{d\gamma}{dt} = \beta(\gamma_{\max} - \gamma) + \frac{\alpha}{(1 - f)}\gamma H(1 - \frac{S_1}{S_2}) \tag{2.5}$$

where $\beta\,[\mathrm{T^{-1}}]$ is a rate coefficient for irreversible sorption.
The redistribution of the solute from the reversible into the irreversible fraction in the kinetic site is given by:

$$\frac{d(\frac{\gamma}{\gamma_{\max}}S_2)}{dt} = \beta(1 - \frac{\gamma}{\gamma_{\max}})S_2 \tag{2.6}$$

Note that $\gamma_{\max} = 1$ represents the original model of Wehrhan et al. [2010]. A special case is defined when irreversible sorption occurs very fast, i. e. $\beta = \infty$, reducing the 2SIS model to the simplified 2SIS model [Wehrhan et al., 2010] with one parameter less. Model descriptions of equilibrium and kinetic sorption either in series (two stages, one rate) or in parallel (two sites, one rate) were proven to be identical in the case of two sorption domains by Altfelder et al. [2001]. This is equally valid for our modified two-stage irreversible sorption model. In this case, the rate parameter between S_1 and S_2 needs to be rearranged. The locally defined sorbed-phase concentrations S_1 and S_2 from the two-stage irreversible sorption model can be defined per unit mass of the total sorbent by $S_{\mathrm{t1}} = fS_1$ and $S_{\mathrm{t2}} = (1 - f)S_2$ to be valid in a two-site model. Accordingly, Eq. 2.4 can then be rewritten as [Altfelder et al., 2001]:

$$\frac{S_{\mathrm{t2}}}{dt} = k_2[(1 - f)k_{\mathrm{f}}C_{\mathrm{w}}^n - S_{\mathrm{t2}}] \tag{2.7}$$

with the rate-coefficient k_2 related to α by: $k_2 = \alpha/(1\text{-}f)$.
The initial condition in the batch container with the total applied

mass C_t [M] is given by:

$$0 = C_t(1 - a_0) - VC_{w,t=0} - M[f + (1-f)f_2]k_f C_{w,t=0}^n \qquad (2.8)$$

$$\gamma_{t=0} = \gamma_{init} \qquad (2.9)$$

where a_0 [-] is the fraction of experimental loss (negative) or gain (positive) of mass compared to total applied mass in the batch system, f_2 is a dimensionless fraction of the kinetic sorption site S_2, accounting for fast or instantaneous initial sorption, and γ_{init} [-] $(0 \leq \gamma_{init} \leq \gamma_{max})$ is the initial fraction of the kinetic sorption site occupied by irreversible sorption. Instantaneous sorption in both the reversible and irreversible kinetic fraction of S_2 is incorporated in the initial condition. Note that for $f_2 = 0$, no instantaneous sorption exists in the kinetic sorption site. C_w is obtained iteratively and depends on the sorption parameters. Hence, all initial concentrations are given at $t = 0$: in the liquid phase C_w, in EAS ($f k_f C_w^n$), RES $[(1 - f)(1 - \gamma_{init})f_2 k_f C_w^n]$, and NER $[(1-f)\gamma_{init}f_2 k_f C_w^n]$. One additional parameter is introduced to estimate the initial concentrations in the reversible and irreversible fraction of the kinetic sorption site, irrespective of the input concentration used.

Global parameter optimization procedure. The set of three ordinary differential equations was solved in Octave (Version 3.2.4) using Hindmarsh's ODE solver Lsode. Octave [Eaton, 2002] is a free programming environment, primarily intended for numerical computations. Parameter optimization was done with the **DiffeRential Evolution Adaptive Metropolis** algorithm (DREAM; Vrugt et al. [2009]). DREAM is a Markov Chain Monte Carlo sampler that can be used to efficiently estimate the posterior probability density function of optimized model parameters in high-dimensional sampling problems [Vrugt et al., 2009]. The optimal parameter values are those that lead to the lowest value of the objective function, Φ, which contains the differences between measured concentrations C and the corresponding model predictions

$\widetilde{C}$:

$$\Phi = \sum_{k=1}^{k=9} \sum_{m=1}^{m=5} \frac{1}{C_k^{\text{input}}} \sum_{i=1}^{i=N} (C_k^{\text{m}}(t_i) - \widetilde{C}_k^{\text{m}}(t_i))^2 \qquad (2.10)$$

where m is the number of measurement classes (liquid phase, EAS, RES, NER, experimental loss), k represents the different input concentrations, and N is the number of sampling times. To give similar weight to the measurements with different input concentrations, all measurements were multiplied with the inverse of their corresponding input concentrations C^{input}.

The posterior distribution functions were taken after convergence, according to the Gelman-Rubin criterion $\widehat{R} < 1.05$ [Vrugt et al., 2009]. Their corresponding 95% percentiles were evaluated as confidence intervals and interpreted as parameter uncertainties.

Multiple extractions. The functional relationship between the liquid phase concentrations $C_1\,[\text{M}\,\text{L}^{-3}]$ measured with LSC and the consecutive microwave extraction steps was mathematically described by the Gustafson and Holden [1990] model:

$$\frac{C_1}{C_0} = (1 + \beta_{\text{GH}}x)^{-\alpha_{\text{GH}}} \qquad (2.11)$$

where $C_0\,[\text{M}\,\text{L}^{-3}]$ is the concentration in the first microwave extract, $x\,[\text{-}]$ is the number of extraction steps, and $\alpha_{\text{GH}}\,[\text{-}]$ and $\beta_{\text{GH}}\,[\text{-}]$ are shape parameters estimated using the shuffled complex evolution algorithm [Duan et al., 1992], which was implemented in Octave. This model allows the concentrations of the microwave extract to be extrapolated to any arbitrary concentration, such as the limit of quantification (LOQ = $5.46{\cdot}10^{-4}\,\mu\text{mol}\,\text{l}^{-1}$), and thus provide the number of possible extraction steps. This method allows us to estimate the mass that can be potentially extracted from the NER based on one microwave extraction. This mass is then assigned to the RES fraction.

2.3 Results and discussion

2.3.1 Multiple extractions

The amount of ^{14}C SDZ that was extracted diminished with each consecutive step (Fig. 2.1). This shows that NER (or bound residues) is a terminology that is based on the experimental protocol, which has also been reported in other studies. Ying et al. [2005], for example, increased the extraction efficiency of triazine herbicides with ethanol from about 50% with the first extraction step to more than 90% after 5 steps.

Irrespective of input concentration and contact time, the points on the plot coalesced and we were able to fit all measurements of each treatment with only one parameter set for each soil. Figure 2.1 shows the Gustafson-Holden model fitted to the multiple
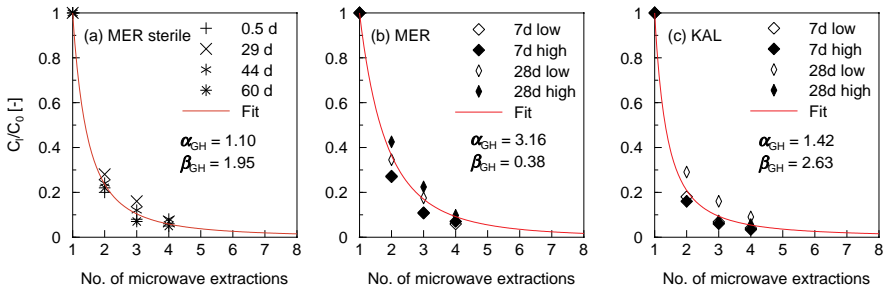
Figure 2.1: Multiple microwave extractions for the plow layer of (a) the sterilized Merzenhausen soil (MER sterile), (b) the Merzenhausen soil (MER), and (c) the Kaldenkirchen soil (KAL). The solid lines represent the fits of the model described by Gustafson and Holden [1990] with the shape parameters α_{GH} and β_{GH} to the ^{14}C-derived SDZ-equivalent concentrations in the microwave extracts, C_l, normalized to the concentrations in the first microwave extracts, C_0, and the symbols represent the measurements in the corresponding extracts.

extraction data for the three soils. The values for the parameters α_{GH} and β_{GH} were different, resulting in soil-specific calibration relationships. By extrapolating the ^{14}C SDZ concentrations in the extracts to the limit of quantification using the soil-specific fits, we were able to estimate the total number of possible microwave extractions, which ranged between 4 (MER sterile with the low input concentration) and 132 (KAL high input concentration).

The RES fraction increased by approximately 60% for MER sterile samples, 70% for the MER soil, and approximately 50% for KAL soil. The differences in the actual amounts of SDZ extracted in the 4 consecutive steps and the potentially extractable amounts were generally higher for the low input concentrations (approximately 25%) than for the high input concentrations (approximately 5–10%).

For example, for the MER soil with a high SDZ input concentration of $17\,\mu\mathrm{mol\,l^{-1}}$, one extraction step (RES fraction) after 28 days yielded $9.9\,\mu\mathrm{mol\,kg^{-1}}$. The sum of the 4 extractions resulted in $17.3\,\mu\mathrm{mol\,kg^{-1}}$, which is an increase of 75%. After 55 (potential) extractions, the RES increased slightly to $17.9\,\mu\mathrm{mol\,kg^{-1}}$. These findings verify the methodology applied, extrapolating after four extractions. When these results were applied to the batch experiments with consecutive extractions, the RES fraction increased by about 80% (MER) or 50% (KAL and MER sterile) for all sampling times. The reduction in the NER fraction was time-dependent for MER and MER sterile (initially 80–90%, decreasing to approximately 50%) and constant over time for KAL (approximately 60%).

Our experimental procedure allowed the potential RES fraction to be estimated based on the concentration measurement in the first microwave extraction using a soil-specific relationship. If only one extraction was conducted for the MER soil example with a high input concentration outlined above, the RES fraction would be underestimated by 50–80%. NER was still present in the soils after correction with the soil-specific equations from the multiple

extraction experiments: about 30% of the total applied mass in MER/KAL and 10% in MER sterile, compared to about 60% in MER/KAL soil and 20% in the MER sterile soil with only one microwave extraction (for the 60-day experiment).

2.3.2 Long-term batch experiments: sterilized soil

Transformation. No transformation products were found in the liquid phase of the sterilized setups, which indicates that transformation is a biologically driven process. The concentrations in the liquid and solid phases add up to approximately 100%, which allows for excluding mineralization. In our study, transformation on mineral surfaces, as described in Meng [2011], did not seem to be the dominant process for the soils investigated. In contrast to the assumption in Kreuzig et al. [2003], sterilization could prevent microbial metabolism longer than 3 days, and we found no cultivatable micro-organisms on the agar plate after 60 days.

Sorption and sequestration dynamics. Figure 2.2a shows the dynamics of distribution of SDZ between all fractions, including the reduced NER, calculated based on the multiple extractions (denoted as extrapolated NER, depicted as shaded areas). Both sorption (distribution of SDZ between liquid and solid phase) and sequestration (redistribution of SDZ between solid phase fractions) were found to be kinetic processes undergoing non-linearity, as also shown e. g. in Kasteel et al. [2010].

Generally, the EAS fraction was low, indicating a low bioavailability. In the NER fraction, there was an indication of an initial sorption at $t = 0$. This was different for the non-sterile treatments (see below), where both the RES and NER fractions showed pronounced initial sorption. This behavior is also reported in the literature for SDZ [Schmidt et al., 2008, Junge et al., 2011], and for other organic contaminants Heistermann et al. [2003].
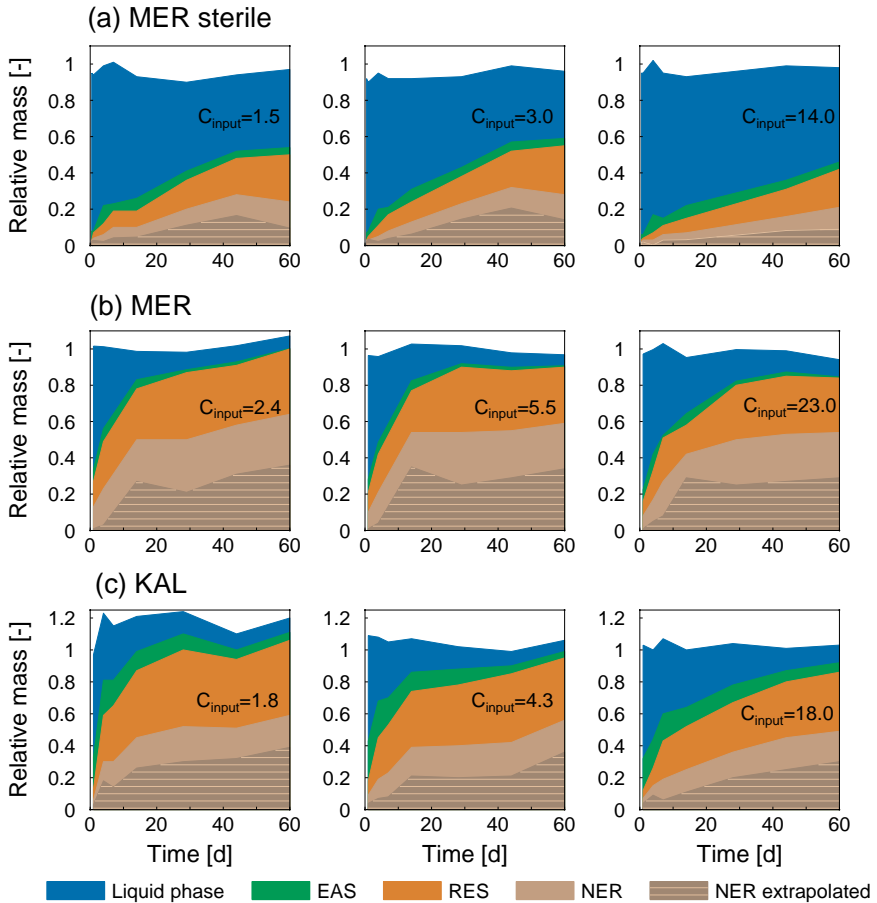
Figure 2.2: Cumulative masses of ^{14}C-labeled sulfadiazine equivalents in the various compartments for (a) the sterilized Merzenhausen soil (MER sterile), (b) the Merzenhausen soil (MER), and (c) the Kaldenkirchen soil (KAL) for the low, medium and high input concentration C_{input} [μmol l^{-1}]. The mass in each compartment was normalized based on the total mass applied. NER extrapolated denotes the reduced non-extractable residues, calculated by extrapolating the results of the multiple extractions.

Parameter optimization using DREAM. Sterilized MER soil
was used to demonstrate the fit of the adapted 2SIS model to the
measured concentrations in all experimental fractions, including
the experimental loss (Fig. 3). The 7-day sorption isotherm was
incorporated to improve the representation of non-linear sorption,
covering a large concentration range. The optimal parameter set
and the 95% confidence intervals (CI) are listed in Table 2.2. Note
that all predictions were performed using only one set of param-
eters. The parameter uncertainties were reasonable (with most
confidence bands below 50% of the corresponding best value) with
very narrow intervals for n and γ_{max}.

The dynamics of the liquid phase concentrations for all three input
concentrations were described well by the model. The relationship
between concentrations in the liquid and the solid phase, given by
the Freundlich isotherm, could be represented for three orders of
magnitude (see bottom of Fig. 3). Sorption non-linearity with
Freundlich n values less than one (here: $n = 0.85$) means that
higher concentrations tended to sorb to a lesser extent than lower
concentrations Sukul et al. [2008b]. In our study, this resulted in
relatively higher C_{w} at higher input concentrations and in lower
sorbed concentrations in the RES and NER fractions (an effect
that was more pronounced in the untreated samples). The EAS
fraction was described reasonably well, despite the large scatter in
the data for the early time steps. The low f value for the equilib-
rium sorption site fraction (0.043) indicated that the sorption of
SDZ was dominated by kinetics. The kinetic sorption site showed a
non-zero concentration at $t = 0$. The introduction of the two addi-
tional parameters f_2 (dimensionless fraction of the kinetic sorption
site undergoing fast or instantaneous initial sorption; here: 0.020)
and γ_{init} (initial fraction of the kinetic sorption site occupied by
irreversible sorption; here: equal to $\gamma_{\mathrm{init}} = 0.54$) led to a better
representation of the measurements in the early phases of sorption
and sequestration compared to the original 2SIS model. A sepa-
rate estimation of γ_{init}, which represents the irreversible sorption

Table 2.2: Parameter estimates for the modified two-stage irreversible sorption model (2SIS) for the sterilized Merzenhausen soil (MER sterile), the Merzenhausen soil (MER), and the Kaldenkirchen soil (KAL), as well as for the correction of the residual phase (RES) by multiple extractions (denoted as ME).

Parameter*	MER sterile	MER	KAL
$k_f\,[\mu\text{mol}^{1-n}\,\text{l}^n\,\text{kg}^{-1}]$	3.2	15.6	17.6
	$(2.5\text{–}4.3)^{\dagger}$	$(13.2\text{–}18.6)$	$(13.0\text{–}25.1)$
$n\,[\text{-}]$	0.85	0.81	0.92
	$(0.81\text{–}0.88)$	$(0.79\text{–}0.83)$	$(0.88\text{–}0.96)$
$\alpha\,[\text{d}^{-1}]$	0.013	0.016	0.016
	$(0.0085\text{–}0.018)$	$(0.013\text{–}0.020)$	$(0.0092\text{–}0.024)$
$f\,[\text{-}]$	0.043	0.018	0.052
	$(0.031\text{–}0.055)$	$(0.014\text{–}0.023)$	$(0.037\text{–}0.069)$
$f_2\,[\text{-}]$	0.02	0.026	0.024
	$(0.0092\text{–}0.035)$	$(0.020\text{–}0.035)$	$(0.0089\text{–}0.045)$
$\beta\,[\text{d}^{-1}]$	$\infty^{\ddagger}$	0.82	∞
		$(0.63\text{–}1.41)$	
$\gamma_{\max}\,[\text{-}]$	0.54	0.64	0.53
	$(0.52\text{–}0.56)$	$(0.63\text{–}0.65)$	$(0.51\text{–}0.55)$
$a_0\,[\text{-}]$	0.045	0.0028	-0.052
	$(0.024\text{–}0.061)$	$(-0.014\text{–}0.023)$	$(-0.093\text{–}-0.0060)$
MSE	0.021	0.021	0.15
	MER sterile ME	MER ME	KAL ME
$\beta\,[\text{d}^{-1}]$	∞	0.37	0.17
		$(0.26\text{–}0.66)$	$(0.10\text{–}0.39)$
$\gamma_{\max}\,[\text{-}]$	0.29	0.34	0.33
	$(0.27\text{–}0.31)$	$(0.26\text{–}0.66)$	$(0.30\text{–}0.35)$
MSE	0.025	0.066	0.15

* k_f is the Freundlich coefficient, n is the Freundlich exponent, α is the rate coefficient for reversible sorption, f is the fraction of equilibrium sorption sites, f_2 is the fraction of kinetic sorption sites, β is the rate coefficient for irreversible sorption inside the kinetic domain, $\gamma_{\max}$ is the maximum fraction of irreversible sorption sites in the kinetic domain, a_0 is the experimental loss, and MSE is the mean of the squared relative errors. [†] 95% confidence interval. [‡] For $\gamma_{\max} = \infty$, the 2SIS model reduces to the simplified 2SIS model with instantaneous irreversible sorption into the max. fraction of the kinetic site.

at $t = 0$ in S_2, resulted in the same value as γ_{max} within the level of parameter uncertainty. Therefore, we fixed the value of γ_{init} as equal to γ_{max}. We used this model framework to simulate instantaneous sorption in the kinetic site with one additional parameter for each phase (f_2 and γ_{init}) irrespective of the input concentration, which is now part of the initial condition. This constitutes an improvement to the model described by Zarfl et al. [2009], in which the initial conditions were set to the values of the first measurement points.

We found a maximum sorption capacity for irreversible sorption: γ_{max} ($= 0.54$). Accordingly, 54% of the sorption capacity in the kinetic domain could be occupied by irreversible sorption, or, in the terminology of the extraction protocol, by NER.

Assuming $1/\alpha$ (rate coefficient for reversible kinetic sorption; here: $0.013\,\mathrm{d}^{-1}$) as the characteristic time-scale of the kinetic sorption, the value of α laid in the range of the experimental duration. As the rate coefficient for irreversible sorption β tended to infinity, we used the simplified 2SIS model, fitting one parameter less. Generally, for large values of β, the results describing distribution in the kinetic site were similar to each other and the value of α was limiting, as it quantified the uptake into the kinetic site. The rate coefficient $\beta >> \alpha$ indicated a fast sequestration in NER Wehrhan et al. [2010]. Hence, with the mass exchange coefficient $\alpha = 0.013\,\mathrm{d}^{-1}$ and β set to infinity, the redistribution of the reversible and irreversible fractions in the kinetic site was much faster than the mass exchange between S_1 and S_2. This is in line with the experimental findings, where the extraction efficiency decreased rapidly over time Kreuzig and Höltge [2005]. The error in the mass balance was acceptable ($a_0 = 0.045$), i. e. the mean estimated mass recovery was 104.5%.

2.3.3 Long-term batch experiments: untreated soils.

Transformation. There was considerable transformation in the untreated soils. In addition to the parent compound and the hydroxylated form (4-OH-SDZ), 2-aminopyrimidine, M1, M2, p-(pyrimidine-2-yl)amino-aniline, and Acetyl-SDZ were found. After 60 days, approximately 80% of the pure SDZ initially applied in the liquid phase had been transformed. Note that at this time step, only 10–15% of the initially applied mass was found in the liquid phase. In the extracts from the solid fractions, similar compositions were measured. This gave confidence in the application of our modeling procedure to estimate the effective behavior of SDZ equivalents based on the sterilized samples.

Sorption and sequestration dynamics. While the sorption affinity was higher in the KAL soil, the tendency to form NER was stronger in MER soil (Fig. 2b and 2c). The initial rapid increase of substance in the strongly bound RES and NER fractions in both the MER and KAL soils in the first two weeks was followed by slower changes. Generally, the strongest tendency to form NER was found in the untreated MER soil, as $\gamma_{\max}$ was highest and f was lowest. Mass balances were generally in the range of $100\pm5\%$, except for the low input concentration in the KAL soil (up to 120%). We have no explanation for this.

An overview of all measured and fitted ^{14}C-derived SDZ-equivalent concentration dynamics for the three soils is given in Fig. 4. The corresponding parameters are listed in Table 2.2. The parameter uncertainties were generally larger for the KAL soil, although we used one fitting parameter less with β set to infinity. This could be due to the slightly different experimental protocol. The numerical mass recoveries were $100\pm5\%$ in MER and KAL.

Sorption affinity, as quantified by the Freundlich coefficient k_f, was higher for the KAL soil ($18.5\,\mu\mathrm{mol}^{1-n}\,\mathrm{l}^{n}\,\mathrm{kg}^{-1}$) than for the MER soil ($14.1\,\mu\mathrm{mol}^{1-n}\,\mathrm{l}^{n}\,\mathrm{kg}^{-1}$). This agrees with the findings of several

other studies using the same two soils [Kasteel et al., 2010, Zarfl et al., 2009, Unold et al., 2009b]. The value for the Freundlich exponent n ranged between 0.82 (MER) and 0.91 (KAL). The higher sorption affinity in the loamy sand compared to the silty loam was most likely due to the speciation of SDZ. The mean pH for the MER soil was 6.7 and for the KAL soil 5.7, which led to a higher fraction of the negatively charged form of SDZ with a lower sorption affinity in the MER soil [Kasteel et al., 2010].

Fitting the Freundlich isotherm to the 7-day sorption isotherm only, the Freundlich parameters k_f and n were: $3.3\,\mu\mathrm{mol}^{1-n}\,\mathrm{l}^n\,\mathrm{kg}^{-1}$ and 0.75 for MER, and $4.0\,\mu\mathrm{mol}^{1-n}\,\mathrm{l}^n\,\mathrm{kg}^{-1}$ and 0.90 for KAL. The deviations are much more pronounced for k_f than for n, as also reported in Sabbah et al. [2005]. The value for k_f is about four times smaller than the true equilibrium parameters, which could cause considerable underestimation of the sorption capacity when a sorption equilibrium is assumed after 7 days. It should be noted that 7 days is a much longer shaking time than generally used, which may lead to drastic misinterpretations of the leaching behavior in the environment Sabbah et al. [2005]. With regard to transport processes, a lower k_f means a lower retardation and consequently a shorter residence time in soils.

2.3.4   Effects of sterilization

The sorption behavior for the sterile treatment differed from that of the non-sterile treatment in several aspects: (i) lower sorption capacity, (ii) slower sequestration, and (iii) 80% of the measured ^{14}C radioactivity was assigned to different transformation products in the non-sterile MER treatment after 60 days. According to Berns et al. [2008], sterilization of soil by autoclaving alters the quantity and quality of soil organic matter. After sterilization, they found a 37-fold increase in the released amount of organic

substances in the MER soil. The composition of the organic matter had also changed, as sterilization removed sugars and proteins from dead microorganisms in the solid phase. Thus, the easily accessible C_{org} became less accessible after sterilization. As sorption occurs to a large extent to the organic matter [Thiele-Bruhn et al., 2004, Wehrhan et al., 2010], the SDZ in our experiments may have sorbed to dissolved organic matter which could have caused the higher measured liquid phase concentrations, as compared to the untreated soil.

The sorption affinity decreased in the sterile treatments ($k_f = 3.2 \, \mu mol^{1-n} \, l^n \, kg^{-1}$, with an unchanged pH value of 6.7) and the extent of equilibrium sorption increased, as indicated by the higher value for f. Additionally, less NER was formed. This may be due to a change in the composition and amount of organic matter or by the stopped microbial activity. The parameter uncertainties were similar to the untreated samples, with a more uncertain estimation for f_2 in the MER sterile. The parameter with the least uncertainty was γ_{max}.

2.3.5   2SIS description for the multiple extractions

For parameter estimation based on the multiple extraction experiments (which resulted in a corrected NER fraction), only the distribution process in the kinetic site was regarded, as the other processes of sorption and sequestration were identical to the experiments with one single extraction step. Consequently, all parameter values, except β and γ_{max}, were taken from the experiments with a single extraction (Table 2.2). As a result of the lower fraction of NER, the value of γ_{max} decreased. As the fraction (readily) available for irreversible sorption generally decreased, β became smaller. The parameter uncertainty was relatively high for the untreated MER soil. This was caused by two (outlier) values for

the RES fractions after 14 days for the medium and the high SDZ input concentration. If these measurements are weighted with zero, we get the following: $\beta = 0.26$ (0.18–0.41) and $\gamma_{\max} = 0.33$ (0.32–0.35).

2.4   Conclusions

We found no transformation products in the liquid phase of sterilized MER soil. This verifies the mainly biologically driven transformation of sulfadiazine in this soil. For the sterilized MER soil samples, the distribution into four measured fractions was mathematically described using a modified formulation of a recently proposed model [Wehrhan et al., 2010], combined with a global optimization procedure. The validity of this model description derived using the sterilized samples was demonstrated with non-treated samples. The observed fast initial sequestration into the two fractions of the less accessible kinetic site was incorporated into the initial conditions. For this, a formulation was used similar to the description of initial sorption to the equilibrium sorption site. The initial redistribution in the kinetic sorption site of the reversible fraction (equivalent to RES) and the irreversible fraction (equivalent to NER) was also described. Thus, instantaneous sorption into the two kinetic domains was properly described by adding only two parameters.

Mathematically evaluating the multiple harsh extractions allowed us to correct the magnitude of the experimentally defined amount of non-extractable residues of SDZ [Förster et al., 2009, Zarfl et al., 2009]. Our method reduced the NER fraction 1.5–2 fold. In summary, it is not possible to estimate the leaching potential of sorbed sulfadiazine to soils using one exhaustive extraction step, as this underestimates the potential amount of substance that can be released.

30
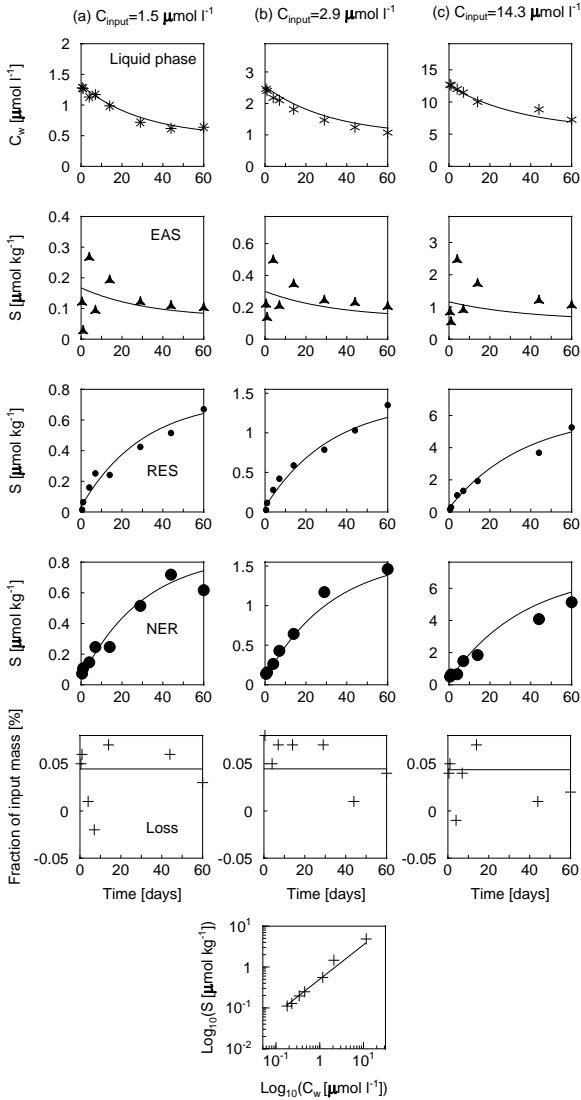
Figure 2.3: Temporal changes of the concentrations in each compartment for the sterilized Merzenhausen soil for the three input concentrations (a) low, (b) medium, (c) high, and (d) the 7-day sorption isotherm. The symbols represent the measurements and the solid lines the fits. The plots are scaled according to the relations in the input concentrations.
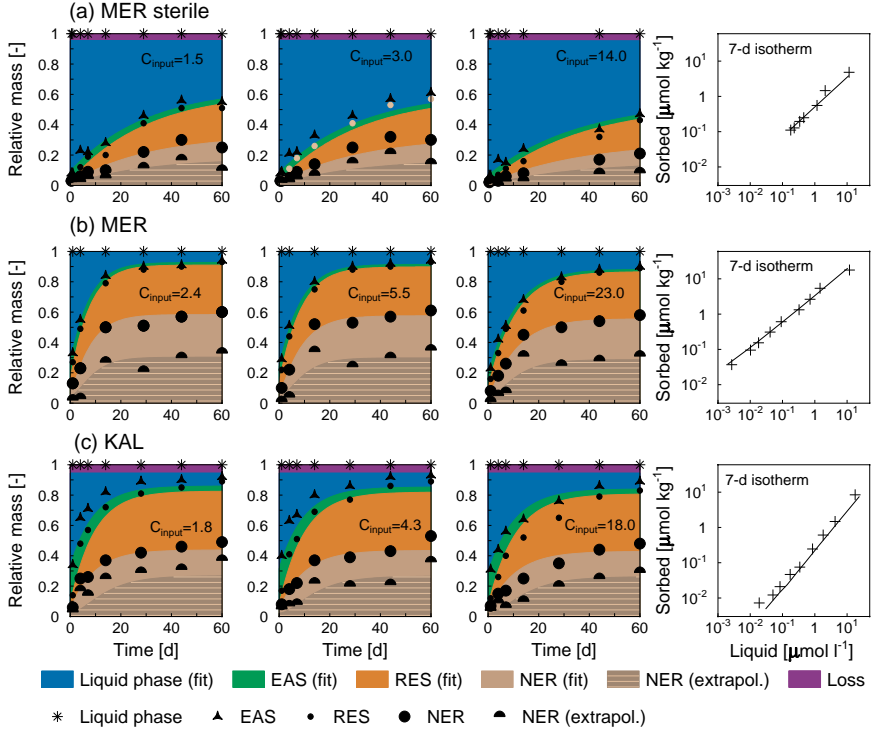
Figure 2.4: Overview of all measured and fitted concentration dynamics for (a) the sterilized Merzenhausen soil (MER sterile), (b) the Merzenhausen soil (MER), and (c) the Kaldenkirchen soil (KAL) for the three input concentrations C_{input} [μmol l^{-1}]. The measured concentrations were normalized by the corresponding recovered masses, except for the 7-day isotherms. For the untreated samples, ^{14}C-derived SDZ equivalents are given. NER extrapolated denotes the reduced non-extractable residues, calculated by extrapolating the results of the multiple extractions.

32

Chapter 3

Dynamics of transformation of the veterinary antibiotic sulfadiazine in two soils [1]

3.1 Introduction

Veterinary pharmaceuticals are unintentionally introduced into the environment, for example by fertilization practices using manure from livestock [Boxall, 2008, Halling-Sørensen et al., 1998]. Consequently, residues of these organic compounds have been found in several environmental compartments [Kümmerer, 2009]. As they are intended to have biological effects and to be persistent, their environmental behavior requires thorough investigation with respect to their fate and effects.

The substance under study is sulfadiazine (IUPAC: 4-amino-N-

(2-pyrimidinyl) benzene-sulfonamide; SDZ). This antibiotic is one of the sulfonamides which are widely used in animal husbandry as well as in human medicine [Hruska and Franek, 2012, Sarmah et al., 2006]. Surface interactions (e.g. sorption) as well as transformation processes are controlling factors for the fate of organic xenobiotics in soils. Aerobic biological transformation constitutes the main route of degradation for veterinary pharmaceuticals in soils [Boxall, 2008], although SDZ is reported not to be readily biodegradable [Baran et al., 2006]. Generally, sulfonamides undergo several transformations to metabolites in soils, in aqueous solution, and organisms - by both biological and physiochemical processes [Garcia-Galan et al., 2012, Schwarz et al., 2010, Sukul et al., 2008a, Lamshöft et al., 2007, Halling-Sørensen et al., 1998]. Sorption of SDZ to soil material is reported to be kinetic and non-linear [Sittig et al., 2012, Wehrhan et al., 2010, Kasteel et al., 2010]. Sittig et al. [2012] identified and numerically described the dynamics of sorption and sequestration of SDZ in a long-term batch study. According to the protocol of Förster et al. [2009], Sittig et al. [2012] extracted the solid phase sequentially and defined the extracts using $0.01\,M\,CaCl_2$/methanol as an "easily assessable fraction" (EAS). The (multiple) extracts with acetonitrile were obtained using a microwave and termed the residual fraction (RES). Both extractable fractions represented a reservoir that can be released from the solid phase. The remaining sorbed substance was regarded as non-extractable residue (NER). If it is sorbed to the soil matrix or to soil organic compounds, a substance is assumed to be protected against transformation [Sukul and Spiteller, 2006, Van Eerd et al., 2003, Bollag et al., 2002]. After numerically evaluating 14-day batch studies, Kasteel et al. [2010] concluded that the transformation of SDZ was restricted to the liquid phase.

Transformation processes of SDZ in soils have hardly been investigated [Gao], especially with regards to the spectrum of sorbed substances [Schwarz et al., 2010]. Wehrhan et al. [2010] pointed out the need for further studies including investigations of the

transformation products (TPs) in batch experiments, noting that the liquid phase should be analyzed as well as the sorbed substance. Recently, new strategies in extractions and analytics have become available to enhance the extraction efficiency of the sorbed solute and facilitate the detection of trace amounts of TPs [Förster et al., 2009, Unold et al., 2009].

To investigate the transformation behavior of SDZ in two different soils, we conducted 60-day batch sorption experiments, analyzing the corresponding samples from (i) the liquid phase in the batch containers, and (ii) the extracts obtained by a sequential extraction procedure. Individual setups with radiolabeled SDZ for different time steps enabled us to simultaneously trace the dynamics of sorption, sequestration, and transformation. A compartment model allowed us to mathematically describe the transformation of the parent compound in the liquid phase as well as the dissipation of the parent and the TPs into a sink, and to estimate all the parameters for the parent compound and the TPs simultaneously. Dissipation time values (duration needed for the disappearance of 50% (DT_{50}) or 90% (DT_{90}), respectively) for transformation, sorption or total dissipation (separate DT_{50} values) enable the fate of SDZ and TPs to be interpreted. Our hypotheses were that (i) the transformation of SDZ in soils occurs immediately or with a time lag, leading in part to new TPs, (ii) the occurrence and nature of species in the liquid phase and in the microwave extracts from the sorbed phase are similar, and (iii) the tendency to transform is dependent on the input concentration of the liquid phase.

3.2 Materials and Methods

3.2.1 Chemicals

[14]C-SDZ was radiolabeled at the C-2-atom in the pyrimidine ring (specific radioactivity: $8.88\,MBq\,mg^{-1}$, purity: 99%, Bayer-HealthCare AG, Wuppertal, Germany). ^{12}C-SDZ with a purity of 99% was purchased from Sigma-Aldrich, Steinheim, Germany. Standards of 2-aminopyrimidine, 4-OH-SDZ, and N-acetyl-SDZ were provided by the Institute of Environmental Research (INFU) at the TU Dortmund University. Demineralized water and chemicals of at least analytical grade were used.

3.2.2 Long-term batch experiments

The setup of the sorption experiments was described in Sittig et al. [2012] (Chapter 2). Briefly, 10 g soil and 10–15 ml application solutions in three different initial concentrations ($\approx$2, $\approx$5, and $\approx$20 μmol l^{-1}) were shaken for a maximum of 60 days. The soil from the unique setups was consecutively extracted at each time step. Here, we used samples from the first three horizons of the Merzenhausen site (M Ap, M Al, and M Bt; Orthic Luvisol; silty loam) and from the upper two horizons from Kaldenkirchen (K Ap, K B1; Gleyic Cambisol; loamy sand). Selected soil properties are listed in Table 3.1. The complete experimental schedule is given in Table 1 in the Supplementary Information (Chapter 3.5).

Table 3.1: Properties of the soils under study.

	Soil texture *			pH [†]	C_{org} [‡]	Fe(total) [§]	Fe (active) [¶]	Sampling depth
	[mass-%]				[mass-%]	[mass-%]	[mass-%]	[cm]
	Sand	Silt	Clay					
M Ap	4.3	82.9	12.8	6.7	1.0	1.7	0.3	20
M Al	1.8	83.0	15.3	6.8	0.3	1.7	0.3	55
M Bt	1.8	78.3	20.0	7.0	0.2	2.1	0.2	80
K Ap	69.7	26.3	4.0	5.7	0.9	0.7	0.3	20
K B1	69.0	27.7	3.3	6.2	0.2	0.5	0.1	45

* Pipette method (diameters: sand $2\,mm$–$64\,\mu m$, silt 2–$64\,\mu m$, clay $< 2\,\mu m$). Analysis with oven-dried and sieved ($2\,mm$) soil. [†] pH measured in $0.01\,M$ $CaCl_2$. [‡] Total organic carbon content determined via combustion with subsequent IR detection. [§] Total Fe content after Li-borate extraction. [¶] Active pedogenic iron oxides extracted with oxalic acid ammonia oxalate after Schwertmann [1964].

3.2.3 Instrumentation and measurements

All analytical methods were detailed described in Sittig et al. [2012] (Chapter 2). Briefly, the separation and quantification of SDZ and their metabolites was usually made by Radio-HPLC (Jasco with LB 509 detector, Berthold Technologies, Bad Wildbad, Germany), using a reversed phase column (Phenomenex SynergiFusion RP 80, 4.6 mm · 250 mm, 4 μm; Phenomenex, Aschaffenburg, Germany). Gradient Elution (flow 1 ml min^{-1}) was conducted with mixture of water (490 ml) and methanol (10 ml), buffered with 0.5 ml of a 25% phosphoric acid solution (solvent A) and methanol (solvent B) under following conditions: 0% B for 6 min, increased linearly from 0% to 27% B in 17 min, from 27% to 37% B in 3 min, from 37% to 47% B in 2 min and to 57% B in 2 min. Under the conditions of 0.25 ml injection of each sample, the detection limit for SDZ and TPs was 12 nM (3 μg l^{-1} SDZ mass equivalents; 100% method). In the case of too low activities, HPLC fractions were taken for additional, more sensitive LSC measurements (2 nM detection limit).

Furthermore, an aliquot of each sample was measured by liquid scintillation counting (LSC, Perkin Elmer, Waltham, MA, USA) for quantification of the total activity (external calibration). Several TPs were detected (partly for the first time). If available, standards were used for their identification. For structure elucidation of the most intense unknown metabolite (M1), we coupled the Radio-HPLC with mass spectrometry (LC-APCI-MS/MS; TSQ Quantum, Thermo Fisher, Waltham, MA, USA), using a Phenomenex Synergi Fusion-RP 80 A column (2 mm · 150 mm, 4 μm, Torrance, CA, USA) with 1 mM ammoniumacetate + 0.1% formic acid (solvent A) and acetonitrile + 0.1% formic acid (solvent B) gradient, conditions according to Sukul et al. [2008a].

3.2.4 Mathematical description of dissipation and transformation in the liquid phase

The concentration dynamics of SDZ and the TPs in the liquid phase were described with a kinetic compartment model (Fig. 3.1), implemented in MATLAB [2007]. With respect to values triggering higher-tier studies for regulatory purposes (endpoints, such as DT_{50} or DT_{90}) the FOCUS [2006] report recommends using the most appropriate model description for the parent compound. We therefore described the observed bi-phasic behavior of SDZ (kinetics not following first-order degradation) with the Gustafson and Holden [1990] dissipation model, using the differential form for parameter estimation [FOCUS, 2006]. This provides an analytical solution to evaluate the endpoints (Eq. 1 in the Supplementary Information (Chapter 3.5)). SDZ was the predecessor for all TPs, whose dissipation kinetics in the liquid phase were described by single first-order kinetics. Our model formulation allowed for the evaluation of additional endpoints: $DT_{50,transf.}$ for the time during which 50% of the substance was transformed, $DT_{50,sorption}$ for the overall sorption, and the DT_{50}'s for transformation of SDZ to the single TPs (ref. Chapter 3.5).

Since we applied the model compound in a radiolabeled form, we were able to achieve mass balance closure. Consequently, we included the measurements of the sink into the parameter estimation process, consisting of sorption and/or undefined further transformation. The system of differential equations was simultaneously solved for the dimensionless liquid phase concentrations (relative to the input) of SDZ and the TPs:

$$\frac{d\,\text{SDZ}}{d\,t} = -\frac{\alpha}{\beta}\text{SDZ}(\frac{t}{\beta} + 1)^{-1} \tag{3.1}$$

$$\frac{d\,\text{TP}_i}{d\,t} = a_i\,\text{SDZ} - b_i\,\text{TP}_i \quad \text{for } i = 1...5 \tag{3.2}$$

$$\frac{d\,\text{Sink}}{d\,t} = b_0\,\text{SDZ} + b_1\,\text{2-amino.} + b_2\,\text{M1} + b_3\,\text{M2} + b_4\,\text{M3}$$
$$+ b_5\,\text{4-OH-SDZ} \tag{3.3}$$

where t is time, α [-] and β [T^{-1}] are shape parameters (both > 0), a_i [T^{-1}] ($i > 0$) are the rates of transformation of SDZ in the liquid phase, b_0 [T^{-1}] is the dissipation of SDZ from the liquid phase due to sorption, and b_i [T^{-1}] ($i > 0$) denotes dissipation of the TP's from the liquid phase due to sorption and/or further transformation. The iterator i stands for the compound, as shown in Fig. 3.1 ($i = 0$: SDZ; $i = 1$: 2-aminopyrimidine; $i = 2$: M1 (unknown); $i = 3$: M2 (unknown); $i = 4$: M3 (unknown); $i = 5$: 4-OH-SDZ). To account for both instantaneous sorption and very rapid transformation, the initial concentrations of SDZ and M1 were incorporated into the estimation for all five soils, as in Sittig et al. [2012]. The initial concentrations for all other TPs were fixed to zero, except for 4-OH-SDZ in M Ap which was also treated as a variable. The initial value of the sink was constrained on the basis of mass balance considerations. Table 2 in the Supplementary Information (Chapter 3.5)) specifies the parameter estimations for the different horizons.

The DREAM$_-$(ZS) algorithm by Vrugt et al. [Vrugt, 2012] was applied for global parameter optimization, minimizing the sum of squared errors between the measured and simulated concentrations. This method additionally yields statistically based estimations for the posterior uncertainty intervals. Initial ranges for all rate parameters were set between zero and one, α between zero and 5, and β between zero and 50.
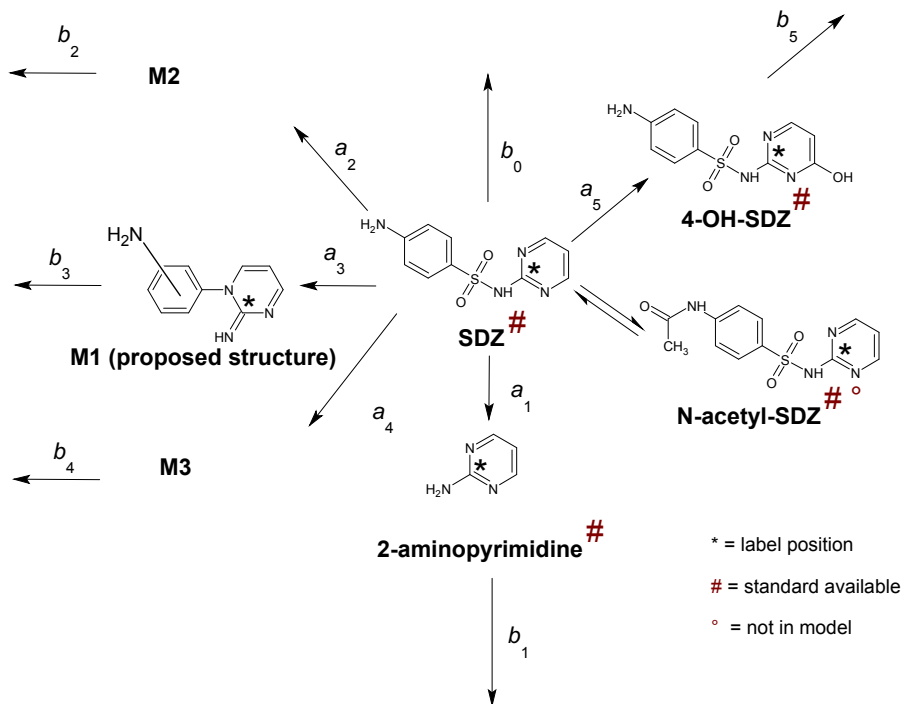
Figure 3.1: Structural formulas of all species and scheme of the compartment model describing the transformation of the parent compound (SDZ) in the liquid phase (rate parameters a) as well as a sink for all species due to adsorption and/or transformation in the solid phase (rate parameters b). The dissipation of SDZ is described with the bi-phasic model after Gustafson and Holden [1990], for the TPs, a single first-order approach was used. Sulfadiazine (SDZ) was assumed as the predecessor for all TPs; the transformation to N-acetyl-SDZ is known to be reversible.

3.3 Results and discussion

3.3.1 Transformation products of SDZ

Characterization of unknown transformation products was proved initially by the most sensitive multiple reaction monitoring (MRM) on all hitherto known (nonlabeled) transitions. The ion chromatograms of the transitions m/z 187 > 145 and m/z 187 > 108 consistently showed one peak assigned to M1. No further peaks (M2, M3) could be recorded, because of their marginal substance amounts.

In a separate experiment - the irradiation of nonlabeled SDZ with UV-light - we produced M1 (besides several other products) in higher concentration for further experiments with regard to structure elucidation. At first, we recorded in the full scan mode the pseudomolecular peak [M+H]+ at m/z 187 Da. Subsequently, by recording of a high resolution mass spectrum by means of ESI-FTICR-MS (LTQ FT Ultra, ThermoFisher Scientific) we received its sum formula $C_{10}H_{11}N_4$. MS/MS investigation showed the following product ion spectrum: m/z 145 Da (100%), 170 Da (31%), 108 Da (26%) (a graphical representation is shown in Fig. 2 in the Supplementary Information (Chapter 3.5))). Due to the fact that M1 is also formed by SO_2 extrusion with the same elemental composition as well as same product ion spectrum and similar retention time as 4-[2-iminopyrimidine-1(2H)-yl] aniline identified by Sukul et al. [2008a], we assume that both compounds are constitution isomeres.

Our irradiated as well as the irradiated sample from Sukul et al. [2008a] show in each case several chromatographic peaks with the transition 187 > 145. Therefore, we assume, that M2 and M3 could be possibly 4-[2-iminopyrimidine-1(2H)-yl] aniline, or isomers therefrom.

In summary, we detected up to seven compounds within the different fractions (liquid phase; easily assessable fraction: EAS; residual fraction: RES) (Fig. 3.1): 2-aminopyrimidine, M1, M2, M3, 4-OH-SDZ, SDZ, and N-acetyl-SDZ.

2-aminopyrimidine was previously depicted as SDZ-metabolite, produced by photolysis, in EC-MS [Hoffmann et al., 2011] as well as microbial by *Microbacterium lacus* [Tappe et al., 2013]. Schwarz et al. [2010] found a similar metabolite originating from the sulfonamide sulfapyridine after a 14-day incubation with fungal laccase from *Trametes versicolor*.

Boreen et al. [2005] described an SO_2 extrusion process like in our M1 for other sulfonamides - after photolysis or as an indirect process, attributed to the interaction with dissolved organic matter. Sukul et al. [2008a] expressed this for the exposition of SDZ in liquid solution to UV-light with 4-[2-iminopyrimidine-1(2H)-yl] aniline, as the major metabolite. In our study, M1 and the possible isomers M2 and M3 also developed in the dark, as was also reported by Unold et al. [2009]. Gao showed the formation of products similar to M1 after transformation of sulfamethazine (N1-(4,6-dimethyl-2-pyrimidinyl)-sulfanilamide) on the surface of Mn-oxides.

4-OH-SDZ is a TP of the metabolism in pigs [Lamshöft et al., 2007], is formed by photolysis [Sukul et al., 2008a] as well as in soils [Unold et al., 2009, Förster et al., 2009, Kasteel et al., 2010], respectively. Wang et al. [2010] showed that 4-OH-SDZ was formed in suspensions of Fe-oxides and oxalate. The formation of N-acetyl-SDZ mainly occurred in pig metabolism [Lamshöft et al., 2007].

3.3.2   Transformation in the two soils

Figure 3.2 shows the concentration dynamics of the liquid phase, EAS, and RES from the two plow layers (M Ap and K Ap), as well as of the liquid phases from the setups with the M Al, M Bt, and the K B1, all for the high input concentration level of $\approx 20\,\mu\mathrm{mol\,l^{-1}}$. Besides the known general differences in terms of sorption dynamics and capacity for both soils [Sittig et al., 2012, Kasteel et al., 2010], there was a trend towards a decrease in sorption with depth of the soil profiles. Kasteel et al. [2010] showed this for the same soils and the first two horizons in 14-day batch sorption experiments, see also the values for M/M_0 in the liquid phase after 60 days (Table 3 in the Supplementary Information (Chapter 3.5))).

There were differences in the transformation patterns between the two soils. Generally, transformation was more pronounced in the MER soil. The transformation tendency decreased for both soils with increasing depth, due to a potentially decreasing microbial activity. This is indicated by the lower organic carbon contents (Table 3.1), which can used as a proxy for microbial activity. In their 14-day batch experiments, Kasteel et al. [2010] found a stronger formation of 4-OH-SDZ in the KAL soil, the SO_2 extrusion product (4-[2-iminopyrimidine-1(2H)-yl] aniline) was much more abundant in the MER soil. In column experiments, a stronger transformation tendency was reported in the KAL soil [Unold et al., 2009].

The formation of 2-aminopyrimidine, M2, M3, and 4-OH-SDZ occurred dynamically throughout the course of the experiment. In the liquid phases for both soils we detected a rapid formation of M1, which was more pronounced for MER. The transformation on goethite surfaces is reported to lead to p-(pyrimidine-2-yl)amino-aniline, a constitutional isomer of M1 as the prevailing species [Meng, 2011]. In our study, M1 was dominant in the liquid phase

for the first 30 days. After fast formation, its fraction stagnated and the percentage remained more or less constant. This dynamic might be due to the fact that the formation of M1 and its dissipation from the liquid phase due to sorption and transformation proceeded at the same rate. At the moment, we have no explanation for this process.

The formation of 4-OH-SDZ was rapid. The patterns differed between the soils from the two sites as well as for the plow layers and the subsequent horizons. While 4-OH-SDZ was formed and further degraded in the M Ap, the formation in the K Ap appeared to be still on the increasing limb of formation after 60 days, although there still might be a degradation which is slower than its formation for the first 60 days. Deeper in the soil profiles we still found the formation of 4-OH-SDZ, although to a far smaller extent. In contrast, Zarfl et al. [2009] found no hydroxylation of SDZ in manure-amended soils for the the period of 220 d.

Trace amounts of N-acetyl-SDZ were found in almost every sample of the K Ap, except for the extracts from the RES fraction where the concentration was more abundant (up to 10%). A qualitative overview for all horizons and all fractions after 60 days is given in Table 3 in the Supplementary Information (Chapter 3.5).

The compositions of the liquid phase and the extract from the RES phase were remarkably similar (Fig. 3.2 and Fig. 1 in the Supplementary Information (Chapter 3.5)). Linear correlation coefficients of 0.94 (M Ap) and 0.96 (K Ap) were evaluated for SDZ in the high input concentration in the two plow layers. This is similarly true of the EAS fraction, even though with a very low amount at the end of the experimental period. Figure 1 in the Supplementary Information (Chapter 3.5) shows details of the correlations between the liquid phase and RES fraction for the two plow layers, revealing similar patterns for all three major species in the KAL soil and good agreement for SDZ and M1 in the MER soil. These findings apparently contradict the common assumption that a sorbed xenobiotic in the RES fraction is not (bio-)available

[Bollag et al., 2002, Alexander, 2000] and therefore not prone to metabolization. However, it must be considered that in batch experiments, i. e. continuously shaking and liquid in excess, conditions are created in which the protection caused by sorption might be reduced.

In our experiments we found TPs which were assigned to biotic as well as abiotic processes. For instance, the hydroxylation of SDZ to 4-OH-SDZ is reported to be driven biotically [Sukul and Spiteller, 2006] as well as abiotically [Wang et al., 2010]. Using batch experiments with sterilized soils, Sittig et al. [2012] showed that the transformation of SDZ is mostly biologically driven, as they did not find any TPs.

Model description

The best-fit parameter values and the 95% posterior uncertainty intervals are listed in Table 3.2. It was difficult to reliably estimate the parameters because in most cases no complete course consisting of increase, peak and subsequent decline of a single TP was observed (Fig. 3.2). The estimations of the rate parameters for the sink of 2-aminopyrimidine, M2, and M3 (b_1, b_3, and b_4) were uncertain, as expressed by the posterior uncertainty intervals that filled the complete parameter range. For the other parameters, the posterior distributions were mostly peaked (not shown). In the 60-day experimental period, we did not observed any decline in the concentrations of these three species, which made it impossible to estimate any significant parameter values. Hence, we fixed those parameters to zero, as we did for the parameter b_2 (dissipation of M1) for M Bt and K B1. This model described the observations well (Fig. 3.3), as was also indicated by the visual impression of low RMSE and high Nash and Sutcliffe [1970] model efficiencies (close to unity). The initial concentration of SDZ could be estimated well, showing uncertainty bands with 10–15% of the best fit.
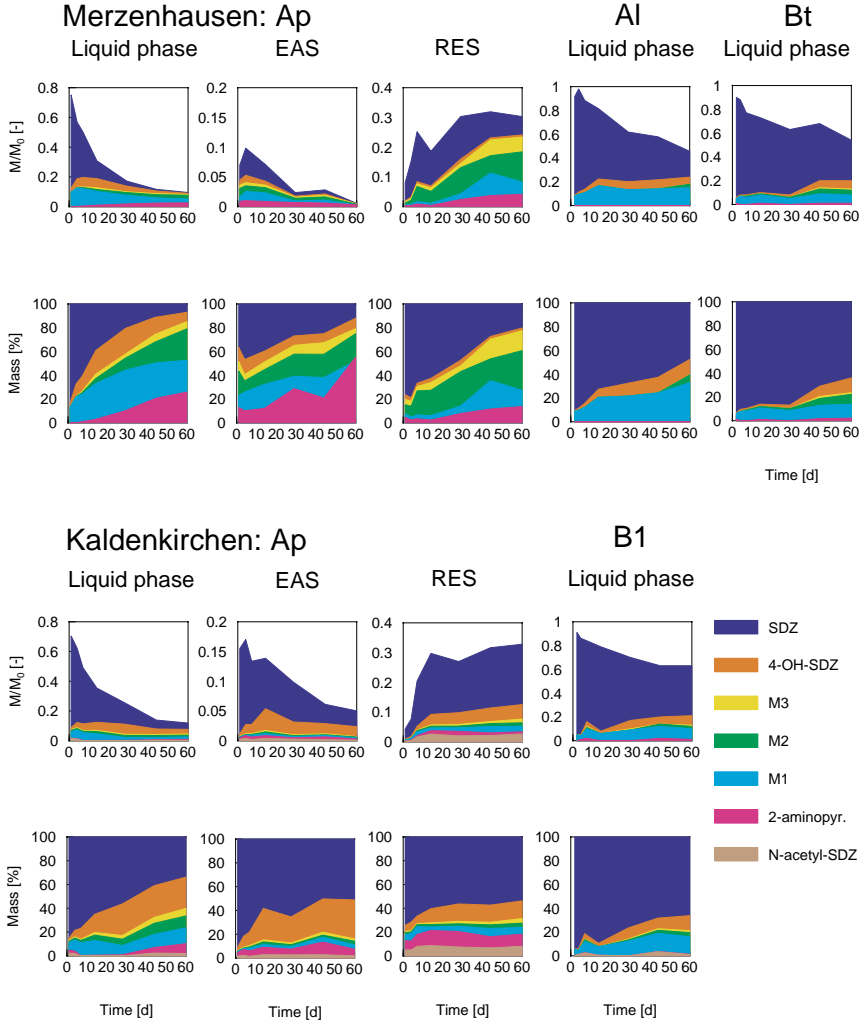
Figure 3.2: Overview of the compositions in the liquid phases of the setups from both soils for the high concentration, totally comprising of five horizons. For the plow layers (Ap), the liquid phases as well as the extracts from the solid phase (EAS: easily assessable fraction; RES: residual fraction) are displayed. All dynamics are shown in absolute values as well as percentages of the respective fraction.

Table 3.2: Parameter values for the compartment model (best-fit values, 95% posterior uncertainty intervals in brackets) and corresponding calculated endpoints for the five horizons from Merzenhausen (M Ap, M Al, and M Bt) and Kaldenkirchen (K Ap and K B1).

Parameter	M Ap	M Al	M Bt	K Ap	K B1
	Shape parameters for the bi-phasic model for the parent				
α [-]	**4.77**	**1.58**	**0.90**	**3.92**	**0.78**
	(3.42–5.00)	(0.94–1.84)	(0.52–1.24)	(2.34–4.42)	(0.46–1.08)
β [d^{-1}]	**30.5**	**46.6**	**38.3**	**44.5**	**25.5**
	(19.9–35.4)	(21.6–49.7)	(16.0–49.7)	(23.8–49.7)	(15.0–49.6)
	Model rate parameters [$\cdot 10^{-3}$ d^{-1}]				
a_1	**2.6**	–	–	**0.32**	–
	(1.0–5.5)			(0.0089–2.3)	–
a_2	**6.6**	**6.1**	**0.46**	**50**	**2.0**
	(0.97–24)	(1.5–21)	(0.028–2.7)	(1.3–58)	(0.36–3.8)
a_3	**2.7**	–	–	**0.84**	–
	(0.91–5.7)	–	–	(0.17–3.2)	–
a_4	**1.0**	–	–	**1.7**	–
	(0.13–3.7)	–	–	(0.11–3.0)	–
a_5	**16**	**2.8**	**1.8**	**8.9**	**2.7**
	(1.1–39)	(1.3–4.6)	(0.28–3.1)	(5.4–16)	(1.4–3.7)
b_0	**97**	**16**	**15**	**6.5**	**10**
	(68–108)	(0.67–23)	(12–17)	(0.36–58)	(8.4–12)
b_1	–	–	–	–	–
	–	–	–	–	–
b_2	**26**	**11**	–	**500**	–
	(15–60)	(1.2–80)	–	(23–770)	–
b_3	–	–	–	–	–
	–	–	–	–	–
b_4	–	–	–	–	–
	–	–	–	–	–
b_5	**46**	–	–	**17**	–
	(8.0–240)	–	–	(3.0–70)	–
	Estimated relative initial concentrations M/M$_0$ [-]				
SDZ	**0.71**	**0.92**	**0.86**	**0.68**	**0.86**
	(0.67–0.74)	(0.88–0.98)	(0.82–0.89)	(0.65–0.70)	(0.83–0.90)
M1	**0.094**	**0.074**	**0.052**	**0.046**	**0.039**
	(0.061–0.11)	(0.011–0.12)	(0.019–0.075)	(0.012–0.10)	(0.0080–0.069)
4-OH-SDZ	**0.010**	**0 (set)**	**0 (set)**	**0 (set)**	**0 (set)**
	(0.00020–0.047)	–	–	–	–
Sink*	**0.19**	**0.0060**	**0.088**	**0.27**	**0.18**
	Goodness-of-fit criteria [-]				
RMSE[†]	0.011	0.027	0.029	0.013	0.023
ME[‡]	0.99	0.98	0.97	0.99	0.96
	Regulatory endpoints [d] SDZ				
DT$_{50,total}$	4.8	26	45	8.6	51
DT$_{90,total}$	19	153	459	36	642
DT$_{50,transf.}$	24	78	307	11	147
DT$_{50,sorption}$	7.1	43	46	107	69
	DT$_{50}$ [d] for transformation of SDZ to:				
2-aminopyr.	267	–	–	2166	–
M1	105	114	1507	14	347
M2	257	–	–	825	–
M3	693	–	–	408	–
4-OH-SDZ	43.3	248	385	77.9	257

* Evaluated based on mass balances [†] Root mean squared error [‡] Nash-Sutcliffe model efficiency [Nash and Sutcliffe, 1970].

Transformation occurred faster in the M Ap than in the K Ap, with higher values for the formation rates of 4-OH-SDZ ($16 \cdot 10^{-3}\,\mathrm{d^{-1}}$ to $8.9 \cdot 10^{-3}$ $\mathrm{d^{-1}}$) and 2-aminopyrimidine ($2.6 \cdot 10^{-3}\,\mathrm{d^{-1}}$ to $0.32 \cdot 10^{-3}\,\mathrm{d^{-1}}$), as well as for the initial concentration of M1 (9.4% to 4.6%).

For all five horizons, the $DT_{50,total}$ values for SDZ were reached within the experimental period of 60 days (Table 3.2). The observed tendency towards a decreasing rate of transformation with depth was reflected in an increase of the values for $DT_{50,transf.}$, and the DT_{50}'s for the transformation of SDZ to the single TPs. Furthermore, a deceleration of the kinetics was indicated by larger differences between DT_{50} and DT_{90}. The importance of the transformation with regard to the sorption strength was reflected in the differences between the values for $DT_{50,transf.}$ and $DT_{50,sorption}$, with the former being up to seven times higher (M Bt). The total disappearance of SDZ from the liquid phase was dominated by sorption for all horizons except the K Ap, where the value for the $DT_{50,sorption}$ was higher than the $DT_{50,transf.}$. This was caused by uncertainties in the estimation of the rate-parameters a_2 (formation of M1) and b_0.

The $DT_{50,total}$ values decreased with decreasing initial concentration (Table 5 in the Supplementary Information (Chapter 3.5)). This was primarily caused by non-linear sorption behavior, where lower concentrations are preferably sorbed. Furthermore, the DT_{50} for the formation of 2-aminopyrimidine, M2, M3, and 4-OH-SDZ tend to decrease with lower input concentrations, while the opposite was found for M1. This indicates that the transformation processes occurred mostly in combination with the solid phase. Additionally, with the lower input concentration, transformation is possibly less reduced due to the less adverse effect on the microbial population. In contrast, M1 might be formed quickly in the liquid phase at the beginning of the experiment and was relatively more abundant in the high input concentration. The exact metabolic pathway of SDZ transformation to the single species in
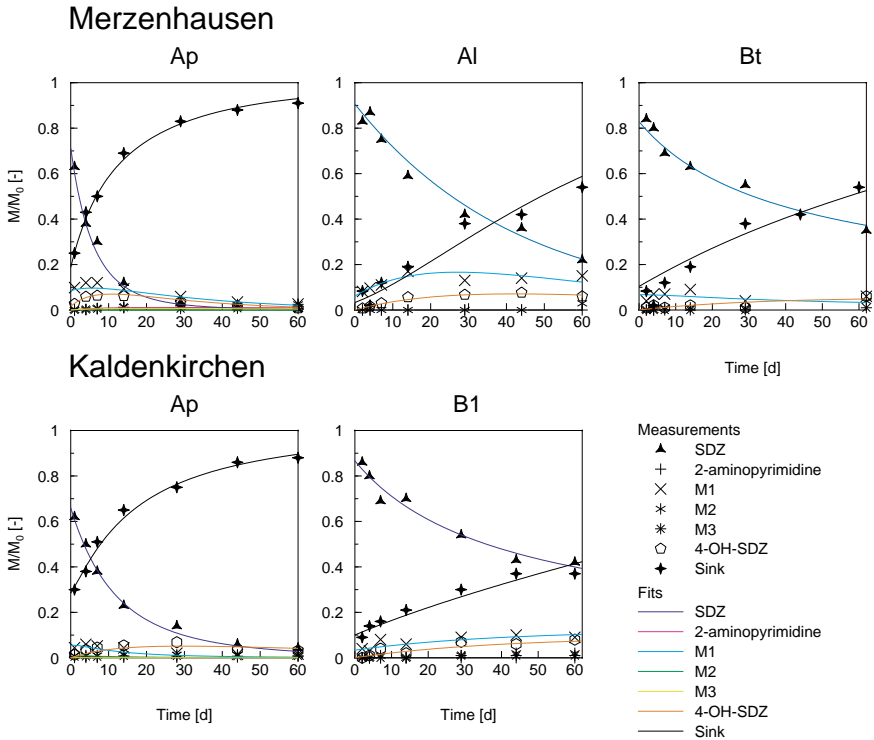
Figure 3.3: Concentration dynamics in the liquid phase for all species as example for the highest of the three concentrations. Symbols represent measurements and lines model calculations.

soils is still unclear, but nevertheless we were able to describe the transformations with SDZ as the predecessor of all TPs (Fig. 3.1).

3.4 Conclusions

In this paper, we studied the dynamics of the transformation of SDZ into up to six transformation products for two soils both

in the liquid phase and in the extracts of the solid phase using long-term batch experiments. Apart from instantaneous transformation, more than 90% of the applied SDZ in the liquid phase and up to 80% in the microwave extracts from the solid phase was transformed after 60 days. The transformation characteristics differed considerably between the two soils under investigation and decreased with soil depth, i. e. with decreasing C_{org} content. Our experiments showed that the compositions of liquid phase and extractable sorbed fraction were similar. Furthermore, the transformation behavior depended on the input concentration. Due to the non-linearity in the sorption behavior, lower input concentrations led to relatively higher amounts of sorbed substance and caused an increase or decrease of transformation, as a function of the species. Our study showed that in addition to investigating the fate of parent compounds, the occurrence and dynamics of transformation products should also be included in such studies.

3.5 Supplementary material

3.5.1 Schedule of the laboratory experiments

Table 3.3 gives the complete schedule of the sorption and sequestration experiments. For each sample, 10 g of the corresponding fine soil ($< 2\,mm$) was used. Unique setups for each time step allowed us to sequentially extract the sorbed solute from the solid phase after separating the liquid and solid phase by vacuum filtration. The samples were constantly shaken in a head-over-head shaker at 7 rotations per minute and in the dark. The procedure is described in detail in Sittig et al. [2012] (Chapter 2).

Table 3.3: Test schedule of the batch sorption experiments with consecutive extraction.

	M Ap	M Al	M Bt	K Ap	K B1
L/S-ratio [-][*]	1.5:1	2:1	1.5:1	2:1	1.5:1
Init. conc. $[\mu\text{mol}\,l^{-1}]$	2.4, 5.5, 23	1.7, 3.5, 17	1.5, 2.9, 13	1.8, 4.3, 18	2.6, 5.2, 24
Sampling times [d]	0.5, 1, 4, 7,	2, 4, 7,	2, 4, 7,	1, 4, 7,	2, 4, 7,
	14, 29, 44, 60	14, 29, 44, 60	14, 29, 44, 60	14, 28, 44, 60	14, 29, 44, 60
No. extractions[†]	3	3	2	2	2

[*] Liquid-to-solid ratio of the soil/$0.01\,\text{M}\,CaCl_2$ solution slurries [†] The subsequent extractions with $0.01\,\text{M}\,CaCl_2$ for 24 h and methanol for 4 h with the M Ap and M Bt soils were replaced with one extraction step for 24 h with a mixture (1:1; v:v) of both liquids.

3.5.2 Modeling the bi-phasic behavior of SDZ and deriving additional endpoints

Applying the Gustafson and Holden [1990] shape parameters as proposed in [FOCUS, 2006], endpoints DT_x [d] for SDZ were evaluated as follows:

$$DT_x = \beta[(\frac{100}{100-x})^{\frac{1}{\alpha}} - 1] \qquad (3.4)$$

Calculating the dissipation of SDZ solely due to sorption $(DT_{50,\text{sorption}})$ was done by: $\ln(2)/b_0$. With respect to the transformation only, $(DT_{50,\text{transf.}}$ or, in other words, $\text{DegT}_{50})$ can be achieved with: $\ln(2)/(\text{sum of all } a\text{'s})$, and transformation to any of the transformation products i: $\ln(2)/a_i$.

3.5.3 Schedule of the simulations

Table 3.4 lists the specifications of the simulations with the DREAM_(ZS) algorithm. The choice of the parameters to be estimated was done following an examination of the data.

3.5.4 Measurements at the end of the 60-day experimental period

Table 3.5 shows the results after 60 days for all five horizons and all three measured fractions (C_w, EAS, and RES).

Table 3.4: Schedule of the simulations.

	Species fitted	No. of para	No. of data	df[*]
M Ap	SDZ, 2-aminopyr.[†] M1, M2[†] M3[†] 4-OH-SDZ	13	42	29
M Al	SDZ, M1[†] 4-OH-SDZ	9	28	19
M Bt	SDZ, M1[†] 4-OH-SDZ[†]	9	24	15
K Ap	SDZ, 2-aminopyr.[†] M1, M2[†] M3[†] 4-OH-SDZ	12	42	30
K B1	SDZ, M1[†] 4-OH-SDZ[†]	9	28	19

[*] Degrees of freedom, the difference between the number of data points and the number model parameters to estimate. [†] Only the a parameter, describing the transformation of SDZ to the corresponding species was fitted in these cases; the parameter for further sorption/transformation of the species, b, was fixed to zero.

3.5.5 Correlations between soil properties and sorption and transformation parameters

Table 3.6 shows the correlations between transformation and both the total organic carbon content (C_{org}) and pH-value in terms of Kendall τ [Kendall, 1938] (between -1 and 1) regarding all five horizons. A trend was visible for both these soil properties: a positive correlation with C_{org} and a negative correlation with pH, with p-values of 0.13 and 0.22, respectively. No trend was observed for the other soil properties.

Table 3.5: Percental compositions of the liquid phases and solid-phase extracts (EAS: easily accessible fraction; RES: residual fraction). Compositions are given for the five horizons from the two soils under study (M: Merzenhausen, K: Kaldenkirchen) after 60 days for the high concentration.

Species	M Ap	M Al	M Bt	K Ap	K B1
	Liquid phase				
SDZ	5.6	47	64	36	66
2-aminopyr.	26	–	1.3	6.3	0.27
M1	27	33	12	13	15
M2	26	6.4	8.3	10	3.4
M3	6.1	–	1.3	6.3	1.7
4-OH-SDZ	7.8	13	12	26	13
Acetyl-SDZ	–	–	0.8	1.9	1.1
M/M_0 *	0.10	0.46	54	0.12	0.63
	EAS				
SDZ	8.7	–	–	53	54
2-aminopyr.	55	–	–	3.7	3.5
M1	–	–	–	3.6	7.0
M2	23	–	–	3.1	1.2
M3	4.4	–	–	1.9	1.1
4-OH-SDZ	8.7	–	–	33	30
Acetyl-SDZ	–	–	–	1.8	3.3
M/M_0 *	0.010	0.019	<1%	0.018	0.062
	RES				
SDZ	20	42	59	62	66
2-aminopyr.	14	5.7	12	2.2	2.7
M1	33	7.7	12	5.7	11
M2	17	34	7.9	3.6	2.0
M3	14	4.3	3.7	3.8	1.7
4-OH-SDZ	2.3	6.3	8.7	15	12
Acetyl-SDZ	–	0.62	5.0	8.0	5.4
M/M_0 *	0.30	0.19	0.068	0.33	0.17

* Mass of ^{14}C relative to initial input mass, constituting parent and transformation products.

Table 3.6: Linear correlations between estimated values for the model parameters and soil properties, evaluated for the soils of each of the sites as well as for all five soils (denoted as total).

		Transformation rate SDZ (sum of a's)	Correlation
	C_{org} [mass-%]		
M Ap	1.0	0.029	
M Al	0.3	0.0089	**Kendall τ**
M Bt	0.2	0.0023	**0.74**
K Ap	0.9	0.062	**p-value**
K B1	0.2	0.0047	**0.13**
	pH		
M Ap	6.7	0.029	
M Al	6.8	0.0089	**Kendall τ**
M Bt	7.0	0.0023	**−0.60**
K Ap	5.7	0.062	**p-value**
K B1	6.2	0.0047	**0.22**
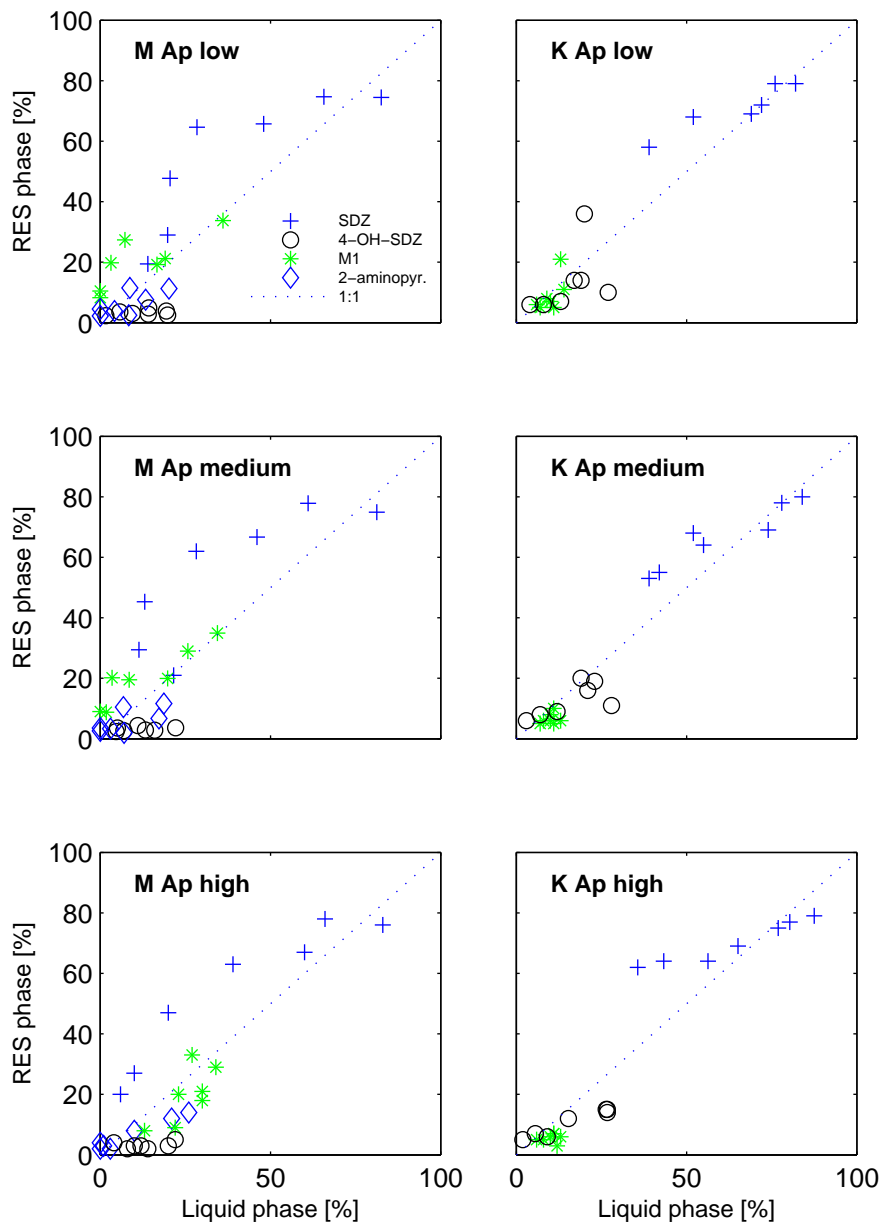
Figure 3.4: Correlations between the relative concentrations of the main species in the liquid phases and in the RES fractions.

MS/MS spectrum of component M1
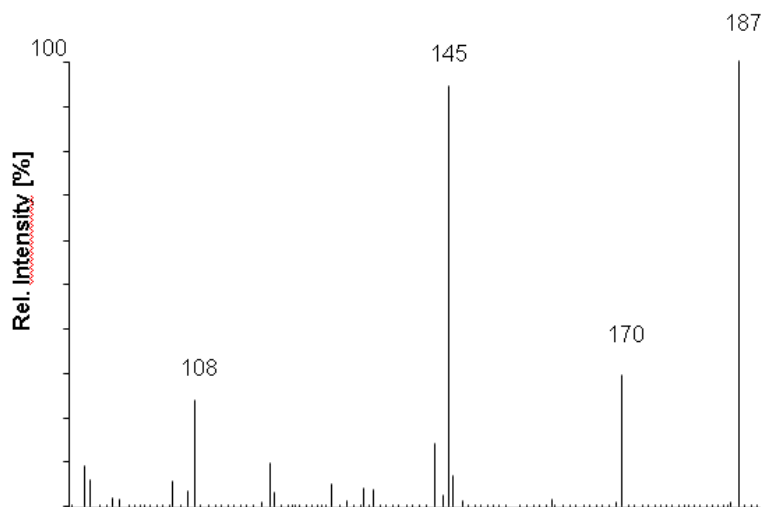
Figure 3.5: Graphical representation of the mass spectrum of M1.

Table 3.7: Modeling endpoints [days] for the three levels of input concentration (high, medium, low).

Soil	Concentration	$DT_{50,total}$	$DT_{90,total}$	$DT_{50,transf.}$	$DT_{50,sorp.}$	DT_{50} for transformation of SDZ to:				
						2-aminopyr.	M1	M2	M3	4-OH-SDZ
M Ap	high	4.8	19	24	7.2	265	106	261	688	43
	medium	2.8	11	17	4.0	196	138	135	282	28
	low	3.0	12	16	4.3	149	354	196	396	22
M Al	high	26	153	78	44	–	115	–	–	247
	medium	20	102	206	10203	–	587	–	–	317
	low	19	98	102	4064	–	158	–	–	288
M Bt	high	45	459	305	48	–	1511	–	–	382
	medium	25	452	316	29	–	4545	–	–	340
	low	17	188	198	24	–	2000	–	–	220
K Ap	high	8.6	36	11	107	2191	14	835	405	78
	medium	5.1	20	14	11	7979	22	207	2332	47
	low	4.8	19	6.3	77	423	19	208	597	10
K B1	high	51	642	150	69	–	352	–	–	261
	medium	29	214	148	40	–	438	–	–	224
	low	23	128	220	29	–	2206	–	–	245

Chapter 4

Transport of sulfadiazine - laboratory estimated soil parameters strongly determined by the choice of the likelihood function

4.1 Introduction

In hydrological modeling, observations are represented by the sum of a deterministic component, the model, and a random component describing the remaining errors, i. e. the residuals between the simulation and the measurements. Parameter inference is often based on the assumption of independent and Gaussian normally-distributed errors between measurements and simulations with a mean of zero and a constant variance. When regarding the residuals as distributed heteroscedastic, i. e. with no constant variance, and furthermore non-normally-distributed (skewed and in different degrees of kurtosis), different parameter

values are estimated and predictive uncertainties may be reduced. Laloy et al. [2010] presented an approach to consider the residuals to be heteroscedastic via Box-Cox [Box and Cox, 1964] transformation. This improved the estimation of parameter uncertainty and model prediction. Schoups and Vrugt [2011] developed a formal likelihood function, which allows for an improved description of the distribution of the residuals in simulations. This approach (including auto-correlated errors) leads to a more accurate statistical description of the errors and tighter predictive uncertainty bands.

Traditionally, all uncertainties associated with model simulation and prediction are interpreted as originating from the parameter uncertainties [Vrugt et al., 2005], i. e. not differentiating in different sources of uncertainties. This ignores the fact, that there are three different main sources of error in a modeling procedure, as demonstrated for this study in Fig. 4.1:

- Input error: errors in the input to the model, which affect the ability of the model to fit the data correctly

- Model structural error: inadequacies in the representation of the model to describe the underlying processes

- Parameter error: the uncertainties of the model due to the uncertainties of the parameter values.

Input errors constitute the measurement errors from input and output [Vrugt et al., 2005]. Measurement errors traditionally are assumed to be normal distributed in the measurements and stemming from the measurement process. Uncertainties in the input, i. e. the control variables, originate from measurements of the initial and boundary conditions. The model structural errors constitute of lacks of including all processes in the model description, as well as from averaging spatial and temporal inhomogeneities.
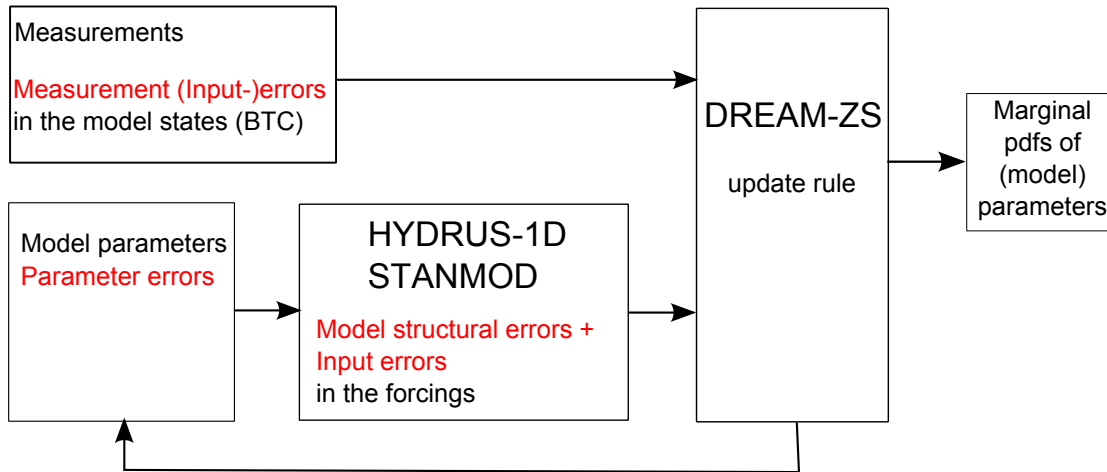
Figure 4.1: Sources of errors and uncertainties in the modeling process, exemplary demonstrated for this study. Measurement errors in forcing and states constitute the input error.

Numerical simulation can be conducted applying a Bayesian framework such as the Markov chain Monte Carlo (MCMC) simulator used in this study: the DiffeRential Evolution Adaptive Metropolis (DREAM) algorithm Vrugt et al. [2008, 2009], here in its variant DREAM_(ZS) Vrugt et al. [2010]. Applying this method, the several sources of uncertainties are respected and represented in the inferred parameter uncertainties in a lumped manner. Consequently, the optimization does not aim at a single best set of parameters, but by adopting a Bayesian viewpoint, strives to identify a distribution of model parameters [Vrugt et al., 2008].

In this study, breakthrough curves of laboratory column experiments were described with a conceptual mathematical model including reversible and irreversible sorption using the HYDRUS-1D model [Simunek et al., 2008, Version 4.14], in combination with DREAM_(ZS). A detailed analysis of the results obtained with the DREAM_(ZS) algorithm was conducted. Therefore, we included the recently presented formulation of the handling of the distribution of residuals in the modeling results by Schoups and Vrugt [2011]. The objectives were (i) to mathematically describe the breakthrough of ^{14}C SDZ equivalent concentrations for the threefold applied veterinary antibiotic sulfadiazine with the HYDRUS-1D model in combination with an MCMC simulator for the experiments with the application via manure and solution, (ii) to compare the results of the parameter estimation with the DREAM algorithm based on two different underlying descriptions of the residuals in the corresponding likelihood functions, i. e. the Standard Least Squares approach (SLS) and the Generalized Likelihood approach (GL) of Schoups and Vrugt [2011], (iii) to show the behavior of SDZ in a realistic standard scenario with soil parameters and meteorological data from a soil profile in Hamburg (Germany), given the estimated parameters resulting from both simulations of the laboratory column experiments.

4.2 Materials and Methods

Sulfadiazine (IUPAC: 4-amino-N-(2-pyrimidinyl)benzene sulfon-amide; SDZ) was used as model compound which was radioactively labeled at the C-2-atom of the pyrimidine ring (purity: 99%, spe-cific radioactivity: 8.88 MBq mg^{-1}; BayerHealthCare AG, Wup-pertal, Germany).

Laboratory transport experiments were conducted using the plow layer (Ap horizon) of a gleyic Cambisol from Kaldenkirchen (KAL), North Rhine-Westphalia (Germany). It was a loamy sand consti-tuting of 69.7 mass-% sand, 26.3 mass-% silt, and 4.0 mass-% clay. The pH measured in 0.01 M CaCl$_2$ was 5.7, the total organic car-bon content was 0.88 mass-%. Undisturbed soil cores (diameter 8 cm, length 10 cm) of the soil under agricultural use were taken approx. 5 cm under the surface. The columns were stored in the dark at 4°C before usage.

4.2.1 Unsaturated column experiments

The laboratory experiments were conducted under unsaturated unit-gradient conditions (matric potential approx. -40 cm) using a computer-controlled system, as described in Unold et al. [2009a] and Appendix A. Manure (approx. 15 g) from feeding experiments, containing a mixture of ^{14}C-SDZ and ^{12}C-SDZ with a ratio of 1:39 and solution with the same SDZ concentration, respectively, were incorporated in the first cm of the column. This was done three times, the total duration of the experiment was approximately four weeks. The experiments were performed at room temperature in the dark to avoid photodegradation. A 0.01 M CaCl$_2$ solution was used as background solution for irrigation.

All samples after breaking through the column were analyzed for

their total radioactivity with Liquid Scintillation Counting (LSC; 2500 TR, Packard Bioscience GmbH, Dreieich, Germany) with a counting time of 15 min and in duplicates. Therefore, an aliquot of the sample was mixed with an appropriate scintillation cocktail (Instant Scint-Gel Plus; Canberra Packard GmbH, Dreieich, Germany). The detection limit was $0.4\,\mathrm{Bq}$, the limit of quantification was $1.2\,\mathrm{Bq}$ ($5.46 \cdot 10^{-4}\,\mu\mathrm{mol\,l^{-1}}$ ^{14}C SDZ).

Hydrophysical transport parameters were estimated applying a pulse input of $0.05\,\mathrm{M}\,\mathrm{CaCl_2}$ for the duration of approximately one hour, before and after all three applications, with measuring the specific electrical conductivity in the outflow online. Furthermore, we used the breakthroughs of the specific electrical conductivities during the applications in the experiment with solution. These tracer breakthroughs were simulated with CXTFIT as included in STANMOD [Simunek et al., 1999, Version 2.08.1130].

4.2.2 Transport model

The HYDRUS-1D model was used to numerically simulate the laboratory breakthrough experiments. This model solves the one-dimensional convection-dispersion equation:

$$\frac{\partial C}{\partial t} + \frac{\rho}{\theta}\frac{\partial S}{\partial t} = -V\frac{\partial C}{\partial z} + D\frac{\partial^2 C}{\partial z^2} - \mu_{\mathrm{irr}}C \qquad , \qquad (4.1)$$

where $C\,[\mathrm{M\,L^{-3}}]$ is the total SDZ-equivalent concentration in the liquid phase, $t\,[\mathrm{T}]$ is time, $\rho\,[\mathrm{M\,L^{-3}}]$ is the soil bulk density, $\theta\,[\mathrm{M\,L^{-3}}]$ is the volumetric water content, $S\,[\mathrm{M\,M^{-1}}]$ is the sorbed solute concentration at the kinetic sorption site, $V\,[\mathrm{L\,T^{-1}}]$ is the pore water velocity, $z\,[\mathrm{L}]$ is the depth, $D\,[\mathrm{L^2\,T^{-1}}]$ is the dispersion coefficient, and $\mu_{\mathrm{irr}}\,[\mathrm{T^{-1}}]$ is the rate-coefficient for irreversible sorption.

The concentration on the kinetic reversible sorption site is de-

scribed by:

$$\frac{\partial S}{\partial t} = \alpha(k_{\mathrm{f}}C^n - S) \qquad (4.2)$$

where $\alpha \, [\mathrm{T}^{-1}]$ denotes the rate coefficient for kinetic sorption, $k_{\mathrm{f}} \, [\mathrm{M}_{\mathrm{solute}}^{1-n} \, \mathrm{L}^{3\mathrm{n}} \, \mathrm{M}_{\mathrm{soil}}^{-1}]$ is the Freundlich coefficient, and $n \, [\text{-}]$ is the Freundlich exponent.

4.2.3 Parameter estimation

Time evolution of a state vector ψ (i.e. the concentrations in the BTC) can be described with a model Ω with the vector of parameters η and the observed forcings (here: irrigation rate, dispersivity etc.) $\widetilde{\nu}$: where both the observation of the states (i.e. measuring the concentrations in the BTC) and forcings is corrupted with an error (input error). A measured concentration c_t is related to the actual state of the system with the measurement operator $\Gamma()$: The difference ϵ_t between the measured, $\mathbf{c}_m = \{c_t; t \in \{1, ..., m\}\}$ and simulated, $\widetilde{\mathbf{c}}_m = \{\widetilde{c}_t; t \in \{1, ..., m\}\}$ BTC values is given by:

$$\epsilon_t(\eta) = c_t - \widetilde{c}_t(\eta) \qquad t = 1, ..., m \qquad . \qquad (4.3)$$

The goal of the classical optimization appraoch is to find a set of model parameters to render the value for ϵ as close to zero as possible and to represent the system under study as consistent as possible [Vrugt et al., 2008]. The residual ϵ usually consists of a combination of input, model structural, output, and parameter errors Schoups and Vrugt [2011].
In this Standard Least
Squares (SLS) approach, the corresponding objective function Φ

is then expressed by:

$$\Phi = \sum_{t=1}^{m} \epsilon_t(\eta)^2 \qquad . \qquad (4.4)$$

This approach ignores input data uncertainty and implies a correct representation of the simulated system with the error residuals to be independent (uncorrelated) and normally distributed with a constant variance and a mean of zero [Vrugt et al., 2008].

Applying a probablistic framework using Bayes theorem, an estimation of the posterior probability density function (pdf) of the parameters is given by maximizing $p(\eta|\mathbf{c}_m)$ [Vrugt et al., 2011]:

$$p(\eta|\mathbf{c}_t) = p(\mathbf{c}_t|\eta)p(\eta) \qquad , \qquad (4.5)$$

where $p(\mathbf{c}_t|\eta) \equiv L(\eta|\mathbf{c}_t)$ denotes the likelihood function, and $p(\eta)$ contains prior information about the parameters before any measurement was conducted. In this work, we assume a uniform distribution of the parameters over their given intervals (no prior knowledge), i. e. a flat or non-informative prior.

The likelihood function $L(\eta|\mathbf{c}_t)$, assuming the Standard Least Squares (SLS) approach, is given by:

$$L(\eta|\mathbf{c}_t) = -\frac{m}{2}\ln(2\pi) - \frac{m}{2}\ln(\sigma^2) - \frac{1}{2}(\sigma^{-2})\sum_{t=1}^{m} \epsilon_t(\eta)^2 \qquad , \quad (4.6)$$

where σ denotes the standard deviation of the measurement error. This assumption may be refined by assuming time-variant value for σ to account for heteroscedasticity.

Alternatively, we applied the recently presented generalized likelihood approach [Schoups and Vrugt, 2011], which eases the SLS assumption. There, the standard deviation σ_t at time t is given by:

$$\sigma_t = \sigma_0 + \sigma_1 \mathbf{c}_t \qquad t = 1, ..., m \qquad . \qquad (4.7)$$

With $\sigma_0 > 0\,[\mathrm{M\,L^{-3}}]$, a constant standard deviation can be assumed (homoscedasticity), while σ_1 [-] allows for a variance which

depends on the measurement itself (heteroscedasticity).

The dimensionless parameters ξ ($\xi > 0$) and β ($-1 > \beta < 1$) describe the skewness and the kurtosis of the skew exponential power (SEP) distribution of the model residuals with zero-mean and unit standard deviation, respectively.

With the SEP$(0,1,\xi,\beta)$, non-normality in the distribution of the model residuals can be assumed:

$$p(\alpha_t|\xi,\beta) = \frac{2\sigma_\xi \omega_\beta}{\xi + \xi^{-1}} \exp\left\{c_\beta |a_{\xi,t}|^{2/(1+\beta)}\right\} \qquad , \qquad (4.8)$$

where $a_{\xi,t} = \xi^{-sign(\nu_\xi + \sigma_\xi a_t)}(\nu_\xi + \sigma_\xi a_t)$, and values for ν_ξ, σ_ξ, c_β, ω_β are evaluated from ξ and β as described in Schoups and Vrugt [2011]. Parameter a_t is part of the model for the residual errors:

$$\Psi_p(B)e_t = \sigma_t\, a_t \quad \text{with}\, a_t \sim \text{SEP}(0,1,\xi,\beta) \qquad , \qquad (4.9)$$

where $\Psi_p(B) = 1 - \sum_{i=1}^{p} \phi_i\, B^i$ represents an autoregressive polynomial with p autoregressive parameters ϕ_i, B is the backshift operator ($B^i\, e_t = e_{t-i}$). a_t is independent and identical distributed with a zero mean and unit standard deviation.

In the Generalized Likelihood form, $L(\eta|\mathbf{c}_t)$ is given as:

$$L(\eta|\mathbf{c}_t) = m \log\frac{2\sigma_\xi \omega_\beta}{\xi + \xi^{-1}} - \sum_{t=1}^{m} \log \sigma_t - c_\beta \sum_{t=1}^{m} |a_{\xi,t}|^{2/(1+\beta)} \qquad .$$
$$(4.10)$$

With this formulation, flexibility for the assumption of the residues is gained. It includes the SLS as a special case - with $\beta = 0$, $\xi = 1$, $\sigma_1 = 0$, and $\phi_1 = 0$. A detailed derivation of the likelihood function is given in the appendix in Schoups and Vrugt [2011].

Estimation of the posterior probability density function of the parameters was done with the DREAM_(ZS) algorithm (**Diffe**R**ential **E**volution **A**daptive **M**etropolis algorithm) [Vrugt et al., 2009]. DREAM_(ZS) is a MCMC sampler that can be used to efficiently estimate the posterior probability density function of optimized model parameters in high-dimensional sampling problems [Vrugt

et al., 2008]. It runs several Markov chains in parallel - after a so-called burn-in period (in which the parameter values become independent of their initial values), the chains are merged. Convergence was controlled by the $\hat{R}$-criterion by Gelman and Rubin [1992] ($\hat{R} < 1.2$). The traditional best solution is part of this distribution, and can be found by locating that point of the sample with maximum posterior density.

The DREAM_(ZS) algorithm generated samples from the posterior distribution of the calibration parameters and was combined with the HYDRUS-1D model, as described in Scharnagl et al. [2011]. The calibration parameters for the transport model and the ones for the statistical description of the residues (to be put in the MCMC simulator) with their uniform distributed prior ranges as well as the control variables (for the HYDRUS 1-D model) are listed in 4.1. Values for the control variables are denoted as resulting from the manure experiment. With each realization of the model parameters given by DREAM_(ZS), a forward run with the HYDRUS-1D model over all three applications was conducted, totally 100000 times. After each single breakthrough, the (simulated) profile constituted the initial condition for the subsequent SDZ application, regarding the concentrations in the liquid phase as well as the reversible sorbed solute. In the first cm, the newly applied mass of SDZ was given as concentration in the liquid phase.

4.2.4 Application to a field scenario

For comparability with already existing studies for pesticides in the EU registration process, we applied our estimated set of parameters to a field scenario of an agricultural site (sandy loam) in Hamburg (Germany), according to FOCUS [2000]. To reach this aim, we took the corresponding soil parameters and meteorologi-

Table 4.1: Input parameter ranges and control variables for the manure experiment.

	Symbol	Unit	Minimum	Maximum
Calibration parameters				
Freundlich coefficient	k_{f}	$[\text{mol}^{1-n}\,\text{l}^{n}\,\text{kg}^{-1}]$	0	0.1
Freundlich exponent	n	-	0.1	1
Rate coefficient reversible sorption	α	$[\text{h}^{-1}]$	0.01	0.6
Rate coefficient irreversible sorption	μ_{irr}	$[\text{h}^{-1}]$	0	0.1
Heteroscedasticity intercept	σ_0	$[\text{mol}\,\text{l}^{-1}]$	0	1
Heteroscedasticity slope	σ_1	-	0	1
Kurtosis parameter	β	-	-1	1
Skewness parameter	ξ	-	0.1	10
Control variables				
Volumetric water content	θ	[-]	0.32	-
Dispersivity	λ	[cm]	0.47	-
Concentration 1st cm (variable)	-	$[\text{mmol}\,\text{cm}^{-3}_{\text{liquid phase}}]$	≈ 0.0005	-
Irrigation rate	q	$[\text{cm}\,\text{h}^{-1}]$	0.17	-
Bulk density	ρ	$[\text{g}\,\text{cm}^{-3}]$	1.44	-
Duration	-	[h]	var.	-
Numerical time-steps	-	[h]	0.1	-

cal data to simulate the water flow and transport process under a transient upper boundary condition. The Freundlich coefficients k_{f} were normalized to the organic carbon content ($k_{\text{OC}} = k_{\text{f}}/\text{C}_{\text{org}}[\%]$). The physically heterogeneous profile had a depth of 1 m; the hydraulic properties are listed in Weihermüller et al. [2011]. The atmospheric boundary conditions are displayed in Fig.4.2. The amount of manure applied was according to the laboratory experiment: $30\,\text{t}\,\text{ha}^{-1}$, with a SDZ concentration in the applied manure of $160\,\text{mg}\,\text{kg}^{-1}$. In the simulation, applications were conducted once every 1st of September during a 20-year period, using the atmospheric data from 1977–1997. For equilibration, the first 973 days were simulated without any application, giving an initial water content in the profile of 25%. The simulations were conducted using the Hydrus-1D model with a simulation of the water flow using Richards Equation and the solute transport (Eq. 4.1). The simulated applications were conducted with incorporation in the first 10 cm of the soil profile. Hydrus-1D was coupled with Matlab, the simulation was run 21 times with giving the results of one run as initial condition for the following, in terms of the water

content (with which the initial concentration in the application layer was evaluated) and the profile with reversibly sorbed solute.
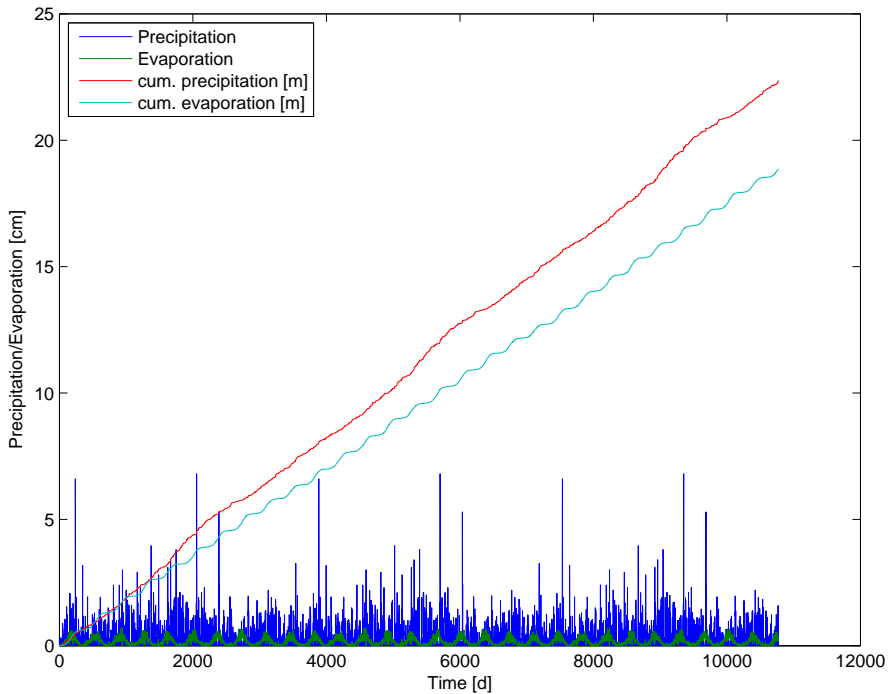

Figure 4.2: Atmospheric conditions for the FOCUS scenario Hamburg [FOCUS, 2000].

4.3 Results and discussion

4.3.1 Simulation of the solute breakthroughs with two different formulations of the likelihood function

The best fits of the hydrophysical parameters are listed in Table 4.2. The experimental mass recoveries for the experiment with manure and solution are displayed Table 4.3. In the experiment with solution, considerably more mass than in the manure experiment was eluted and therefore measured in the BTC. Consequently, the mass sorbed in the profile and removed twice with the corresponding application layer was higher in the manure experiment.

Figure 4.3 shows the BTC in the experiments with manure and solution, respectively. The shapes of the BTC were different - with higher peak concentrations for the experiment with solution and more pronounced tailing in the manure experiment. Apparently, the measurement errors were very small, as was confirmed by a non-parametric time-difference approach [Vrugt et al., 2005]: 3E-08 and 5E-08 mol l^{-1} for the experiment with manure and solution, respectively. The corresponding error distribution showed homoscedasticity - for the simulations with the SLS approach, this value was given for σ_0.

Table 4.2: Hydrophysical parameters gained with the breakthroughs of the specific electrical conductivities, $0.05\,\text{M CaCl}_2$ pulses and during the applications, simulated using STANMOD. The values for q are the applied irrigation rates.

	v^*	$D^\dagger$	$\boldsymbol{\lambda}^\ddagger$	$\boldsymbol{\theta}^\S$	$q^\P$
	$[\text{cm h}^{-1}]$	$[\text{cm}^2\,\text{h}^{-1}]$	$[\text{cm}]$	$[\text{-}]$	$[\text{cm h}^{-1}]$
Manure					
before applications	0.50	0.14	0.28	0.33	0.17
A1	–	–	–	–	–
A2	–	–	–	–	–
A3	–	–	–	–	–
after applications	0.51	0.24	0.47	0.32	0.16
Solution					
before applications	0.58	0.24	0.41	0.34	0.20
A1	0.57	0.39	0.68	0.35	0.20
A2	0.63	0.32	0.51	0.32	0.20
A3	0.58	0.37	0.64	0.32	0.19
after applications	0.52	0.13	0.26	0.38	0.19

* Pore water velocity. † Dispersion coefficient. ‡ Dispersivity. § Volumetric water content. ¶ Irrigation rate.

Table 4.3: Experimental mass recoveries, given as percental amounts in the several fractions.

	Manure	**Solution**
BTC	49.3 %	74.2 %
Profile	39.4 %	23.3 %
1st cm A2*	7.7 %	2.78 %
1st cm A3†	7.7 %	2.84 %
Total	104.1 %	103.1 %

* Amount removed in the first cm before the second application † Amount removed in the first cm before the third application
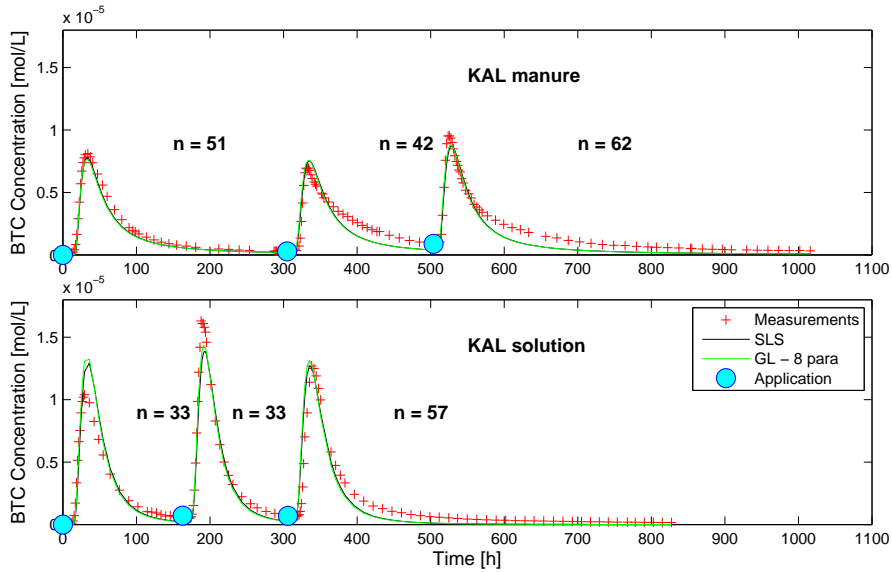
Figure 4.3: Breakthrough curves after application with manure and solution. Simulations (lines) were conducted with the DREAM algorithm, estimating one set of parameters for all three applications, applying the Standard Least Squares (SLS) and the Generalized Likelihood (GL) approach, respectively. For the latter, three or four statistical parameters of the distribution of the residuals were estimated additionally to the four transport parameters.

The errors between measurements and simulations were essentially determined by errors in the model structure. This was clearly visible in the manure experiment, in which probably other processes occurred than those regarded in our model, such as a constant release from this fraction that is assumed to be irreversibly bound in our model and described by a first-order decay. Another possible source of errors are the additional model inputs, e. g. the irrigation rate, the dispersivity (determined with the tracer experiment), or the estimation of the volumetric water content.

The estimated parameters for transport and statistical distribution of the residuals are displayed in Table 4.3.1. With the classical SLS approach, the uncertainty became zero, as this approach implies a perfect model with no model structural errors or input errors. There was only one best set of parameters found (without uncertainty), as any change in the parameter values results in a model simulation that is unlikely given the very small measurement error. The use of the Generalized Likelihood approach allows for a representation of the effects of input and structural errors.

The choice of the likelihood function used as well as the number of estimated parameters (with the GL approach) had a strong influence on the values for the estimated parameters of our model description.

Table 4.4: Results of the simulations with the DREAM algorithm in combination with the HYDRUS 1-D model, applying the standard least squares (SLS) and a generalized likelihood approach (GL) as formulation for the likelihood function.

		k_f*	n†	μ_{irr}‡	α§	σ_0¶	σ_1‖	β**	ξ††	RMSE	L‡‡	95%-CI residuals	
	Units	$[\mathrm{mol}^{1-n}\,\mathrm{l}^n\,\mathrm{kg}^{-1}]$	[-]	$[\mathrm{h}^{-1}]$	$[\mathrm{h}^{-1}]$	$[\mathrm{mol}\,\mathrm{l}^{-1}]$	–	–	–	$[\mathrm{mol}\,\mathrm{l}^{-1}]$		$[\mathrm{mol}\,\mathrm{l}^{-1}]$	
	Range	0–0.1	0.1–1	0–0.1	0.01–3	0–1	0–1	−1–1	0.1–10				
						KAL manure							
SLS	Best	4.4E-04	0.36	0.044	0.27	–	–	–	–	6.1E-07	−33645	-1.3E-06	1.1E-06
(σ from	2.5%	4.4E-04	0.36	0.044	0.27	–	–	–	–				
error analysis)	97.5%	4.4E-04	0.36	0.044	0.27	–	–	–	–				
GL	Best	5.4E-04	0.37	0.042	0.24	7.2E-07	0.022	0.99	–	6.3E-07	1982	-1.3E-06	1.1E-06
7 para	2.5%	3.9E-04	0.34	0.040	0.21	1.4E-08	2.1E-03	0.65	–				
	97.5%	8.4E-04	0.41	0.047	0.29	9.5E-07	0.18	1.00	–				
GL	Best	3.0E-04	0.32	0.044	0.28	4.2E-07	0.045	0.47	0.19	6.4E-07	2001	-1.3E-06	1.1E-06
8 para	2.5%	3.2E-04	0.33	0.042	0.23	1.4E-07	3.6E-03	0.47	0.23				
	97.5%	5.9E-04	0.38	0.049	0.28	9.8E-07	0.14	1.00	0.83				
						KAL solution							
SLS	Best	0.012	0.66	0.040	1.12	–	–	–	–	1.3E-06	−39328	-3.6E-06	2.7E-06
(σ from	2.5%	0.012	0.66	0.040	1.12	–	–	–	–				
error analysis)	97.5%	0.012	0.66	0.040	1.12	–	–	–	–				
GL	Best	1.2E-03	0.45	0.021	1.79	9.1E-08	0.27	0.99	–	1.4E-06	1556	-5.2E-06	2.9E-06
7 para	2.5%	9.4E-04	0.42	0.018	1.61	4.1E-08	0.09	0.85	–				
	97.5%	2.0E-03	0.49	0.026	2.08	9.1E-07	0.29	1.00	–				
GL	Best	0.011	0.65	0.037	1.22	8.6E-07	0.15	0.98	0.70	1.4E-06	1556	-4.4E-06	1.8E-06
8 para	2.5%	6.1E-03	0.60	0.036	0.72	5.6E-08	0.090	0.70	0.26				
	97.5%	0.018	0.70	0.050	1.82	1.0E-06	0.47	1.00	0.83				

* Freundlich coefficient (sorption affinity). † Freundlich exponent. ‡ the first-order decay rate coefficient. § rate coefficient for reversible sorption. ¶ intercept for the standard deviation of the errors between measurement and model. ‖ slope for the standard deviation of the errors between measurement and model. ** kurtosis parameter. †† skewness parameter. ‡‡ likelihood.

Application with manure lead to a lower value for k_f, with higher non-linearity, as indicated with a lower value for n. The value for the first-order rate coefficient for decay, μ_irr, was very similar for five out of the total six approaches (approx. $0.04\,\mathrm{h}^{-1}$), with the exception of the Generalized Likelihood simulation with estimation of seven parameters for the experiment with solution. A higher value for the rate coefficient of reversible sorption, α, was generally estimated for the experiment with solution.

The estimation of the parameters for the statistical distribution of the residuals in the GL approach lead to very small values for the intercept of the residuals, σ_0 (homoscedastic part), and very different values for the slope (representing heteroscedasticity), σ_1. The kurtosis parameter β tended to unity, with the exception for the eight-parameter estimation with the manure experiment. A skew distribution of the residuals was indicated with values different from unity for the skewness parameter ξ. The RMSE was considerably smaller for the manure experiment, probably caused by a better representation of the peaks.

Applying the SLS approach and assuming homoscedasticity produced no marginal posterior distribution functions. The very small measurement error indicated by the very smooth measured BTC lead to a parameter uncertainty with the classical SLS approach which is virtually zero. Hence, the optimal value has no uncertainty. The SLS approach gives no information about a systematic error, as the non-parametric error estimator only confirms a random error. Most model calibration theories are based on a perfect model, this strategy does not seem applicable here. The assumption of a perfect model was extended by Schoups and Vrugt [2011] to a Generalized Likelihood function to include non-ideal models. The is indicated by the differences in the parameter estimates. The GL allows for other sources of error than only the parameter errors, which then increases the parameter uncertainty.
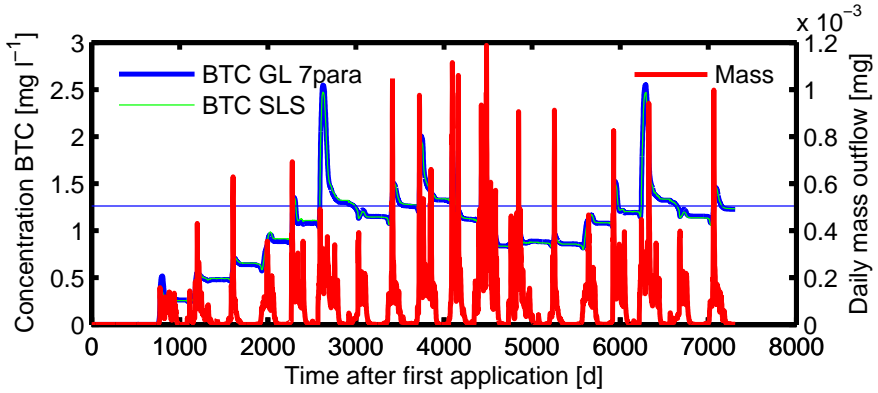
Figure 4.4: Breakthrough of SDZ-equivalents at the end of the 1-m profile from the FOCUS scenario Hamburg, starting after the first application: concentration (straight line: medium concentration after establishment of a plateau $1.3\,\mu g\,l^{-1}$) and mass outflow.

4.3.2 Field scenario

Figure 4.2 shows the breakthrough curves and daily eluted masses for the 20-year experiment, applying the parameters from the estimation using the SLS and the GL approach, respectively. Table 4.5 displays the results, demonstrated on some assorted indicators. In most cases, the mass outflow coincides with the high concentrations. The average concentration after establishment of the plateau of $0.91\,\mu g\,l^{-1}$ exceeds the critical value for drinking water ($0.1\,\mu g\,l^{-1}$).

The resulting differences after application of the parameters from the two simulation approaches were very small. There were only slight differences in the peak concentrations and their corresponding arrival times.

Table 4.5: Results of the simulations of the real world scenario, based on the parameters inferred with the two different approaches of parameter estimation, demonstrated on some assorted indicators.

	Unit	SLS	GL 7para
LMF	[-]	0.5610	0.5663
Arrival time approx.	[d]	756	751
Peak conc.	$[\mathrm{mg\,l^{-1}}]$	2.47	2.55
Time peak conc.	[d]	2627	6292
Medium conc. (after plateau)	$[\mathrm{mg\,l^{-1}}]$	1.26	1.27
80%-percentile mean yearly conc.	$[\mathrm{mg\,l^{-1}}]$	1.49	1.50

4.4 Conclusions

We have shown the numerical simulations of results from laboratory column experiments with radio-labeled antibiotic sulfadiazine. Our model description with a convective-dispersive approach was able to represent the results of the column experiments with threefold applications quite well, using one set of parameters. We conducted a parameter optimization using a MCMC simulator, applying two different approaches for the objective function: a Standard Least Squares approach and a Generalized Likelihood formulation. The differences between the predicted breakthrough curves using the different methods were much smaller than the deviation between the predictions and the measurements. A non-parametric error estimator showed the overall dominance of the model structural error. Hence, we were hardly able to demonstrate the influence of the choice of the likelihood function. This was further demonstrated with the application of the estimated parameters on a real-world scenario used for the prediction of groundwater concentrations, which lead to only minor differences after using of the two different sets of parameters.

Chapter 5

Column transport experiments with multiple applications of SDZ in manure and in liquid solution

5.1 Introduction

Via the application of manure for fertilizing purposes on agricultural fields, veterinary antibiotics are unintentionally introduced into the environment. Their presence in the different environmental compartments can have several consequences, e. g. the development and spreading of resistance genes, affection of the microbial functionalities and finally transfer into the human food-chain [Kümmerer, 2009]. Besides sorption and transformation, the fate of an organic compound in soil is determined by the transport behavior through the soil profile with the possibility of ultimately reaching the groundwater [Boxall, 2008].

The substance under study here is sulfadiazine (IUPAC: 4-amino-N-(2-pyrimidinyl) benzene sulfonamide; SDZ), an antibiotic from the group of the sulfonamides. In laboratory experiments, Wehrhan et al. [2007] showed the high mobility of SDZ. The transport through soil columns packed with a silty loam in terms of peak concentrations and eluted mass fractions was influenced by concentration and pulse duration. Sorption to the soil matrix governing the transport processes was found to be a non-linear and kinetic process. Unold et al. [2009a] applied SDZ in two different matrices: together with manure from pig-feeding experiments and in liquid solution, respectively. In the experiments with manure, they reported smaller eluted mass fractions and lower peak concentrations in the breakthrough curves accompanied by an accumulation in the first layer of the laboratory column. Aust et al. [2010] showed in field-lysimeter studies the leaching of SDZ after application with manure. This demonstrated the possibility of this route of entry with concentrations above the trigger values. Kreuzig and Höltge [2005] investigated the simultaneous occurrence of leaching and degradation when SDZ is applied together with manure. They point out the need for experiments in combination with manure. In laboratory lysimeter experiments they observed a retention in the first layer (and the formation of non-extractable residues). Kwon [2011] demonstrated the leaching of three sulfonamides applied together with manure compost in laboratory column experiments and postulate a promoted leaching as consequence of the elevated pH caused by manure application.

SDZ undergoes several transformation processes both in soil and solution. This was shown in several studies with batch and column experiments [Sittig et al., 2014, Kasteel et al., 2010, Unold et al., 2009a, Sukul et al., 2008a]. After passage through the animal, SDZ is partly transformed, mostly into 4-OH-SDZ and acetyl-SDZ [Lamshöft et al., 2007].

We performed laboratory soil column experiments with radiolabeled SDZ for the duration of approximately one month using

undisturbed soil cores from the plow layers of a silty loam and a loamy sand. We measured the ^{14}C-SDZ equivalent concentrations as well as the transformation products. SDZ was applied threefold during the experimental period via incorporation into the first centimeter, with manure stemming from pig-feeding experiments and in liquid solution in two different concentrations, respectively. This procedure simulates the way of entry for veterinary pharmaceuticals applied as fertilizers on agricultural fields. The objectives were to investigate (I) the effects of this realistic scenario of multiple applications and the benefits in comparison to experiments with single applications, (II) the influence of manure on the transport process, (III) the transformation of the parent compound during movement through the soil, and (IV) the fate of the manure-borne metabolites during the experiments. Numerical studies applying the HYDRUS-1D model [Simunek et al., 2008, Version 4.14] in combination with the DREAM_ZS algorithm by Vrugt et al. (J. Vrugt et al., Posterior exploration using differential evolution adaptive Metropolis with sampling from past states, manuscript in preparation, 2012) allowed us to describe the breakthrough curves of all six experiments, each with one set of parameters for all three applications. Our hypotheses were (I) the application together with manure significantly influences the transport behavior, (II) sorption to the soil column is concentration dependent, (III) the effective transport and transformation processes are considerably distinct in the two soils. Our study points at the fate of SDZ after multiple application to soil, in terms of mass breakthrough and transformation products.

5.2 Materials and methods

5.2.1 Laboratory experiments

Sulfadiazine (IUPAC: 4-amino-N-(2-pyrimidinyl)benzene sulfonamide; SDZ) was used as model compound which was radioactively labeled at the C-2-atom of the pyrimidine ring (purity: 99%, specific radioactivity: $8.88\ \mathrm{MBq\,mg^{-1}}$; BayerHealthCare AG, Wuppertal, Germany).

Laboratory transport experiments were conducted using the plow layers (Ap horizons) of a Gleyic Cambisol from Kaldenkirchen (KAL; loamy sand) and an Orthic Luvisol from Merzenhausen (MER; silty loam), both sites are situated in North Rhine-Westphalia (Germany). Selected soil properties are listed in Table 2.1. Undisturbed soil cores (diameter 8 cm, length 10 cm) of the soils under agricultural use were taken approximately 5 cm under the surface. The columns were stored in the dark at 4°C before usage. The soil column experiments were conducted using a $0.01\,\mathrm{M}$ $CaCl_2$ background solution under unsaturated conditions with a pressure-controlled setup as described in Unold et al. [2009a] to establish unit-gradient conditions and therefore identical water content throughout the column. Before the experiments, the column were slowly saturated from bottom to top for the duration of about 3 days. By this means, the development of preferential flow paths and the entrapment of air could be avoided. Irrigation was conducted from top to bottom with a rate of $0.2\,\mathrm{cm\,h^{-1}}$, using an irrigation device equipped with 18 needles. To investigate the hydrodynamic properties, a pulse of a $0.05\,\mathrm{M}$ $CaCl_2$ solution was applied for the duration of approximately one hour and the specific electrical conductivity in the outflow was measured directly, as described in Unold et al. [2009a].

SDZ was applied by incorporation in the soil of the first centimeter

for each of the six experiments, either $10\,\mu$mol together with manure, or in liquid solution in two concentrations (10 and $1\,\mu$mol), all with a mass of $15\,$g. The liquid solutions were adjusted with NaOH to the pH of the manure: 8.3. By means of measuring the specific electrical conductivity in the outflow of the column, we had an additional "tracer" breakthrough, assuming the ions in the manure and the solution respectively behave like a conservative tracer. The applied solutions were free of transformation products. The total radioactivity was measured with liquid scintillation counting, the composition of the liquid samples with Radio-HPLC, both procedures are described in Sittig et al. [2014]. The manure stemmed from feeding experiments conducted at Bayer AG Monheim where the radio-labelled SDZ was applied to pigs and the manure (total SDZ concentration: $0.63\,$mmol$\,$kg^{-1}) was collected [Lamshöft et al., 2007]. With the same protocol as used in this study (McIlvaine buffer), Lamshöft et al. [2007] found Ac-SDZ and 4-OH-SDZ in fractions of 21 and 26%, respectively. All transformation products found in our studies are described in Sittig et al. [2014]. Due to a storage time of approximately five years, the original composition of the manure changed: we found no Ac-SDZ and 18% of 4-OH-SDZ.

5.2.2 Numerical evaluations

Simulations of the conservative tracer experiments were conducted with CXTFIT as included in STANMOD [Simunek et al., 1999, Version 2.08.1130], on the basis of the equilibrium CDE. Breakthroughs of the ^{14}C SDZ equivalent concentrations were simulated as described in Chapter 4.2.2 conducting parameter estimation with coupling DREAM_(ZS) and HYDRUS-1D.

5.3   Results and discussion

5.3.1   Breakthrough curves of the Cl⁻ tracer

Figure 5.1 shows the BTC of the $CaCl_2$ tracer pulses in all six experiments, both before and after the series of three SDZ applications, the time is expressed in terms of dimensionless pore volumes (exchange of one water filled pore space). The shapes were similar before and after the applications. Even though there were differences in the 'after' experiments: all five peaks (for the manure experiment with the MER soil, only the 'before' experiment was measured) were lower, and in both the experiments with solution with the MER soil and in the manure experiment with the KAL soil the arrival time for the peak was shorter. The curves generally had regular shapes and could be well described using the equilibrium CDE (displayed as lines in Fig. 5.1). Hence, no preferential flow paths were indicated. Table 5.1 lists the dispersivities for all experiments, according to the simulations with CXTFIT as included in STANMOD [Simunek et al., 1999, Version 2.08.1130]. The dispersivities describing the breakthrough of the SDZ applications were estimated on the basis of the breakthroughs of the specific electrical conductivity, measured online during the experiment.

The dispersivities were higher in the experiments with MER soil, indicating a higher heterogeneity. This became visible in the shapes of the BTC, with more stretched courses and lower peak concentrations in the MER experiments. Compared to the MER soil, the peak concentrations arrived later (up to 0.6 pore volumes) and were considerably higher in the KAL soil (up to twofold). In 4 out 5 cases, the estimated dispersivities were higher after the three applications than before.
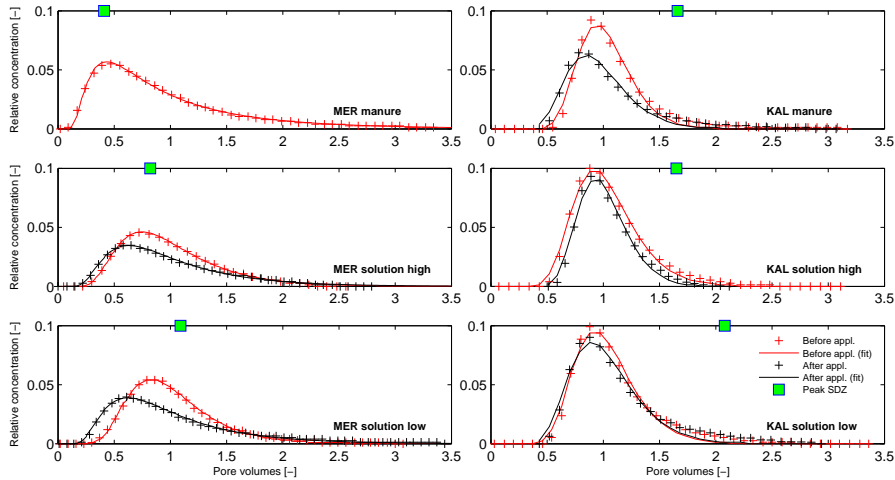
Figure 5.1: Measured (markers) and simulated (lines) breakthrough curves of the chloride tracer pulses before and after the three SDZ applications in all six experiments with the soil from Merzenhausen (MER) and Kaldenkirchen (KAL), respectively. The arrival time of ^{14}C-SDZ equivalent concentrations in terms of exchanged pore volumes shows the delay in comparison to the conservative tracer chloride.

Table 5.1: Dispersivities [cm] for all six column experiments, based on the equilibrium CDE.

		KAL	MER
manure	**before**	0.28	3.46
	A1	–	1.74
	A2	–	0.92
	A3	–	1.51
	after	0.47	–
sol. high	**before**	0.41	1.09
	A1	0.68	1.37
	A2	0.51	1.13
	A3	0.64	1.39
	after	0.26	1.72
sol. low	**before**	0.38	0.73
	A1	0.50	0.66
	A2	0.41	0.74
	A3	0.38	1.18
	after	0.47	1.77

5.3.2 Breakthrough curves of the ^{14}C-SDZ equivalent concentrations

Figure 5.2 shows the course of the ^{14}C-SDZ equivalent concentrations at the column outflow in the experiments with the Merzenhausen and Kaldenkirchen soil, respectively. For further process elucidation, the concentrations were log-transformed. The breakthrough curves had regular shapes, not indicating any preferential flow phenomena. As characteristic feature they all showed a fast initial increase and an extended tailing, whereas the first was more pronounced in the MER soil and the latter similar for both soils.

Generally, the peak concentrations arrived earlier in the MER soil,

with the first peak after 0.4 (manure), 0.8 (liquid high), and 1.1 (liquid low) pore volumes, respectively. In the KAL soil, the first peaks were at 1.7, 1.7, and 2.1 pore volumes. This confirms the findings of Unold et al. [2009a], who found the peaks arriving in MER soil approximately 0.6 pore volumes earlier. In contradiction to their findings, in our experiments the peak heights for the MER soil were higher than for the KAL soil, with the latter having lower dispersivities. Figure 5.1 demonstrates the occurrence of the peak concentrations in comparison to the conservative tracer chloride: in the MER experiment, the peaks for tracer and the SDZ ^{14}C-SDZ equivalent concentrations arrived approximately at the same time, whereas the tracer arrived considerably earlier in the KAL soil. The peaks in the experiments with the KAL soil arrived approximately at identical times in the experiment with the manure and the high liquid phase concentration, whereas it was a little later in the experiment with the low concentration. In the MER soil, the peak with the manure application arrived the earliest, followed by high liquid phase concentration and low concentration. This trend was visible in all subsequent applications. A lower sorption affinity in the MER soil is indicated by higher amounts of the solute in the outflow ($\approx$20%), clearly higher peak concentrations ($\approx$100%) and a lower mass sorbed in the profile (20–40%), respectively. This confirms previous studies with the same soils (Unold et al. [2009a], Kasteel et al. [2010]). As expected, the undisturbed soil columns from the two sites differed remarkably, since both the assumed heterogeneity of the flow paths and the surface area are greater in the MER soil. Furthermore, there was a difference in the distribution between neutral anionic SDZ species, as noted in Table XXX in Chapter 2, since the pH values were about 5.7 in the KAL experiments and ca. 6.7 for MER. Other factors reported to lead to an increased sorption affinity are clay and organic matter content [Boxall, 2008]. In both soils, a concentration dependency was observed: in the low liquid phase concentrations, the BTC concentrations were relatively lower and

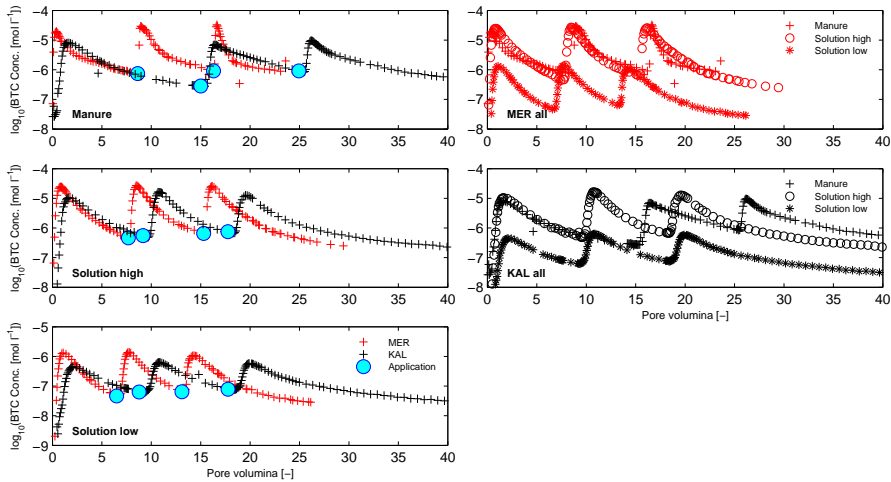the characteristics of the tailing were more pronounced than in the experiments with higher concentrations.

Figure 5.2: Breakthrough curves of the ^{14}C-SDZ equivalent concentrations for the experiments with the soils from Merzenhausen (MER) and Kaldenkirchen (KAL), respectively. The application concentrations for the experiments with manure and the high concentration in the liquid phase were identical, the low liquid phase constituted 10% of these concentrations, hence the scaling. On the left: the six BTC, sorted by application; on the right: sorted by soil. The data was log-transformed for plotting.

Table 5.2: Percental experimental mass recoveries for the six column experiments, separated by the single fractions.

	Manure	Solution high	Solution low
	Merzenhausen		
BTC	62.80	88.10	59.40
Profile	23.90	14.50	34.20
1st cm A2	7.70	1.90	3.60
1st cm A3	7.10	1.60	4.00
Total	101.50	106.10	101.20
	Kaldenkirchen		
BTC	49.30	74.19	50.49
Profile	39.36	23.31	43.90
1st cm A2	7.72	2.78	4.89
1st cm A3	7.70	2.84	5.37
Total	104.08	103.13	104.65

5.3.3 Concentration profiles

Figure 5.3 shows all six concentration profiles in terms of ^{14}C-SDZ equivalent concentrations at the end of the specific experiments. In the experiments with manure, an accumulation in the uppermost centimeter of the column was observed. The influence of the manure application in comparison to the liquid solution is reflected in the mass balances (Table 5.2): besides a lower total amount of SDZ in the BTC, a higher amount of substance sorbed to the solid phase was measured. Furthermore, the amount removed in the first centimeter before the second (A2) and third (A3) application was higher.

In the experiments with the MER soil, a lower sorption affinity in comparison to the KAL soil is reflected by the lower amount of sorbed substance: approx. 15% in all three experiments. This

confirms the findings of Unold et al. [2009a]. A non-linearity in terms of liquid phase concentrations is reflected in the higher relative sorbed amount of solute in the experiments with the low liquid phase concentration.

5.3.4 Modelling results

Figure 5.4 shows the BTC of measured and fitted concentrations, Table 5.3 lists the results of the parameter estimation based on our model description. The fits are based on the Standard Least Squares approach (residues are assumed to be constant and normal distributed). Due to the very low measurement errors, the estimated parameters showed no posterior distribution and therefore no information on parameter uncertainty was gained (Chapter 4). According to the visual impression, the fits lead to good results. Nevertheless, the model revealed structural deficits, in particular in the description of the KAL manure experiment.
The concentration profiles according to the numerical simulations (Fig.5.3) partly resulted in an overestimation, especially for the experiments with the solutions in the experiments with KAL soil. Estimating the model parameter on the basis of the first breakthroughs (Table 5.3) did not clearly alter the results in terms of the RMSE regarding all three BTC.
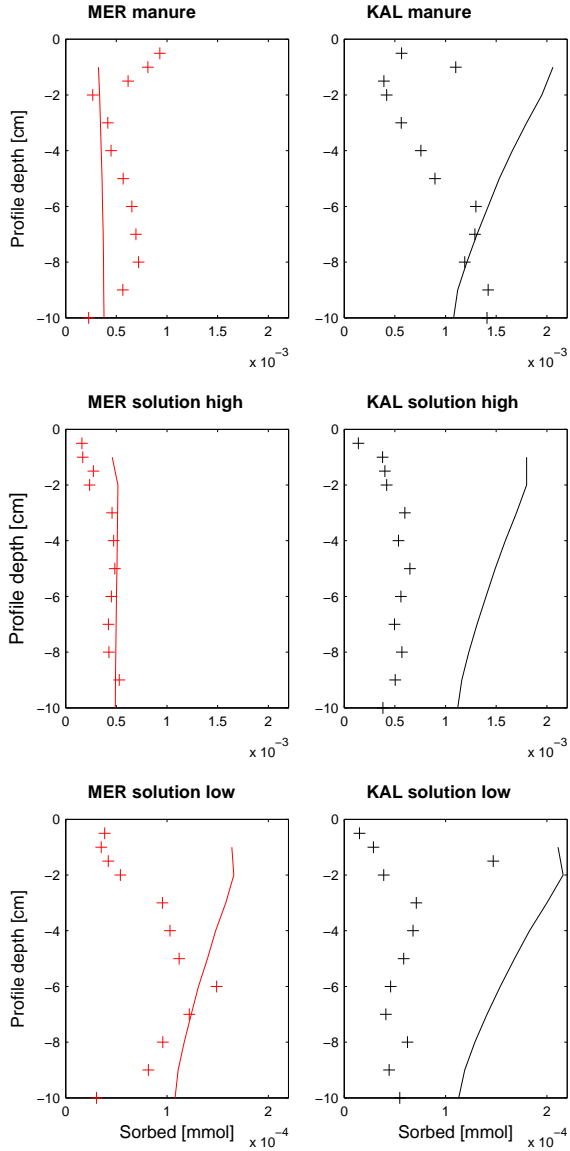
Figure 5.3: Concentration profiles in all six experiments with the columns from both sites - Merzenhausen (MER) and Kaldenkirchen (KAL), both measured at the end of the experimental period (markers) and as result of the numerical simulations (lines).
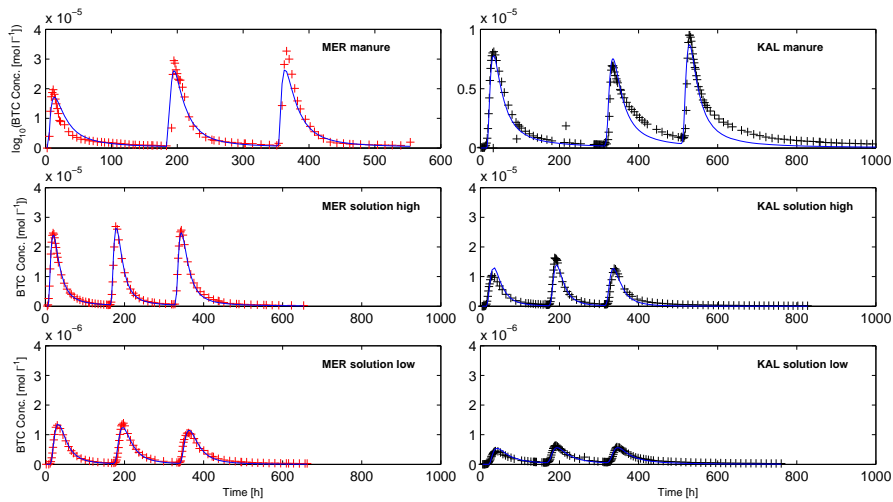
Figure 5.4: Measured and fitted BTC of the ^{14}C-SDZ equivalent concentrations for all six experiments with the soils from Merzenhausen (MER) and Kaldenkirchen (KAL).

Table 5.3: Results of the simulations for all three BTC simultaneously as well as on the basis of the first BTC only.

	k_f [*]	n [†]	μ_{irr} [‡]	α [§]	RMSE [¶]	95%-CI residuals [‖]	
	$[\text{mol}^{1-n}\,\text{l}^n\,\text{kg}^{-1}]$ $[0\text{--}0.1]$	[-] $[0.1\text{--}1]$	$[\text{h}^{-1}]$ $[0\text{--}0.1]$	$[\text{h}^{-1}]$ $[0.01\text{--}3]$	$[\text{mol}\,\text{l}^{-1}]$	$[\text{mol}\,\text{l}^{-1}]$	
			MER manure				
All 3 BTC	3.3E-05	0.13	3.2E-05	0.28	2.6E-06	-5.5E-06	5.6E-06
Only 1st BTC	4.0E-05	0.23	0.051	2.94	7.4E-06	-9.5E-07	2.0E-05
			MER liquid high				
All 3 BTC	1.1E-04	0.28	7.1E-03	0.32	6.3E-07	-1.6E-06	1.0E-06
Only 1st BTC	6.9E-05	0.24	6.2E-03	0.30	8.0E-07	-3.1E-06	1.1E-06
			MER liquid low				
All 3 BTC	6.7E-04	0.53	0.023	0.31	8.1E-08	-2.4E-07	1.9E-07
Only 1st BTC	2.8E-04	0.46	0.022	0.25	9.0E-08	-3.5E-07	1.3E-07
			KAL manure				
All 3 BTC	4.4E-04	0.36	0.044	0.27	6.1E-07	-1.3E-06	1.1E-06
Only 1st BTC	5.3E-04	0.37	0.038	0.24	7.3E-07	-1.9E-06	8.1E-07
			KAL liquid high				
All 3 BTC	0.012	0.66	0.040	1.1	1.3E-06	-3.6E-06	2.7E-06
Only 1st BTC	1.2E-03	0.44	0.033	0.40	2.4E-06	-7.5E-06	4.2E-06
			KAL liquid low				
All 3 BTC	3.8E-04	0.44	0.058	0.34	4.2E-08	-1.0E-07	9.4E-08
Only 1st BTC	2.0E-04	0.39	0.061	0.24	6.9E-08	-2.1E-07	1.1E-07

[*] Freundlich coefficient. [†] Freundlich exponent. [‡] rate of irreversible sorption. [§] rate-coefficient for kinetic reversible sorption. [¶] Root mean squared error of the residuals for all three BTC [‖] 95% residual interval.

The modelled concentration profiles were able represent the measured values quite well for the MER experiments, whereas the total amounts of sorbed SDZ were overestimated in the KAL experiments. Irreversible sorption, represented by an first order decay in our model clearly dominated the sorbed amount in the profile.

5.3.5 Breakthrough curves of the transformation products

Figure 5.5 shows the BTC of all species in absolute concentrations. We found up to six TP's besides the parent compound. For further elucidation, the courses of the percental compositions are shown in Fig. 5.6.
The manure contained 4-OH-SDZ and Ac-SDZ originating from

the pig metabolism [Lamshöft et al., 2007]. The compositions of the outflow in terms of the several species were different for the experiments with manure and solution. While in the manure experiment with both soils 4-OH-SDZ was dominant among the TP's, the application with solution lead to M1 as the dominating TP in all four cases. The fraction of SDZ at the end of the experimental period was highest in the MER manure experiment ($\approx$77%), and with it considerably lower than in the same experiment with KAL soil ($\approx$64%). Surprisingly, the course of the composition remained unchanged in the MER manure experiment and did not follow the dynamics of the applicaitons with solution, while it changed in the KAL soil.

The fraction of 4-OH-SDZ was highest after application with solution in low concentration (up to 25% in the KAL soil), while it was considerably lower in the high concentration (approximately 3%).

The Ac-SDZ which was originally in the manure did not break through in the experiment with KAL soil, but with the MER soil it still constituted up to 5%.

Generally, there were hardly any differences between the first and the subsequent BTC: the fraction of TP's was reduced with the new applications, and the following course of transformation was a repetition of the preceding breakthrough. Nevertheless, in two out of six experiments (MER solution high and KAL manure) there was a trend towards higher fractions of TP's with longer experimental time.

There was a concentration dependency in the transformation in the experiments with liquid solution, i. e. in lower concentration the tendency to transformation was more pronounced, an effect which became more visible in the higher concentration ranges shortly after application and more for KAL than for MER.

Transformation in the two soils in batch experiments is described in Sittig et al. [2014] (Chapter 3).
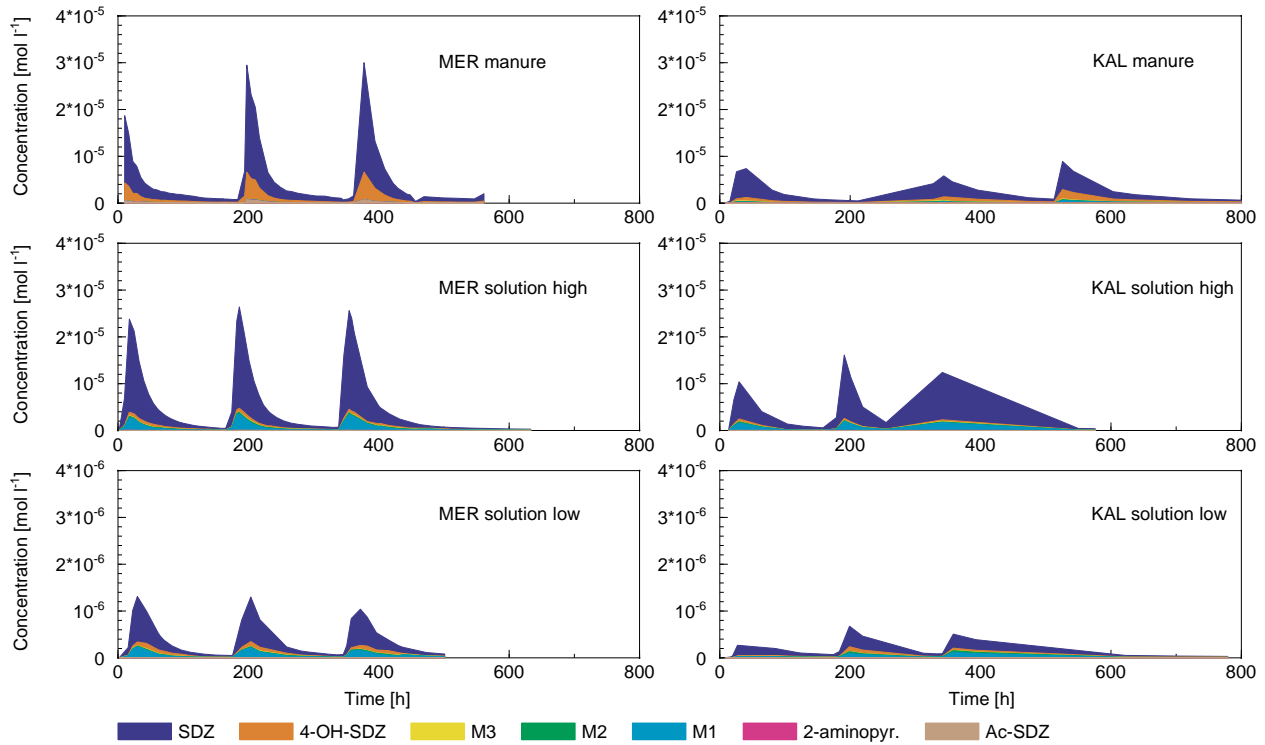
Figure 5.5: Transformation products in the outflow of the column for all six experiments. Note that the number of measurements was generally higher in the experiments with the MER soil.
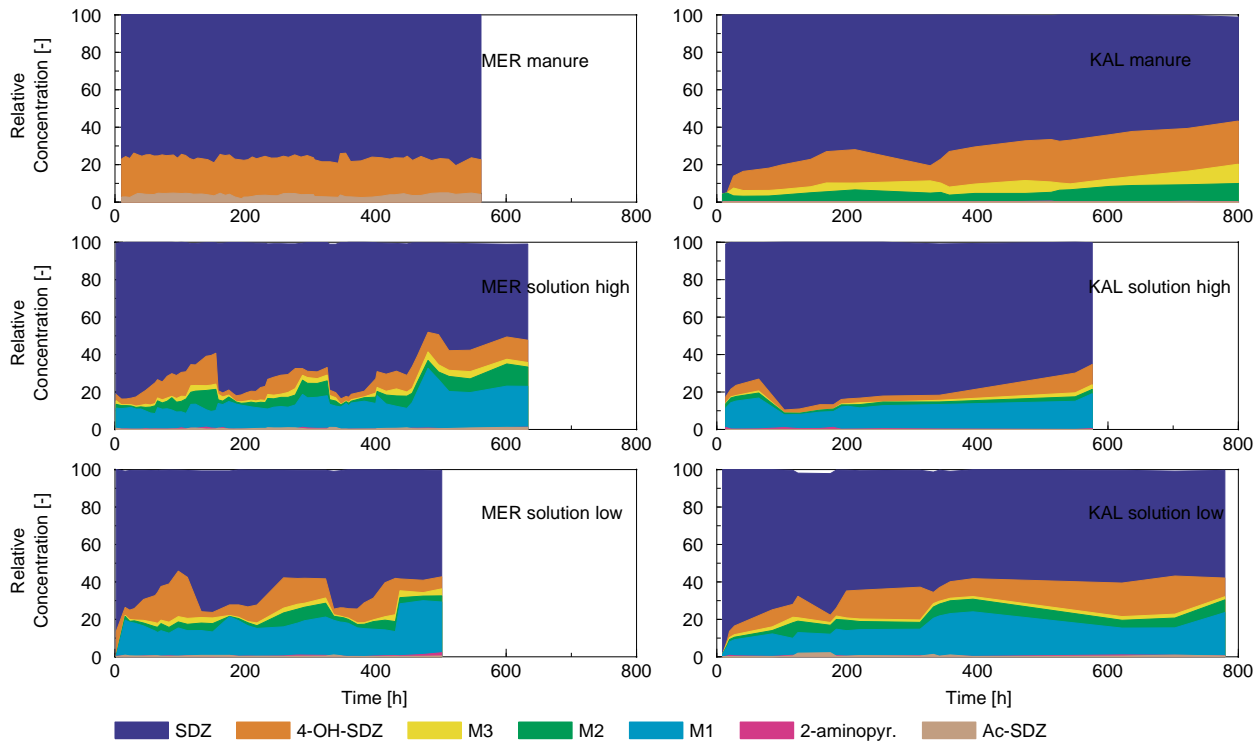
Figure 5.6: Same as Fig. 5.5, but as percental values.

5.4   Conclusions

In this chapter we studied the transport and transformation behavior of SDZ in two different soils in long-term laboratory column experiments. Several aspects were investigated by threefold applications together with manure and aqueous solution in two different concentrations, respectively.

In comparison to the solution with an identical concentration, the manure reduced the eluted amount of about 30% and additionally lead to a considerably different spectrum of metabolites. The experiment with 10% of this concentration in aqueous phase clearly demonstrated the non-linear sorption behavior, since the percental elution was in the same range as for the manure and the sorbed amount was twice as high as for the high concentration. The experimental setup using three successive applications did not reveal any obvious advantages in comparison to experiments with single applications. Our experiments showed the possible transport of SDZ and its metabolites through the vadose zone. Furthermore, the overall fate is strongly dependent on concentration level and soil properties. Our study serves to an enhanced understanding of the environmental fate of SDZ.

Chapter 6

Final remarks

6.1 Synthesis

Sorption and transformation in both batch (Chapter 2 and 3) and column experiments (Chapter 4 and 5) were investigated using two different soils. This gave insights into the behavior of SDZ in soils, with and without the presence of manure (in column experiments), which constitutes the main pathway for its entrance in the environment.

With the static batch experiments, long-term (60 days) sorption, sequestration, and transformation behavior under closed conditions could be investigated.

The column studies gave insights in the transport and sorption processes as a result of threefold application. The arrival time of SDZ was approximately identical with the one from the tracer experiment for the silty loam, while it was considerably later with the loamy sand (up to 100%).

Using results from both these laboratory experiments numerical studies could be conducted - describing both sorption and transformation in the batch studies and transport in the columns after multiple applications. In case of the batch studies an enhanced

model description based on the two-stage irreversible sorption model, presented by Wehrhan et al. [2010] was presented. The transition between different stages of sequestration was numerically shown: equilibrium and kinetic, both reversible and irreversible. Furthermore, the dependence of the term non-extractable residues on the experimental protocol was demonstrated, since it was possible to continuously extract sorbed substance by conducting successive extraction with a harsh method. Furthermore, this clearly demonstrated that SDZ was not covalently bound but prone to be continuously released. For the column transport experiments, a rate-limited sorption approach with first-order irreversible sorption (2S2Rirr) was applied. This allowed for the evaluation of an realistic standard scenario and therefore for a prediction of concentrations in the leachate in soil profiles.

After application, SDZ relatively quick forms sequestered residues. The possible subsequent release of this fraction from soil material was indicated, in both the batch and the column experiments. Fast adsorption and slow desorption serves for the buildup of a long-term reservoir in soils, not only constituting of the parent but as well as of metabolites.

A different spectrum of metabolites in the batch experiments and in the column experiments was found: while M1 and 4-OH-SDZ were formed instantaneously in batch and column experiments with application in liquid solution, the formation of 2-aminopyrimidine took longer. Therefore, no 2-aminopyrimidine was found in the outflow of the column experiments. The species M1 showed similar patterns in batch and column experiments (applied in liquid solution): a spontaneous formation and, subsequently a more or less constant level. The behavior of the species M2 is similar as well: a slow formation. Additionally, 4-OH-SDZ was seemingly formed and further degraded in the course of the experimental time for both types of experiments.

6.2   Outlook

Further studies should investigate the influence of several aspects of the fate of SDZ in the environment, such as the influence of changing moisture conditions (wetting-rewetting cycles) on the sequestration behavior, the influence of application together with manure on the transformation in batch experiments, and the effects of several irrigation modes on soil columns with multiple applications.

Including the transformation processes in the simulation of the column experiments, will give further insights in the fate of SDZ in the vadose zone.

Appendix A

Experimental setup of the column experiments

The column experiments described in Chapter 4 were conducted using the laboratory setup depicted in Fig. A.1. This construction built by personnel from the Agrosphere (IBG-3; Institute for Bio- and Geoscience) served to irrigate the soil columns and to apply suction at the outlets of up to three mounted columns. The system was software-controlled with a LabView based system.

Irrigation was done using a peristaltic pump (REGLO Digital MS-2/12, ISMATEC Laboratoriumstechnik GmbH, Wertheim-Mondfeld, Germany) which lead the 0.01 M $CaCl_2$ solution to the irrigation head equipped with 12 needles. The irrigation rate was controlled gravimetrically using a balance (Kern DS 8K0 1, Gottl. Kern & Sohn GmbH, Balingen-Frommern, Germany). Applying suction at the outlet of the columns allowed for establishing unit-gradient conditions, i. e. the water content in the column was identical over the whole length and the flow was solely driven by gravity, not due to differences in the matric potential. Identical pressure heads over the whole column length were established by adjusting the pressure of the suction in a way that the measurements of two tensiometers (T5, UMS GmbH, Mnchen, Germany) at 2.5

and 7.5 cm became identical (approximately $-40\,\mathrm{mBar}$).
After measuring the electrical conductivity, 15 ml of the percolation solution was released to a fraction collector by closing an electrical circuit with two water-level sensors.
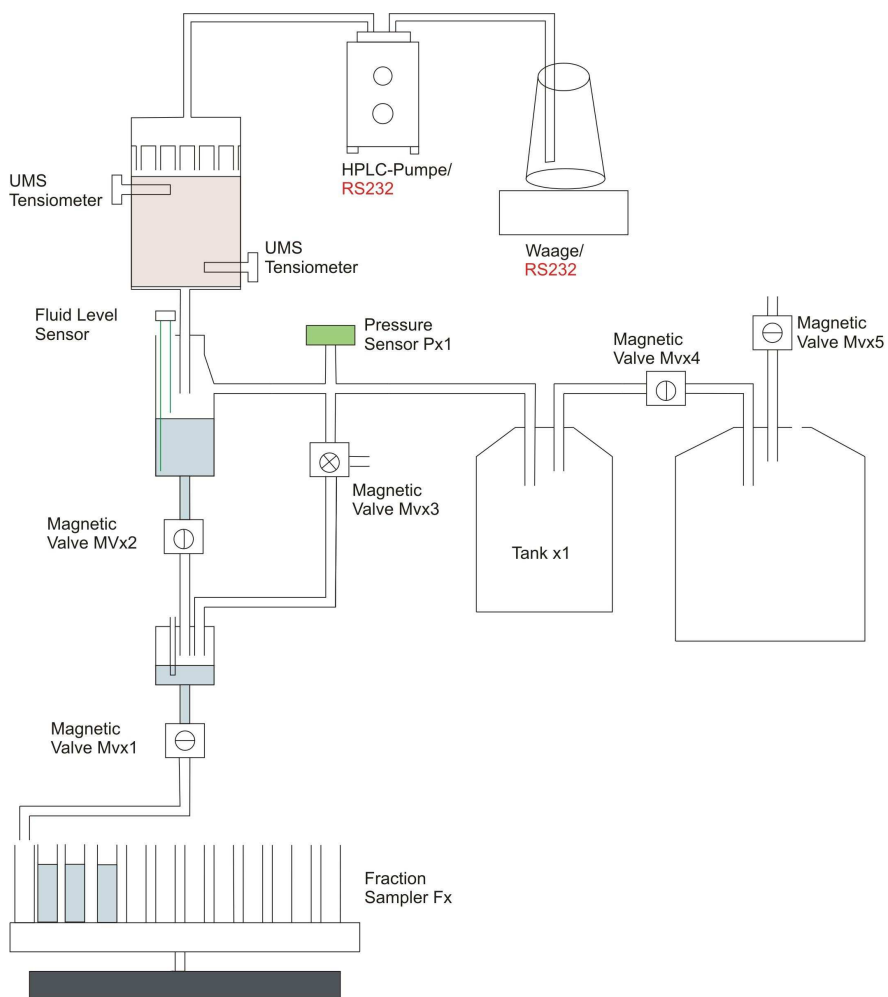
Figure A.1: Scematic overview of the column installation used for the experiments described in Chapter 4–5.

108

Bibliography

M. Alexander. Aging, bioavailability, and overestimation of risk from environmental pollutants. *Environ. Sci. Techn.*, 34:4259–4265, 2000.

S. Altfelder, T. Streck, M. Maraca, and T. Voice. Nonequilibrium sorption of dimethylphthalate—compatibility of batch and column techniques. *Soil Sci. Soc. Am. J.*, pages 102–111, 2001.

M.-O. Aust, S. Thiele-Bruhn, J. Seeger, F. Godlinski, R. Meissner, and P. Leinweber. Sulfonamides Leach from Sandy Loam Soils Under Common Agricultural Practice. *Water, Air, & Soil Pollution*, 211:143–156, 2010.

W. Baran, J. Sochaka, and W. Wardas. Toxicity and biodegradability of sulfonamides and products of their photocatalytic degradation in aqueous solutions. *Chemosphere*, 65:1295–1299, 2006.

A. Berns, H. Philipp, H.-D. Narres, P. Burauel, H. Vereecken, and W. Tappe. Effect of gamma-sterilization and autoclaving on soil organic matter structure as studied by solid state NMR, UV and flourescence spectroscopy. *Eur. J. Soil Sci.*, 59:540–550, 2008.

H. Bialk, A. Simpson, and J. Pedersen. Cross-coupling of sulfonamide antimicrobial agents with model humic constituents. *Environ. Sci. Technol.*, 39:4463–4473, 2005.

J. Bollag, M. Strynar, and M. Ahn. Characterization of enzymatic or abiotic immobilization of xenobiotics in soil. *Dev. Soil Sci.*, 28:289–299, 2002.

A. Boreen, W. Arnold, and K. McNeill. Triplet-sensitized photodegradation of sulfa drugs containing six-membered heterocyclic groups: identification of an SO_2 extrusion photoproduct. *Environ. Sci. Technol.*, 39:3630–3638, 2005.

G. Box and D. Cox. An analysis of transformations. *J. Roy. Stat. Soc. B 26*, pages 211–252, 1964.

A. Boxall. *Fate of Veterinary Medicines Applied to Soils, in: Pharmaceuticals in the Environment*, pages 103–119. Springer Berlin Heidelberg, 2008.

A. Boxall. New and emerging water pollutants arising from agriculture. background report on the oecd study "Water quality and agriculture: meeting the policy challenge", available online: http://www.oecd.org/agriculture/water. 2012.

A. Boxall, D. Kolpin, B. Halling-Sørensen, and J. Tolls. Are veterinary medicines causing environmental risks? *Environ. Sci. Technol.*, 37:286A–294A, 2003.

P. Burauel and F. Führ. Formation and long-term fate of nonextractable residues in outdoor lysimeter studies. *Environ. Pollut.*, 108:45–52, 2007.

J. C. Chee-Sanford, R. I. Mackie, S. Koike, I. G. Krapac, Y.-F. Lin, A. C. Yannarell, S. Maxwell, and R. I. Aminov. Fate and transport of antibiotic residues and antibiotic resistance genes following land application of manure waste. *J. Environ. Qual.*, 38:1086–108, 2009.

T. Christian, R. Schneider, H. Färber, D. Skutlarek, M. Meyer, and H. Goldbach. Determination of antibiotic residues in manure, soil, and surface waters. *Acta hydrochim. hydrobiol.*, 31: 36–44, 2003.

Council of the European Union. Regulation (EC) No 1831/2003 of the European Parliament and of the Council of 22 September 2003 on additives for use in animal nutrition. 2001.

A. de la Torre, I. Iglesias, M. Carballo, P. Ramirez, and M. Jesus Munoz. An approach for mapping the vulnerability of European Union soils to antibiotic contamination. *Sci. Total Environ.*, 414:672–679, 2012.

C. Ding and J. He. Effect of antibiotics in the environment on microbial populations. *Appl. Microb. Biotechn.*, 87(3):925–941, 2010.

L. Du and W. Liu. Occurrence, fate, and ecotoxicity of antibiotics in agro-ecosystems. A review. *Agronomy for Sustainable Development*, 32:309–327, 2011.

Q. Duan, S. Sorooshian, and V. Gupta. Effective and efficient global optimization for conceptual rainfall-runoff models. *Water Resour. Res.*, 28:1015–1031, 1992.

Düngeverordnung. Verordnung ber die Anwendung von Düngemitteln, Bodenhilfsstoffen, Kultursubstraten und Pflanzenhilfsmitteln nach den Grundsätzen der guten fachlichen Praxis beim Düngen. *BGBl I*, page 118, 1996.

EAEM. European agency for the evaluation of medicinal products. note for guidance: Environmental risk assessment for veterinary medicinal products other than GMO-containing and immunological products; emea/cvmo/055/96-final. 1997.

J. Eaton. Gnu octave manual. 2002.

FOCUS. "FOCUS groundwater scenarios in the EU review of active substances" Report of the FOCUS Groundwater Scenarios Workgroup, EC Document Reference Sanco/321/2000 rev.2, available at: http://viso.ei.jrc.it/focus/gw/docs/FOCUS_GW_Report_Main.pdf (verified: 08.05.2012). page 202 pp., 2000.

FOCUS. "Guidance document on estimating persistence and degradation kinetics from environmental fate studies on pesticides in eu registration" report of the focus work group on degradation kinetics, EC document reference sanco/10058/2005 version 2.0. page 434 pp., 2006.

M. Förster, V. Laabs, M. Lamshöft, T. Pütz, and W. Amelung. Analysis of aged sulfadiazine residues in soils using microwave extraction and liquid chromatography tandem mass spectrometry. *Anal. Bioanal. Chem.*, 391:1029–1038, 2008.

M. Förster, V. Laabs, M. Lamsöft, J. Groeneweg, S. Zühlke, M. Spiteller, M. Krauss, M. Kaupenjohann, and W. Amelung. Sequestration of manure-applied sulfadiazine residues in soils. *Environ. Sci. Technol.*, 43:1824–1830, 2009.

M. Garcia-Galan, T. Frümel, J. Müller, M. Peschka, T. Knepper, S. Diaz-Cruz, and D. Barcelo. Biodegradation studies of N4-acetylsulfapyridine and N4-acetylsulfamethazine in environmental water applying mass spectrometry techniques. *Anal. Bioanal. Chem.*, 402:2885–2896, 2012.

A. Gelman and D. Rubin. Inference from iterative simulation using multiple sequences. *Stat. Sci.*, 7:457–472, 1992.

E. Gullberg, S. Cao, O. G. Berg, C. Ilback, L. Sandegren, D. Hughes, and D. I. Andersson. Selection of Resistant Bacteria at Very Low Antibiotic Concentrations. *Plos Pathog.*, 7, 2011.

D. Gustafson and L. Holden. Nonlinear pesticide dissipation in soil: a new model based on spatial variability. *Environ. Sci. Technol.*, 24:1032–1038, 1990.

B. Halling-Sørensen. Algal toxicity of antibacterial agents used in intensive farming. *Chemosphere*, 40(7):731–739, 2000.

B. Halling-Sørensen, S. Nielsen, P. Lanzky, F. Ingerslev, H. Holten Lützhoft, and S. Jorgensen. Occurrence, fate and effects of pharmaceutical substances in the environment - a review. *Chemosphere*, 36:357–393, 1998.

U. Hammesfahr, R. Bierl, and S. Thiele-Bruhn. Combined effects of the antibiotic sulfadiazine and liquid manure on the soil microbial-community structure and functions. *J. Plat Nutr. Soil Sc.*, 174:614–623, 2011.

G. Hamscher, H. Pawelzick, H. Höper, and H. Nau. Different behavior of tetracyclines and sulfonamides in sandy soils after repeated fertilization with liquid manure. *Environ. Toxicol. Chem.*, 24:861–868, 2005.

M. Heistermann, B. Jene, G. Fent, M. Feyerabend, R. Seppelt, O. Richter, and R. Kubiak. Modelling approaches to compare sorption and degradation of metsulfuron-methyl in laboratory micro-lysimeter and batch experiments. *Pest. Manag. Sci.*, 59: 1276–1290, 2003.

T. Hoffmann, D. Hofmann, E. Klumpp, and S. Küppers. Electrochemistry-mass spectrometry for mechanistic studies and simulation of oxidation processes in the environment. *Anal. Bioanal. Chem.*, 399:1859–1868, 2011.

K. Hruska and M. Franek. Sulfonamides in the environment: a review and a case report. *Vet. Med.Czech.*, 57:1–35, 2012.

S. Jechalke, C. Kopmann, I. Rosendahl, G. J., J. Weichelt, E. Krögerrecklenfort, N. Brandes, M. Nordwig, G. Ding, J. Siemens, H. Heuer, and K. Smalla. Increased abundance and transferability of resistance genes after field application of manure from sulfadiazine-treated pigs. *Environ. Microbiol.*, 79: 1704–1711, 2013.

T. Junge, K. Meyer, K. Ciecielski, A. Adams, A. Schäffer, and B. Schmidt. Characterization of non-extractable ^{14}C- and ^{13}C-

sulfadiazine residues in soil including simultaneous amendment of pig manure. *J. Environ. Sci. Health B*, 46:137–149, 2011.

R. Kasteel, C. Mboh, M. Unold, J. Groeneweg, J. Vanderborght, and H. Vereecken. Transformation and sorption of the veterinary antibiotic sulfadiazine in two soils: a short-term batch study. *Environ. Sci. Technol.*, 44:4651–4657, 2010.

M. Kendall. A New Measure of Rank Correlation. *Biometrika*, 30: 91–89, 1938.

C. Kopmann, S. Sven Jechalke, I. Rosendahl, J. Groeneweg, E. Krögerrecklenfort, U. Zimmerling, V. Weichelt, J. Siemens, J. Amelung, H. Heuer, and K. Smalla. Abundance and transferability of antibiotic resistance as related to the fate of sulfadiazine in maize rhizosphere and bulk soil. *FEMS Microbiol Ecol*, 83:125–134, 2013.

R. Kreuzig and S. Höltge. Investigations on the fate of sulfadiazine in manured soil: laboratory experiments and test plot studies. *Environ. Toxicol. Chem.*, 24:771–776, 2005.

R. Kreuzig, C. Kullmer, B. Matthies, S. Höltge, and H. Dieckmann. Fate and behaviour of pharmaceutical residues in soils. *Fresenius Environ. Bull.*, 12:550–558, 2003.

K. Kümmerer. Antibiotics in the aquatic environment–a review–part I. *Chemosphere*, 75:417–34, 2009.

J.-W. Kwon. Mobility of veterinary drugs in soil with application of manure compost. *Bull. Environ. Contam. Toxicol.*, 87:40–44, 2011.

E. Laloy, D. Fasbender, and C. Bielders. Parameter optimization and uncertainty analysis for plot-scale continuous modeling of runoff using a formal bayesian approach. *J. Hydrol. 380*, pages 82–93, 2010.

M. Lamshöft, P. Sukul, S. Zühlke, and M. Spiteller. Metabolism of ^{14}C-labelled and non-labelled sulfadiazine after administration to pigs. *Anal. Bioanal. Chem.*, 388:1733–1745, 2007.

A. Lueking, W. Huang, S. Soderstrom-Schwarz, M. Kim, and W. Weber. Relationship of soil organic matter characteristics to organic contaminant sequestration and bioavailability. *J. Environ. Qual.*, 29:317–323, 2000.

R. Luthy, G. Aiken, M. Brusseau, S. Cunningham, P. Gschwend, J. Pignatello, M. Reinhard, S. Traina, W. Weber, and J. Westall. Sequestration of hydrophobic organic contaminants by geosorbents. *Environ. Sci. Technol.*, 31:3341–3347, 1997.

MATLAB. *Version 7.5.0.342 (R2007b)*. The MathWorks Inc., Natick, Massachusetts, USA, 2007.

N. Meng. *Fate of the antibiotic sulfadiazine in Yangtze River sediments: transformation, sorption and transport. PhD Thesis.* RWTH Aachen University, retrieved 07/18/2012 from: http://darwin.bth.rwthaachen.de/opus3/volltexte/2011/3804/pdf/3804.pdf, 2011.

S. Mohring, I. Strzysch, M. Fernandes, T. Kiffmeyer, J. Tuerk, and G. Hamscher. Degradation and elimination of various sulfonamides during anaerobic fermentation: a promising step on the way to sustainable pharmacy? *Environ. Sci. Technol.*, 43: 2569–2574, 2009.

J. Nash and J. Sutcliffe. River flow forecasting through conceptual models, Part I - A discussion of principles. *J. Hydrol.*, 10:282–290, 1970.

J. Ollivier, D. Schacht, R. Kindler, J. Groeneweg, M. Engel, B. Wilke, K. Kleineidam, and M. Schloter. Effects of repeated application of sulfadiazine-contaminated pigmanure on the abundance and diversity of ammonia and nitrite oxidizers

in the root-rhizosphere complex of pasture plants under field conditions. *Frontiers in microbiology*, 4, article 22, 2013.

B. Pan, P. Ning, and B. Xing. Part V - sorption of pharmaceuticals and personal care products. *Environ. Sci. Pollut. Res.*, 16:109–116, 2009.

R. Reichel, I. Rosendahl, E. T. Peeters, A. Focks, J. Groeneweg, R. Bierl, A. Schlichting, W. Amelung, and S. Thiele-Bruhn. Effects of slurry from sulfadiazine- (SDZ) and difloxacin- (DIF) medicated pigs on the structural diversity of microorganisms in bulk and rhizosphere soil. *J. SoilBio*, 62:82–91, 2013.

I. Rosendahl, J. Siemens, E. Groeneweg, J. Linzbach, V. Laabs, C. Herrmann, H. Vereecken, and W. Amelung. Dissipation and sequestration of the veterinary antibiotic sulfadiazine and its metabolites under field conditions. *J. Environ. Qual.*, 45:5216–5222, 2011.

I. Sabbah, W. Ball, D. Young, and E. Bouwer. Misinterpretations in the modeling of contaminant desorption from environmental solids when equilibrium conditions are not fully understood. *Environ. Eng. Sci.*, 22:350–366, 2005.

A. Sarmah, M. Meyer, and A. Boxall. A global perspective on the use, sales, exposure pathways, occurrence, fate and effects of veterinary antibiotics (VA's) in the environment. *Chemosphere*, 65:725–759, 2006.

B. Scharnagl, J. Vrugt, H. Vereecken, and M. Herbst. Inverse modelling of in situ soil water dynamics: investigating the effect of different prior distributions of the soil hydraulic parameters. *Hydrol. Earth Syst. Sci. 15*, pages 3043–3059, 2011.

K. Schauss, A. Focks, H. Heuer, A. Kotzerke, H. Schmitt, S. Thiele-Bruhn, K. Smalla, B.-M. Wilke, M. Matthies, W. Amelung, J. Klasmeier, and M. Schloter. Analysis, fate and

effects of the antibiotic sulfadiazine in soil ecosystems. *Trends in Analytical Chemistry*, 28:612–618, 2009.

B. Schmidt, J. Ebert, M. Lamshöft, B. Thiede, R. Schumacher-Buffel, R. Ji, P. F.-X. Corvini, and A. Schäffer. Fate in soil of ^{14}C-sulfadiazine residues contained in the manure of young pigs treated with a veterinary antibiotic. *J. Environ. Sci. and Heal. B*, 43:8–20, 2008.

G. Schoups and J. Vrugt. A formal likelihood function for parameter and predictive inference of hydrologic models with correlated, heteroscedastic, and non-gaussian errors. *Water Resour. Res.*, 46, 2011.

J. Schwarz, M.-O. Aust, and S. Thiele-Bruhn. Metabolites from fungal laccase-catalysed transformation of sulfonamides. *Chemosphere*, 81:1469–1476, 2010.

U. Schwertmann. Differenzierung der Eisenoxide des Bodens durch photochemische Extraktion mit saurer Ammoniumoxalat-Lösung. *Z. Pflanzenernaehr. Dueng. Bodenkd.*, 105:194–202, 1964.

V. K. Sharma. Oxidation of Inorganic Compounds by Ferrate(VI) and Ferrate(V): One-Electron and Two-Electron Transfer Steps. *Environ. Sci. Technol.*, 44:5148–5152, 2010.

J. Simunek, M. Sejna, H. Saito, M. Sakai, and M. van Genuchten. The HYDRUS-1D software package for simulating the one-dimensional movement of water, heat, and multiple solutes in variably-saturated media. version 4.0. *Dep. of Environ. Sci.*, pages Univ. of California, Riverside, 2008.

L. Simunek, M. T. v. Genuchten, M. Sejna, N. Toride, and F. J. Leij. STANMOD. Studio of Analytical Models for solving the Convection-Dispersion Equation. Version 2.0., 1999.

S. Sittig, R. Kasteel, J. Groeneweg, and H. Vereecken. Long-term sorption and sequestration dynamics of the antibiotic sulfadiazine - a batch study. *J. Environ. Qual.*, 41:1497–1506, 2012.

S. Sittig, R. Kasteel, G. J., D. Hofmann, B. Thiele, S. Köppchen, and H. Vereecken. Dynamics of transformation of the veterinary antibiotic sulfadiazine in two soils. *submitted to: Chemosphere*, 95:470–477, 2014.

K. Stoob, H. Singer, S. Müller, R. Schwarzenbach, and C. Stamm. Dissipation and transport of veterinary sulfonamide antibiotics after manure application to grassland in a small catchment. *Environ. Sci. Technol.*, 41:7349–7355, 2007.

P. Sukul and M. Spiteller. Sulfonamides in the environment as veterinary drugs. *Rev. Environ. Contam. Toxicol.*, 187:67–101, 2006.

P. Sukul, M. Lamshöft, S. Zühlke, and M. Spiteller. Photolysis of ^{14}C-sulfadiazine in water and manure. *Chemosphere*, 71:717–725, 2008a.

P. Sukul, M. Lamshöft, S. Zühlke, and M. Spiteller. Sorption and desorption of sulfadiazine in soil and soil-manure systems. *Chemosphere*, 73:1344–1350, 2008b.

W. Tappe, M. Herbst, D. Hofmann, S. Köppchen, S. Kummer, B. Thiele, and J. Groeneweg. Degradation of sulfadiazine by microbacterium lacus strain SDZm4, isolated from lysimeters previously manured with slurry from sulfadiazine-medicated pigs. *Appl. Environm. Microbiol.*, 79:2572–2577, 2013.

S. Thiele-Bruhn. Pharmaceutical antibiotic compounds in soils - a review. *J. Plant. Nutr. Soil. Sci.*, 166:145–167, 2003.

S. Thiele-Bruhn, T. Seibicke, H.-R. Schulten, and P. Leinweber. Sorption of sulfonamide pharmaceutical antibiotics on whole soils and particle-size fractions. *J. Environ. Qual.*, 33:1331–1342, 2004.

J. Tolls. Sorption of veterinary pharmaceuticals in soils: a review. *Environ. Sci. Technol.*, 35:3397–3406, 2001.

J. Topp, R. Chapman, M. Devers-Lamrani, A. Hartmann, R. Marti, L. Martin-Laurent, F. Sabourin, A. Scott, and M. Sumarah. Accelerated biodegradation of veterinary antibiotics in agricultural soil following long-term exposure, and isolation of a sulfamethazine-degrading *Microbacterium* sp. 2013.

M. Unold, J. Simunek, R. Kasteel, J. Groeneweg, and H. Vereecken. Transport of manure-based applied sulfadiazine and its main transformation products in soil columns. *Vadose Zone J.*, 8:677–689, 2009.

M. Unold, J. Simunek, R. Kasteel, J. Groeneweg, and H. Vereecken. Transport of manure-based applied sulfadiazine and its main transformation products in soil columns. *Vadose Zone J.*, 8:677–689, 2009a.

M. Unold, R. Kasteel, J. Groeneweg, and H. Vereecken. Transport and transformation of sulfadiazine in soil columns packed with a silty loam and a loamy sand. *J. Contam. Hydrol.*, 103:38–47, 2009b.

L. Van Eerd, R. Hoagland, R. Zablotowicz, and J. Hall. Pesticide metabolism in plants and microorganisms. *Weed Sci.*, 51:472–495, 2003.

J. Vrugt. Posterior exploration using differential evolution adaptive metropolis with sampling from past states. *manuscript in preparation*, 2012.

J. Vrugt, G. Diks, H. Gupta, W. Bouten, and J. Verstraten. Improved treatment of uncertainty in hydrologic modeling: combining the strengths of global optimization and data assimilatiom. *Water Resour. Res. 41.*, 2005.

J. Vrugt, C. ter Braak, C. Clark, and B. Robinson. Treatment of input uncertainty in hydrologic modeling: Doing hydrology backward with markov chain monte carlo simulation. *Water Resour. Res.*, 44:–, 2008.

J. Vrugt, C. ter Braak, C. Diks, B. Robinson, J. Hyman, and D. Higdon. Accelerating markov chain monte carlo simulation by differential evolution with self-adaptive randomized subspace sampling. *Int. J. Nonlinear Sci.*, 10:273–290, 2009.

J. Vrugt, C. ter Braak, and J. Hyman. Differential evolution adaptive metropolis with snooker update and sampling from past states. *SIAM journal on Optimization, In Preparation*, 2010.

J. Vrugt, C. ter Braak, C. Diks, and G. Schoups. Advancing hydrologic data assimilation and treatment of model, parameter, and state uncertainty using particle markov chain monte carlo simulation: Theory, concepts and applications. *submitted to Adv. Water Resour.*, 2011.

Y. Wang, J. B. Liang, X. D. Liao, L.-s. Wang, T. C. Loh, J. Dai, and Y. W. Ho. Photodegradation of sulfadiazine by goethite and oxalate suspension under UV light irradiation. *Ind. Eng. Chem. Res.*, 49:3527–3532, 2010. doi: 10.1021/ie9014974.

A. Wehrhan, R. Kasteel, J. Simunek, J. Groeneweg, and H. Vereecken. Transport of sulfadiazine in soil columns: experiments and modelling approaches. *J. Contam. Hydrol.*, 89: 107–35, 2007.

A. Wehrhan, T. Streck, H. Groeneweg, H. Vereecken, and R. Kasteel. Long-term sorption and desorption of sulfadiazine in soil: experiments and modeling. *J. Environ. Qual.*, 39:654–666, 2010.

L. Weihermüller, R. Kasteel, J. Vanderborght, J. Simunek, and H. Vereecken. Uncertainty in pesticide monitoring using suction cups: evidence from numerical simulations. *Vadose Zone J. 10*, pages 1287–1298, 2011.

J.-F. Yang, G.-G. Ying, L.-H. Yang, J.-L. Zhao, F. Liu, R. Tao, Z.-Q. Yu, and P. Peng. Degradation behavior of sulfadiazine in soils under different conditions. *J. Environ. Sci. and Heal. B*, 44:241–248, 2009.

G. Ying, R. Kookana, and M. Mallavarpu. Release behavior of triazine residues in stabilised contaminant soils. *Environ. Pollut.*, 134:71–77, 2005.

C. Zarfl, J. Klasmeier, and M. Matthies. A conceptual model describing the fate of sulfadiazine and its metabolites observed in manure-amended soils. *Chemosphere*, 77:720–726, 2009.